New Developments in Screen Printing For Advances in Electroanalysis

Fang Tan

(MMU Student ID: 07457999)

Submitted in partial fulfilment of the requirements of Manchester Metropolitan University for the degree of Masters by Research

2013

School of Science and the Environment,
Division of Chemistry and Environmental Science, Manchester Metropolitan University, Chester Street, Manchester M1 5GD, Lancashire, UK.

ABSTRACT

Within the discipline of electrochemistry, the sub-section that concerns itself with quantification is electroanalysis, which is the basis of portable and sensitive sensors; this is exemplified in the billion dollar glucose market where their development allows diabetics to measure their blood glucose on-the-spot without recourse to the clinic. Screen-printing is a suitable method to fabricate such a sensor which is mass-produced yet reproducible and economical in nature. In order for the next-generation of biosensors (such as the glucose sensors), advances in screen-printed electrode design needs to be made; this is exactly what this Master's Thesis aims to achieve.

This thesis first considers the fabrication of platinum screen-printed macroelectrodes, which are analytically explored and benchmarked towards the sensing of selected target analytes. Next, palladium screen-printed macroelectrodes are fabricated and characterised via microscopy and cyclic voltammetry, in particular, the electroanalytical applications are explored towards the sensing of formaldehyde, hydrazine and its potential use in gas sensors for the sensing of hydrogen and methane with comparisons made to existing literature reports. Note that such an electrode made entirely via screen-printing has not been reported before in the literature.

In order to improve mass transport properties, shallow recessed screen-printed electrodes are designed and fabricated and benchmarked towards the sensing of NADH and nitrite. The electroanalytical sensing of nitrite is further testing within canal water samples showing the robust nature of the sensors analytical performance. Additionally these unique sensors were found to be electrochemically useful in sensing towards hydrazine and hydrogen peroxide. Finally, carbon screen-printed microelectrode arrays are fabricated and are benchmarked towards the sensing of acetaminophen, dopamine and nitrite. Note that this is

the first example of an array which exhibits diffusional independence (the current literature reports only arrays that have diffusional interaction) and as such gives rise to analytically useful measurements. This screen printed microelectrode array is also shown to be possible to be produced with gold working electrodes which are benchmarked towards the determination of Chromium (VI).

TABLE OF CONTENTS

ACKNOWLEDGEMENTS

I would like to express my deep gratitude to Dr. Craig Banks, my research supervisor, for his patient guidance, enthusiastic encouragement and useful critiques of this research work. I would also like to thank Dr. Dimitrios Kampouris, for his advice and assistance in keeping my progress on schedule. My grateful thanks are also extended to Mr. Jonathan Metters for all his help and making the screen printed electrodes.

I would also like to extend my thanks to the technicians of the laboratory of the Manchester Metropolitan University chemistry department for their help

Finally, I wish to thank my parents for their support and encouragement throughout my study.

List of Tables

List of Figures

CHAPTER 1. INTRODUCTION

1.1 INTRODUCTION TO SCREEN PRINTING

Screen printing technology is a well-established technique for the fabrication of electroanalytical sensors.[1-5] One prominent commercialisation of screen printed electrodes was the personal glucose biosensor used by those suffering with diabetes, which is billion dollar per annum global market.[6-9] Society is in a constant stare of growth and development and it is inevitable that demands for sensing devices related to clinical and industrial applications will increase; this is particularly true in the former case within UK where the recent budget cuts in NHS are pushing the onus onto individual self-monitoring. In order to achieve this, inexpensive and disposable, yet highly accurate and rapid, devices are greatly sought. Additionally the portability of such devices is of fundamental importance. Decentralised sensing is ever more necessary and thus traditional techniques utilising highly expensive, immovable analytical equipment such as Gas Chromatography-Mass Spectrometers are not feasible for sensing outside the realms of standard laboratories.[10] Examples of cases where portable, economical and sensitive sensors are highly desirable include; utilisation in hospitals where there is a suspected drug over-dose, the personal monitoring of diseases such as diabetes[6] (as detailed earlier), the detection of potential pollutants of toxins within environmental samples[11] such as river water, the screening of drinking water at different sources,[12] and also the rapid determination of naturally occurring biomolecules.[2]

Screen printed electrodes not only address the issue of cost effectiveness but they also satisfy the previously much sought after criterion of highly reproducible and sensitive methods of detection towards target analytes, whilst maintaining the low cost production through scales

of economy. The adaptability of screen printed electrodes is also of great benefit in areas of research; the ability to modify the electrodes with ease, through differing inks commercially available for the reference, counter, and working electrodes, allows for highly specific and finely calibrated electrodes to be produced for specific target analytes.[1]

Screen printing involves printing a thixotropic fluid through a mesh screen which defines the shape and size of the desired electrode. The thixotropic fluid contains a variety of substances including graphite, carbon black, solvents and polymeric binder.[4, 13, 14] Figure 1.1 depicts a schematic representation of the process of screen printing, where multiple layers and complex designs can be implemented. The inks utilised have a relatively high viscosity (3–10 Pa.s at a sheer rate of $230s^{-1}$) but when forced through the screen mesh by the squeegee blade, the ink undergoes sheer thinning allowing it to penetrate through the screen mesh which defines the final shape/design. Upon contact with the substrate, typically a ceramic or plastic material, the ink returns to its viscous state forming the intended shape/design with definition. Such final shapes/designs have thicknesses in the range of 20 to 100 mm and as such are thicker than those obtained by other printing methodologies, thus they are consequently termed ‘‘thick film technology’’. Note that the thickness can be readily controlled by the thickness of the stencil design and the mesh.[15, 16] Such designs can be printed onto ceramic substrates[17] or plastic substrates[17-19] depending on the intended application. In the latter case the cost is generally lower and the carbon print is better adhered to the substrate than in the former case.

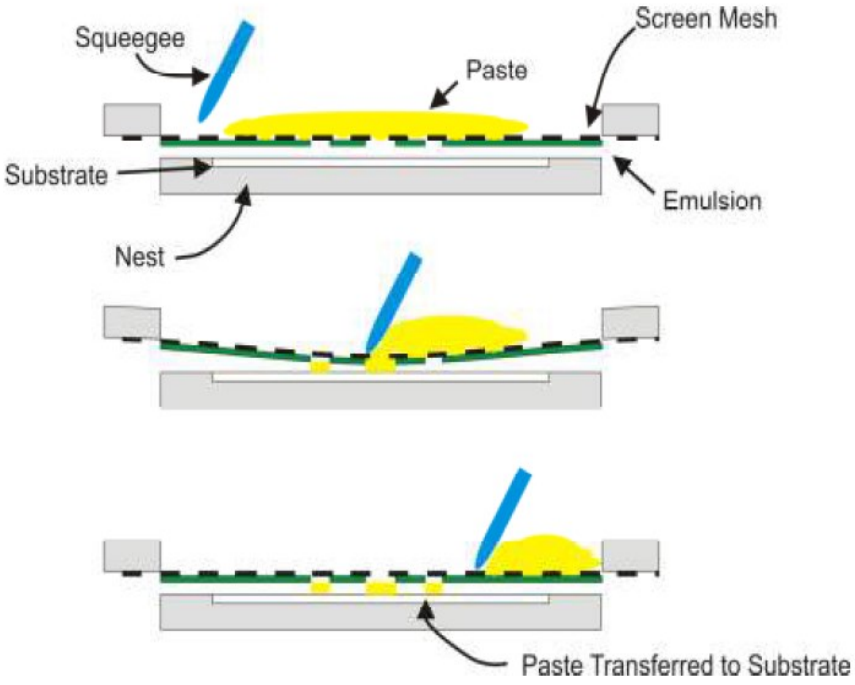

Figure 1.1: Schematic representation of the process screen printed manufacturing of electrodes (cross sectional side view) outlining the basic processes involved. Figure reproduced from reference.[5]

Note that there are many research efforts into developing screen printed biosensors and consequently there is a substantial wealth of literature and as such there are authoritative reviews on utilising screen printed enzymatic electrode biosensors, see for example references.[20-24] In order for screen printed derived sensors to continually move forward, researchers need to design and implement new types. The aims of this work are exactly that, to produce novel electrochemical sensing platforms which can form the basis of such sensors. Screen-printed electrodes in this thesis utilise the technique of electrochemistry and consequently a brief description of this technique now follow. Screen printed electrodes have been utilised within many notable pieces of work without the additional pre-treatment or modification of the electrodes used. The ability to achieve highly sensitive electrochemical responses without the requirement of further modification to the screen printed electrodes is clearly desirable with the reduced pre-treatment/ modification improving the potential commercial development of such work, where minimum costs and ease of production are

essential. Highly sensitive detection of cadmium (II) has been achieved allowing bio-monitoring within artificial and diluted oral (saliva) fluid.[25] Electrochemical analysis with the application of screen printed electrodes enabled detection limits in the low mg L^{-1} with anodic stripping voltammetry utilising the presence of the bismuth film which provides an enhanced sensitivity for the electroanalytical deposition of cadmium (II) coupled with a simple change in pH of the oral (saliva) fluid sample permitting quantitative measurements. Such work highlights the efficiency and flexibility of screen printed electrodes, even in such electrochemically challenging media. Screen printed derived sensors have ease of use, scale of economies, are disposable in nature and require a reduced volume of the analyte (~ microlitres) making them a natural choice in sensing applications over conventional (solid) carbon electrodes and other fabrication approaches due to screen printings adaptability such as lithography. As has been highlighted screen printed sensors offer great longevity with abundant potential future applications. There are many advantages of using screen printed electrodes over conventional carbon based electrodes and we therefore expect many more reports to be published where screen printed sensors are employed both; without modification ‘‘as-is’’ and through novel and advantageous modification. New directions in this area will likely include the use of a range of nanomaterials to improve electron transfer processes yet being completely scalable in terms of fabrication whilst also pushing towards smaller and well-defined geometries which have applications in screen-printed microelectrode arrays and ‘lab on a chip’ approaches with the overall ethos of simpler, cheaper, disposable, scalable and ease of use.

The aim of this thesis is to design, fabricate and evaluate new screen-printed electrodes to impart improvements in their electroanalytical performances. Before presenting such new electrode configurations, an introduction to electroanalysis and a general

introduction into the technique of electrochemistry is given, which is used exclusively within this thesis.

1.2 ELECTROANALYSIS

Electro-analytical techniques are concerned with the interaction between electricity and chemistry, specifically the measurements of electrical quantities, such as current, potential, or charge, and their relationship to chemical parameters. In contrast to many chemical measurements that involve bulk solutions, electrochemical processes take place at the electrode-solution interface. These electrochemical techniques can be characterised into two principle type; potentiometric and potentiostatic measurements, differentiated via the electrical signal used for quantification. Equally both techniques require at least two electrodes (conductors) and a contacting sample (electrolyte) solution, this constitutes the electrochemical cell. The surface of the electrode represents the junction between an ionic conductor and an electronic conductor. The electrode that responds to the target analyte(s) is termed the working electrode, the second, termed the reference electrode; is of constant potential (that is, independent of the properties of the solution). Electrochemical cells can be classified as electrolytic (consuming energy from an external source) or galvanic (producing electrical energy). Controlled-potential (potentiostatic) techniques deal with the study of charge-transfer processes at the electrode-solution interface based on dynamic (no zero current) situations. In this situation, the electrode potential is used to drive an electron-transfer reaction, where the resulting current is measured. This is effectively "electron pressure", forcing a chemical species to either gain or lose an electron (reduction and oxidation respectively). The advantages of using controlled-potential techniques include high sensitivity and selectivity towards electroactive species where extremely low limits of

detection (nanomolar) can be achieved with very small sample volumes (5-20µL) in addition to the extensive array of electrode materials now available, permitting the assay of unusual environments.

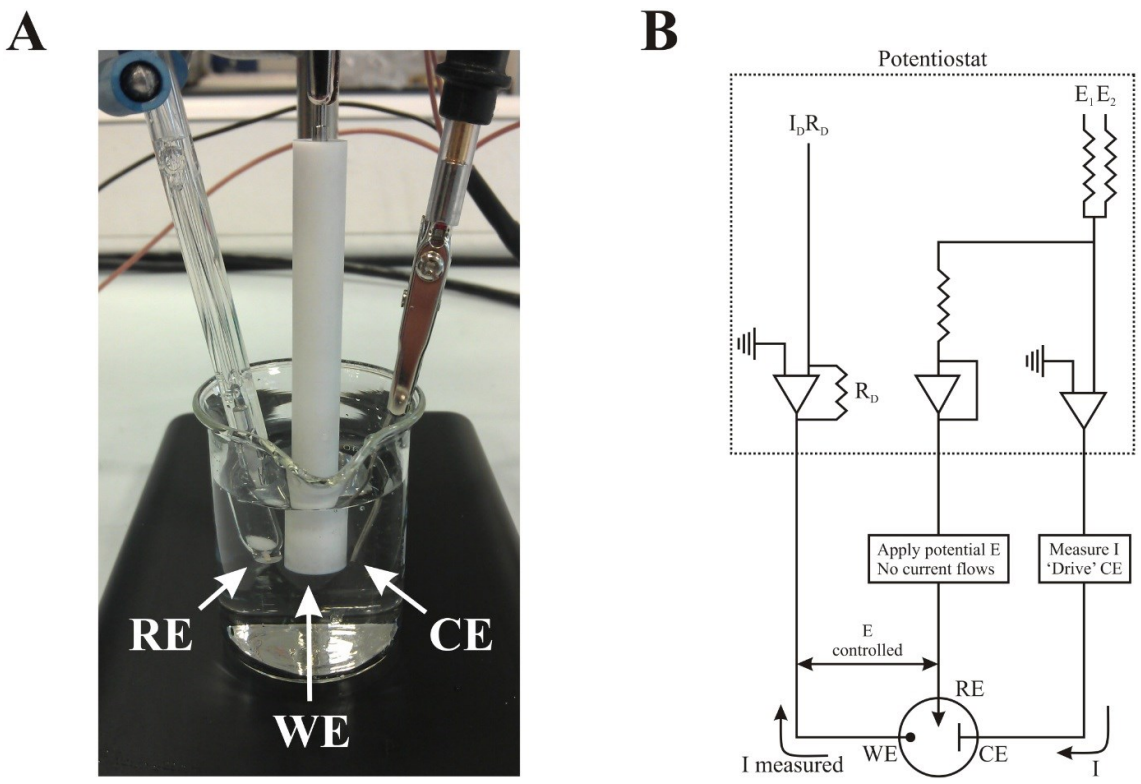

Figure 1.2 A: A typical experimental set-up showing the reference electrode (RE, saturated calomel electrode), the working electrode (WE) and the counter electrode (CE, a platinum rod) immersed into an electrolyte solution. **B**: A simple electronic scheme equivalent to the electrochemical cell. A commercial potentiostat is required for running electrochemical experiments.

Shown in Figure 1.2 is a typical experimental set-up where the three electrode system is being utilised. The reference electrode can be an Ag/AgCl or a Saturated Calomel Electrode (SCE) which can either be commercially obtained or fabricated within the laboratory. The counter electrode should be a non-reactive high surface area electrode such as platinum or carbon and the working electrode can be a plethora of configurations and compositions. This

approach is simplified using screen printed electrodes where *all* the electrodes are on one disposable strip.

1.3 FARADAIC PROCESSES

The intention of controlled-potential electro-analytical experiments is to obtain a current response that is interrelated to the concentration of the target analyte. This is achieved by recording the transfer of electron(s) during the redox process of the analyte:

$$O + ne^- \rightleftharpoons R \tag{1.1}$$

where O and R are the oxidised and reduced forms, respectively, of the redox couple. This reaction will occur in a potential region that makes the electron transfer thermodynamically or kinetically favourable. Within systems that are controlled by the law of thermodynamics, the potential of the electrode can be used to establish the concentration of the electroactive species [$C_O(0, t)$ and $C_R(0, t)$ where C_O and C_R simply represent the concentration of the oxidised and reduced forms respectively] at the surface (distance from surface (x) = 0) at time (t) according to the *Nernst equation*:

$$E = E^o + \frac{2.3\,RT}{nF} \log \frac{C_O\,(0,t)}{C_R(0,t)} \tag{1.2}$$

while at standard conditions (298 K):

$$E = E^o + \frac{0.059}{n} \log \frac{C_O\,(0,t)}{C_R(0,t)} \tag{1.3}$$

where E is the potential at which the peak is truly measured, E^o is the standard potential for the redox reaction, R is the universal gas constant (8.314 J K^{-1} mol^{-1}), T is the temperature (Kelvin), n is the number of electrons transferred in the reaction, and F is the Faraday constant (96,485.33 C mol^{-1}).

Alternatively the *Nernst equation* can be expressed as:

$$E = E^{o} + (RT/nF)\, ln(A_P/A_R) \quad (1.4)$$

where A_P and A_R are the standard activities of the products and reactants respectively.

On the negative side of E^o, the oxidised reactants tend to be reduced thus the forward reaction (*i.e.* reduction) becomes more favourable. The current produced, resulting from the change in oxidation state of the electroactive species is termed the faradaic current because it obeys Faraday's law (that is the reaction of 1 mole involves a change of *n* x 96,485.33 C). The faradaic current is a direct measure of the rate of redox reaction. The resulting current-potential plot, known as a *voltammogram* (see later), is a display of current signal (vertical axis) versus the excitation potential (horizontal axis). The exact shape and magnitude of the voltammetric response is governed by the processes involved in the electrode reaction. The total current is the summation of the faradaic currents for the sample and blank solution, as well as the non-faradaic charging background current.

The reaction route undertaken at the electrode can be quite complicated, sometimes involving a sequence of different phases. The rate of such a reaction is determined by the slowest step in the sequence. Simple reactions involve only the mass transport of the electroactive species to the electrodes surface, the electron transfer across the interface, and the transport of the product back to the bulk solution. More complex reactions involve additional chemical and surface reactions that precede or follow the actual electron transfer. The overall rate of the reaction, and thus the measured current, may be limited by the mass transport of the reactant or the rate of electron transfer. The slowest process will be the rate determining step. Determining whether a given reaction is controlled by the mass transport or electron transfer depends on the type of compound being measured and the experimental conditions (electrode material, media, operating potential, mode of mass transport, time scale,

etc.), therefore the rate determining step of a given system may thus depend on the potential range under investigation. If the overall reaction is governed solely by the rate at which the electroactive species reaches the electrodes surface (*i*.e. a facile electron transfer), the current is said to be mass-transport limited. Such reactions are called *Nernstian* or reversible, because they obey thermodynamic relationships.

1.4 CYCLIC VOLTAMMETRY

Cyclic voltammetry is the most extensively used technique for acquiring qualitative information about electrochemical reactions. It is used extensively within this thesis/transfer report. It tenders the rapid identification of *redox* potentials distinctive to the electroactive species, providing considerable information about the thermodynamics of a redox process, kinetics of heterogeneous electron-transfer reactions, coupled electrochemical reactions or adsorption processes. Cyclic voltammetry consists of scanning (linearly) the potential of the working electrode using a triangular potential wave form (Figure 1.3).

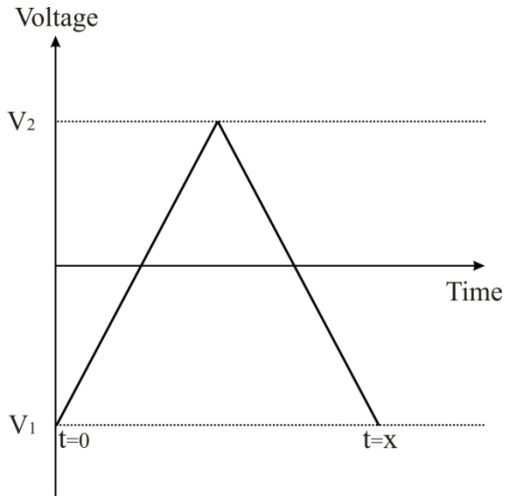

Figure 1.3: Voltage (potential) – time excitation signal utilised in cyclic voltammetric experiments.

Depending on the information sought, either single or multiple cycles can be performed. For the duration of the potential sweep, the potentiostat measures the resulting current that arises via the applied voltage (potential). The plot of current versus potential (voltage) is termed a 'cyclic voltammogram'. A cyclic voltammogram is complex and dependent on time along with many other physical and chemical properties. An illustration of a typical (reversible) redox couple is shown in Figure 4. Assuming only O, oxidised is present initially, a negative potential scan is selected for the first half-cycle, originating from a potential where no reduction transpires. As the applied potential advances towards the characteristic E^{o} for the redox process (unique to each process), the cathodic current increases until a peak is reached. Once the potential region (or window) in which the reduction process arises is traversed, the direction of the sweep potential is reversed. In this stage of the scan, R molecules (generated in the first phase of the sweep) that accumulate near the surface of the electrode; are re-oxidised back to O, resulting in an anodic (current) peak.[26]

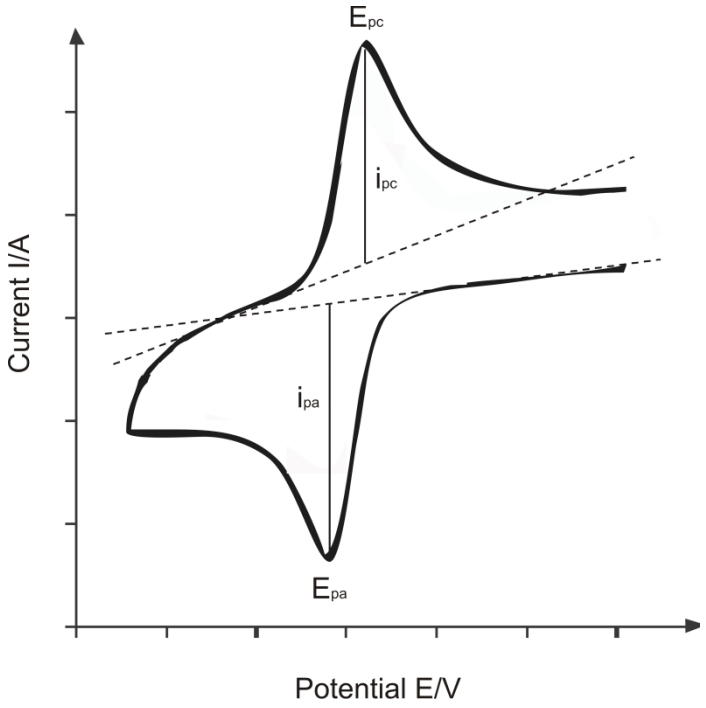

Figure 1.4: Typical cyclic voltammogram for a reversible redox process, where E_{pa} and E_{pc} correspond to the potential values at which the maximum anodic and cathodic peak currents (i_{pa} and i_{pc}, respectively) are recorded.

The characteristics of the peaks distinguished in a cyclic voltammetry attribute to diffusion layers that occur near the electrodes surface (see introduction). The resulting current peaks are thus reflections of the continuous change in the concentration gradient with time. Therefore, increased peak current can be attributed to the achievement of diffusion control, while the current drop (beyond the peak) exhibits a $t^{-1/2}$ dependence (independent of the applied voltage/potential). Thus the reversal current displays a similar shape to the forward reaction.

1.5 INTERPRETATING DATA

The cyclic voltammogram is characterised by several key parameters. The two peak currents (I_p) and peak potentials (E_p) (observed visually), provide the basis for the diagnostic analysis of the voltammetric response. (See Fig. 1.4)

The peak current for a reversible redox couple is given by the *Randles–Ševćik equation*:

$$I_p = 0.4463 \left(\frac{F^3}{RT}\right)^{1/2} n^{3/2} A D^{1/2} C v^{1/2} \qquad (1.5)$$

where I_p is the voltammetric peak current, F is the Faraday constant, A is the electrode area (in cm^2), D is the diffusion coefficient of the analyte (in $cm^2\ s^{-1}$), v is the applied scan rate (in $V\ s^{-1}$), C is the concentration of the electro-active species (in $mol\ cm^{-3}$) and n is the number of electrons transferred in the electrochemical process. Accordingly, the current is directly proportional to the concentration (useful for electroanalysis - see equation 1.10) and increases with the square root of the scan rate. The ratio of forward-to-reverse current peaks should be equivalent for a simple reversible couple. However, the peak ratios can be strongly affected by chemical reactions coupled with the redox system. Peak currents (or heights), are normally measured by extrapolating the preceding baseline current.

The position (or potential) of the peaks (E_p) is related to the standard potential of the redox process. The formal potential for a reversible system is centred between $E_{p,a}$ and $E_{p,c}$:

$$E^o = \frac{E_{p,a} + E_{p,c}}{2} \qquad (1.6)$$

The peak separation (at 298 K) is given by:

$$\Delta E_p = 2.218 \frac{RT}{F} \tag{1.7}$$

Accordingly, a fast one electron process should exhibit a ΔE_p of 57 mV at 298K. Note both peak potentials are independent of scan rate. For multiple electron transfer (reversible processes) the voltammogram will consist of several discrete peaks if the E^{o} values of the individual processes are consecutively higher and distinctly separated. When a redox reaction is slow, or coupled with a chemical reaction, the situation changes significantly. It is these 'non-ideal' processes that are frequently of greatest chemical interest, for which the diagnostic power of cyclic voltammetry is most useful.

For an irreversible system (those with slow electron exchange), the individual peaks are reduced in magnitude and widely separated. Totally irreversible systems are characterised by a shift in the peak potential (see Figure 1.5):

$$E_{\mathrm{P}} = E^{o} - \frac{RT}{\propto n'F}\left[0.78 - \ln(\frac{k^{o}}{D^{1/2}}) + \ln\left(\frac{\propto n'Fv}{RT}\right)^{1/2}\right] \tag{1.8}$$

where α is the transfer coefficient, v is the applied voltammetric scan rate and n' is the number of electrons involved in the charge-transfer step. As such, E_{P} occurs at potentials higher than E^{o}, with the over potential related to k^{o} (the electrochemical rate constant) and α; the voltammogram becomes increasingly 'drawn out' as αn decreased.

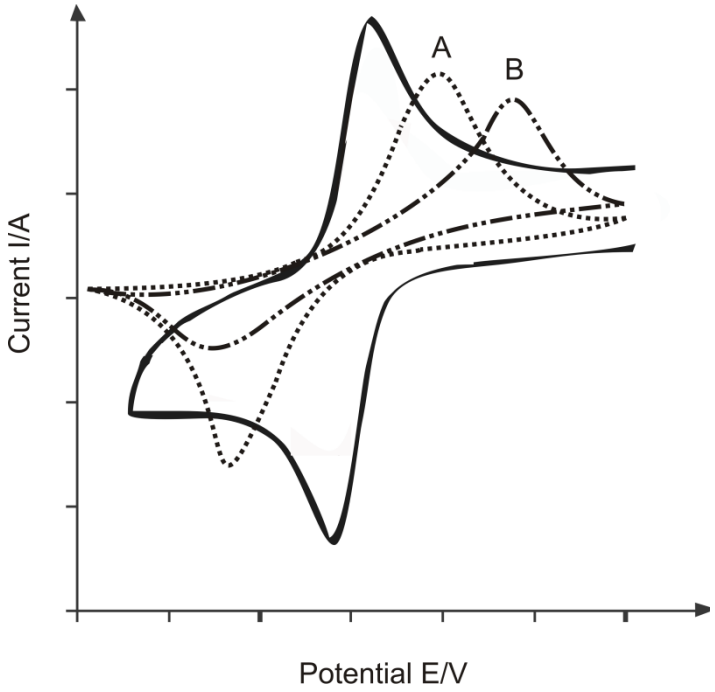

Figure 1.5: Examples of cyclic voltammograms for a quasi-reversible (curve A, dotted) and irreversible (curve B, dash-dot) redox processes. The solid line represents a typical cyclic voltammogram for a reversible redox process.

The peak current in this case (at standard conditions), given by:

$$i_p = (2.99\ x10^5)n(\alpha n_a)^{1/2}ACD^{1/2}v^{1/2} \qquad (1.9)$$

where n is the total number of electrons transferred and n' is the number of electrons involved in the charge-transfer step, D is the diffusion coefficient, α is the symmetry coefficient, n_a is the number of electrons in the rate determining step, C_0 is the bulk concentration of the analyte, A is the electrode area and v is the applied voltammetric sweep scan rate. Assuming a value of 0.5 for α, the reversible-to-irreversible current peak ratio is 1.27; thus the resulting peak current for the irreversible process is approximately 80% of that attained for the reversible system.

Quasi-reversible processes are controlled via both charge transfer and mass transport. The rate of the electron kinetics is measured via the electron chemical rate constant (k^o), whilst the rate of mass transport is measured by the mass transport coefficient:

$$m_T = \frac{D}{\delta} \tag{1.10}$$

Where δ is the diffusion layer thickness, and as discussed earlier, is dependent on time (t) according to:

$$\delta \sim \sqrt{6Dt}$$

$$t \sim \frac{RT}{Fv}$$

The distinction between fast and slow electrode kinetics relates to the dominant rate of mass transport given by:

$$k^o >> m_T \text{ (reversible)}$$

$$k^o << m_T \text{ (irreversible)}$$

The transition limits between a system that is reversible and irreversible can be defined through the parameter Λ, [27]:

$$\Lambda = \frac{k^o}{\left(\frac{FDv}{RT}\right)^{1/2}} \tag{1.11}$$

Three classifications of systems at stationary macroelectrodes (at 298 K, assuming $\alpha \sim 0.5$) are evident:

Reversible	$\Lambda \geq 15$	$\Lambda \geq 0.3v^{1/2}$ cm s^{-1}

Quasi-reversible	$15 > \Lambda > 10^{-3}$	$0.3v^{1/2} > k^{o} > 2 \times 10^{-5}\ v^{1/2}$ cm s^{-1}
Irreversible	$\Lambda \leq 10^{-3}$	$k^{o} \leq 2 \times 10^{-5}\ v^{1/2}$

These conditions show that reversible and irreversible behaviour observed for a given electrochemical rate constant is dependent on the applied scan rate. At sufficiently fast scan rates, at least in principle, all processes can appear electrochemically irreversible (Figure 1.6).

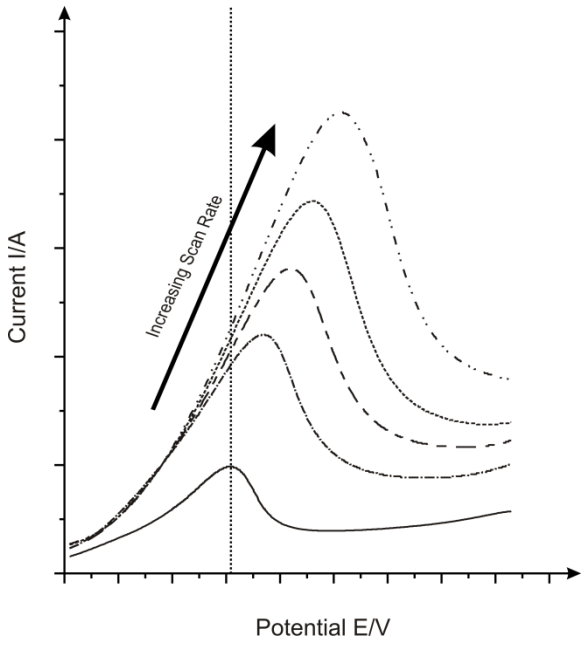

Figure 1.6: Example of shifting peak potentials with increased scan rates.

Cyclic voltammetry offers an indispensable tool for the determination of the experimental electrochemical rate constant. Numerical calculations developed by Nicholson[28] provide a basis for calculating the electrochemical rate constant (k^{o}) via the peak separation potential ($\Delta E_p = E_{p,a} - E_{p,c}$) observed during cyclic voltammetric analysis. This method relates k^{o} to the peak separation (ΔE_p) through the dimensional parameter ψ as described in the following equation:

$$\psi = \frac{\gamma k^{o}}{(\pi a D_{o})^{1/2}} \tag{1.12}$$

where $a = nF\nu/RT$, ν is the scan rate and $\gamma = \frac{D_O}{D_R}$, this represents the ratio of diffusion constants for the oxidized and reduced forms. Thus if $\gamma = 1$, the equation becomes;

$$\psi = \frac{k^o}{\left[\pi D_o \frac{nF\nu}{RT}\right]^{1/2}} \tag{1.13}$$

or

$$k^o = \psi \left[\pi D_o \frac{nF\nu}{RT}\right]^{1/2} \tag{1.14}$$

The equations above are applicable to peak separations between 61 and 212 mV, outside of these values the limits of the simulation software used to calculate these values are reached. ΔE_p values as a function of ψ. The shape of the voltammogram is a function of $k^o/\sqrt{\pi aD}$ (where $a = nF\nu/RT$). As $k^o/\sqrt{\pi aD}$ increases, the system approaches the reversible case. Small values of $k^o/\sqrt{\pi aD}$ (i.e. at rapid scan rates, ν) the system displays irreversible behaviour. Thus, voltammograms undergoing quasi-reversible behaviour are increasingly drawn out displaying larger peak separations compared to those found for a reversible system (see Figure 1.5).

In all cases, the detection limit is reported in this thesis is based upon the 3-sigma ($3\boldsymbol{\sigma}$) approach as reported by International Union Pure and Applied Chemistry (IUPAC). $3\boldsymbol{\sigma}$ refers to a theory of knowledge that gives rise to a methodology for prediction and for the ability to understand the present and foresee the coming outcome can be dramatically improved.

1.6 REFERENCES

1. J. P. Hart, S. A. Wring, *Anal. Chem.*, 1997, **16**, 89.
2. J. P. Hart, S. A. Wring, *Electroanalysis*, 1994, **6**, 617.
3. M. A. Sirvent, A. Merkoci, S. Alegret, *Sens. Actuators*, 2000, **69**, 153.
4. A. Morrin, A. J. Killard, M. R. Smyth, *Anal. Lett.*, 2003, **36**, 2021.
5. J. P. Metters, R. O. Kadara, C. E. Banks, *Analyst*, 2011, **136**, 1067.
6. K. C. Honeychurch, J. P. Hart, *Trends Anal. Chem.*, 2003, **22**, 456.
7. A. Heller, B. Feldman, *Chem. Rev.*, 2008, **108**, 2482.
8. J. D. Newman, A. P. F. Turner, *Biosens. Bioelectron.*, 2005, **20**, 2435.
9. R. Wilson, A. P. F. Turner, *Biosens. Bioelectron.*, 1992, **7**, 165.
10. K. Z. Brainina, *Anal. Chem.*, 2001, **56**, 303.
11. A. M. Gurban, L. Rotariu, M. Tudorache, C. Bala, T. Noguer, *Sensors for Environment, Health and Security*, 2009, **2**, 401.
12. A. O. Simm, C. E. Banks, R. G. Compton, *Electroanalysis*, 2005, **17**, 335.
13. R. O. Kadara, N. Jenkinson, C. E. Banks, *Sens. Actuators*, 2009, **137**, 556.
14. J. Wang, B. Tian, V. B. Nascimento, L. Angnes, *Electrochim. Acta*, 1998, **43**, 3459.
15. H. Kipphan, *Handbook of Print Media, Springer, Heidelberg*, 2011.
16. F. D. Barlow, A. Elshabini, *Ceramic Interconnect Technology Handbook, CRC Press, Florida*, 2007.
17. www.dropsens.com, Accessed Nov. 2010.
18. www.kanichi-research.com, Accessed Nov. 2010.
19. http://www.zensor.com.tw/, Accessed Nov. 2010.
20. M. Tudorache, C. Bala, *Bioanal. Chem.*, 2007, **388**, 565.
21. O. D. Renedo, M. Alonso-Lomillo, M. J. Arcos Martinez, *Talanta*, 2007, **73**, 202.
22. J. P. Hart, A. Crew, E. Crouch, K. C. Honeychurch, R. M. Pemberton, *Anal. Lett.*, 2004, **37**, 789.
23. J. D. Newman, A. P. F. Turner, *Essay in Biochem*, 1992, **27**, 147.
24. M. Albareda-Servent, A. Merkoci, S. Alegret, *Sens. Actuators*, 2000, **69**, 153.
25. M. Khairy, R. O. Kadara, D. K. Kampouris, C. E. Banks, *Anal. Methods*, 2010, **2**, 645.
26. J. Wang, *Analytical Electrochemistry 2nd Edition Wiley-VCH: New York*, 2001.
27. A. J. Bard, L. R. Faulkner, *Electrochemical Methods 2nd Edition; Wiley: New York*, 2001.
28. R. S. Nicholson, *Anal. Chem.*, 1965, **37**, 1351.

EXPERIMENTAL SECTION

All chemicals used were of analytical grade and were used as received without any further purification and were obtained from Sigma-Aldrich. All solutions were prepared with deionised water of resistivity not less than 18.2 MΩ cm. Voltammetric measurements were carried out using a Palmsens (Palm Instruments BV, The Netherlands) potentiostat. All measurements were conducted using a screen printed three electrode configuration consisting of a platinum geometric working electrode area of 3 mm diameter, carbon counter electrode and Ag/AgCl reference. Connectors for the efficient connection of the screen printed electrochemical sensors were purchased from Kanichi Research Services Ltd.[1] Screen-printed carbon electrodes were fabricated in-house with appropriate stencil designs using a microDEK 1760RS screen-printing machine (DEK, Weymouth, UK). A carbon–graphite ink formulation previously utilised[2] was first screen-printed onto a polyester flexible film (Autostat, 250 mm thickness). This layer was cured in a fan oven at 60 degrees for 30 minutes. Next a Ag/AgCl reference electrode was included by screen-printing Ag/AgCl paste (Gwent Electronic Materials Ltd, UK C2040308D2) onto the plastic substrate. Last a dielectric paste ink (Gwent Electronic Materials Ltd, UK D2070423D5) was printed to cover the connection and define the 3 mm diameter graphite working electrode. After curing at 60 degrees for 30 minutes the screen-printed electrode is ready to use. Finally a platinum polymer paste comprising dendritic platinum (83–87%) with particles sizes in the low micrometres range (Gwent Electronic Material Ltd, UK C2050804D9) was screen-printed on top of the carbon working electrode surface. Canal water was sampled at the edge of the canal bank (Rochdale Canal, Oxford Road, Manchester, UK) and collected in a polycarbonate bottle which was washed three times with canal water before being taken back to the laboratory. The sample was stored at room temperature and used within a day of sampling and was simply modified to pH 7 using a phosphate buffer before electroanalytical

measurements were commenced. Scanning electron microscope (SEM) images and surface element analysis were obtained with a JEOL JSM-5600LV model having an energy-dispersive X-ray microanalysis package. Electrodes were fabricated by a Banks group member (J. P. Metters).

All chemicals used were of analytical grade and were used as received without any further purification and were obtained from Sigma-Aldrich. All solutions were prepared with deionised water of resistivity not less than 18.2 MΩ cm.

Voltammetric measurements were carried out using a μ- Autolab III (ECO-Chemie, The Netherlands) potentiostat. All measurements were conducted using a screen-printed three electrode configuration with a geometric working electrode area of 3 mm diameter, with an SCE being used rather than the printed Ag/AgCl reference. Connectors for the efficient connection of the screen printed electrochemical sensors were purchased from Kanichi Research Services Ltd.

Screen-printed carbon electrodes were fabricated in-house with appropriate stencil designs using a microDEK 1760RS screen-printing machine (DEK, Weymouth, UK). A carbon–graphite ink formulation previously utilised[2] was first screen printed onto a polyester flexible film (Autostat, 250 μm thickness). This layer was cured in a fan oven at 60 degrees for 30 minutes. Next a silver/silver chloride reference electrode was included by screen-printing Ag/AgCl paste (Gwent Electronic Materials Ltd, UK C2040308D2) onto the plastic substrate. Last a dielectric paste ink (Gwent Electronic Materials Ltd, UK D2070423D5) was printed to cover the connection and define the 3 mm diameter graphite working electrode. After curing at 60 degrees for 30 minutes the screen-printed electrode is ready to use. Finally to construct the PdSPE a palladium polymer paste consisting of a mixture of powder and dendritic palladium with particles size in the range of low micrometers (67 – 68 % palladium content) (Gwent Electronic Material Ltd, UK, C2031105D2) working electrode was printed on top of

the carbon working electrode surface and once more cured in a fan oven at 60 degrees for 30 minutes.

Scanning electron microscope (SEM) images and surface element analysis were obtained with a JEOL JSM-5600LV model having an energy-dispersive X-ray microanalysis package. Electrodes were fabricated by Banks group member (J. P. Metters).

All chemicals used were of analytical grade and were used as received without any further purification and were obtained from Sigma-Aldrich. All solutions were prepared with deionised water of resistivity not less than 18.2 MΩ cm. Voltammetric measurements were carried out using a Palmsens (Palm Instruments BV, The Netherlands) potentiostat. All measurements were conducted using a screen-printed three electrode configuration consisting of a carbon–graphite geometric working electrode area of 250 μm radii; both the carbon disc-shaped and platinum disc-shaped shallow recessed screen-printed electrodes (denoted throughout as drSPE/PtdrSPE respectively) or 50 μm in width with respect to the pentagon-shaped shallow recessed screen printed electrode (denoted throughout as prSPE), carbon–graphite counter electrode and Ag/AgCl reference. Screen-printed recessed electrodes were fabricated in-house with appropriate stencil designs using a microDEK 1760RS screen-printing machine (DEK, Weymouth, UK). A carbon–graphite ink formulation (Gwent Electronic Materials, UK C2000802P2) was first screen-printed onto a polyester flexible film (Autostat, 250 micron thickness). This layer was cured in a fan oven at 60 degrees for 30 minutes. Next a silver/silver chloride reference electrode was included by screen-printing Ag/AgCl paste (Gwent Electronic Materials Ltd, UK C2040308D2) onto the plastic substrate. Last a dielectric paste ink (Gwent Electronic Materials Ltd, UK D2070423D5) was printed to cover the connection and define the carbon–graphite working electrode, and the resultant recessed surface. After curing at 60 degrees for 30 minutes the screen-printed electrode is ready to use. The PtdrSPE were made in the same fashion using a platinum polymer paste

comprising dendritic platinum (83–87%) with particles sizes in the low micrometers range (Gwent Electronic Material Ltd, UK C2050804D9) in place of the previously utilised carbon–graphite ink formulation. Canal water was sampled at the edge of the canal bank (Rochdale Canal, Oxford Road, Manchester, UK) and collected in a polycarbonate bottle which was washed three times with canal water before being taken back to the laboratory. The sample was stored at room temperature and used within a day of sampling and was simply modified to pH 7 using a phosphate buffer before electroanalytical measurements were commenced. Scanning electron microscope (SEM) images and surface element analysis were obtained with a JEOL JSM-5600LV model having an energy-dispersive X-ray microanalysis package. Electrodes are fabricated by a Banks group member (J. P. Metters).

All chemicals used were of analytical grade and were used as received without any further purification and were obtained from Sigma-Aldrich. All solutions were prepared with deionised water of resistivity not less than 18.2 MΩ cm. Voltammetric measurements were carried out using a Palmsens (Palm Instruments BV, The Netherlands) potentiostat.

The screen-printed microelectrode arrays electrodes were fabricated in-house with appropriate stencil designs using a microDEK 1760RS screen-printing machine (DEK, Weymouth, UK). A carbon-graphite ink formulation (Gwent Electronic Materials, UK C2000802P2) was first screen-printed onto a polyester flexible film (Autostat, 250 micron thickness). This layer was cured in a fan oven at 60 degrees for 30 minutes. Next a silver/silver chloride reference electrode was included by screen-printing Ag/AgCl paste (Gwent Electronic Materials Ltd, UK C2040308D2) onto the plastic substrate. Last a dielectric paste ink (Gwent Electronic Materials Ltd, UK D2070423D5) was printed to cover the connection and define the carbon-graphite working electrode, and the resultant recessed surface. After curing at 60 degrees for 30 minutes the screen printed microelectrode array is ready to use. The gold screen-printed microelectrode array was made in the same fashion

using a gold polymer paste comprising dendritic gold (83-87%) with particles sizes in the low micrometers range (Gwent Electronic Material Ltd, UK C2041206P2) which has previously been reported upon within the literature[3] in place of the previously utilised carbon-graphite ink formulation. Figure 5.1 are optical and scanning electron microscope images showing the configuration of the screen-printed microelectrode array. All measurements were conducted using the screen-printed microelectrode array configuration which comprises 6 carbon-graphite geometric working electrodes with radii of 50 μm separated by an average of 2272 (± 0.3) μm arranged in a circular configuration around a common carbon-graphite counter and a Ag/AgCl reference electrode.

Canal water was sampled at the edge of the canal bank (Rochdale Canal, Oxford Road, Manchester, UK) and collected in a polycarbonate bottle which was washed three times with canal water before being taken back to the laboratory. The sample was stored at room temperature and used within a day of sampling and was simply acidified with H_2SO_4 to a concentration of 0.05 M before electroanalytical measurements were commenced.

Scanning electron microscope (SEM) images and surface element analysis were obtained with a JEOL JSM-5600LV model having an energy-dispersive X-ray microanalysis package. Electrodes are fabricated by a Banks group member (J. P. Metters).

References

1. http://kanichi-research.com, Accessed November 2011.
2. P. M. Hallam, D. K. Kampouris, R. O. Kadara, C. E. Banks, *Analyst*, 2010, **135**, 1947.
3. J. P. Metters, R. O. Kadara, C. E. Banks, *Analyst*, 2012, **137**, 896.

CHAPTER 2

PLATINUM SCREEN PRINTED ELECTRODES FOR THE ELECTROANALYTICAL SENSING OF HYDRAZINE AND HYDROGEN PEROXIDE.

2.1 Abstract

In this chapter, the fabrication of platinum screen printed macro electrodes are reported which are electrochemically characterised and evaluated as to their potential analytical application towards the sensing of hydrazine and hydrogen peroxide. In the case of hydrazine a linear range of 50 to 500 µM is possible with a limit of detection (3σ) of 0.15 µM achievable using cyclic voltammetry which can be reduced to 0.12 µM using chronoamperometry. The novelty of these platinum screen printed electrodes is highlighted in that the platinum on the screen printed electrode surface resides as an oxide, which is favourable for the electrochemical oxidation of hydrazine, which needs to be formed *via* extensive potential cycling when using a traditional platinum electrode hence the platinum screen printed sensors alleviate these requirements. The electroanalytical reduction of hydrogen peroxide is shown to be feasible with a linear range over 100 and 1000 µM with a limit of detection (3σ) of 0.14 µM which is competitive with other reported analytical protocols.

2.2 Introduction

The transition from the electrochemical development systems into the field is a perilous journey. One tried and tested approach for electro-analytical based sensors is through the use of screen-printed electrodes which has helped the implementation of electrochemical biosensors for the sensing of glucose in blood used globally by diabetics.[1] The technique of screen printing is a well-established process producing disposable and cost effective electrodes that can be utilised in electrochemical sensors and biosensors with many academic research groups and industrial enterprises producing new and advantageous electrode configurations.[2] The most commonly utilised screen printed electrodes are constructed of graphite where a commercially purchased ink consisting of graphite and carbon black particles with a polymeric binder and solvents are screen printed onto a suitable substrate which is then cured at a suitable temperature.[2, 3] Many advantageous geometric designs have been reported[2] and new electrodes of different compositions have been produced such as graphite electrodes consisting of Prussian Blue[4, 5] and Cobalt Phthalocyanine[6] mediators utilised in biosensors, metal oxides,[7-13] carbon nanotubes[14, 15] modified screen printed electrodes and gold[16-18] and silver[16] nanoparticles modified electrodes fabricated via electrochemical formation. Similarly other screen printed electrodes comprising entirely gold have been reported.[19-35] It is important to note that in these configurations the whole geometric working electrode comprises the noble metal rather than being modified later. Recently we have reported the fabrication of gold screen printed electrodes applied towards the sensing of highly toxic chromium (VI)[36] and biologically important chromium (III)[37] has been reported highlighting the facile reduction and oxidation of each analyte respectively. Interestingly in the electro-analytical sensing of chromium (VI), gold oxide surfaces are highly desired and typically gold electrodes need to be potential cycled to induce the formation of gold oxide[16, 38] but in the case of the gold screen printed electrodes, this

requirement is alleviated due to the gold electrode surface consisting of predominantly gold oxide without recourse to a pre-treatment. The economical use of the noble metal also acts to ensure that a low cost sensor is feasible without the sensitivity of the electrode being compromised. With the ultimate objective of a screen printed sensor being to ensure facile monitoring of key analytes, such developments which ensure to keep pre-treatments such as potential cycling to a minimum are of great interest! Surprisingly there are very few literature reports concerning the fabrication of platinum screen printed electrodes;[5, 39, 40] consequently in this thesis, the fabrication and characterisation of platinum screen-printed electrodes is presented and their response towards the important target analytes hydrazine and hydrogen peroxide is critically evaluated. Note that hydrazine is an increasingly important industrial molecule utilised within rocket fuel and missile systems and corrosive inhibitors, in addition to the ever expanding fuel cell development.[41, 42] The need for facile detection of hydrazine is further compounded with the knowledge that it is a neurotoxin and molecule which is found to have carcinogenic and mutagenic effects.[42, 43] Reports have detailed the sensing of hydrazine including methods based on flow injection analysis (FIA),[44, 45] ion chromatography,[46] chemiluminescence (CL) and various types of spectroscopy.[47-49] However, the processes involved in many of these methods are extremely complex, and the linear ranges are relatively narrow and have low precision. Fortunately, electrochemical techniques offer the opportunity for portable, cheap and rapid methodologies. Platinum is one such electrode which has been successfully utilised for the sensing of hydrazine, offering faster electrode kinetics over that of the traditional, more sluggish carbon based electrodes. Drawbacks to the use of a traditional platinum electrode evidently centre on the expense and uneconomical nature of such materials. Similarly hydrogen peroxide is of importance, acting as a common intermediate in both environmental and biological systems and is a product of the oxidation of glucose by Glucose oxidase.[50] As such the investigation of its detection is of

interest and has had substantial attention, with the application of various techniques such as chemiluminescence,[51] oxidimetry[52] and electrochemistry.[53-55] Although a handful of studies describing the fabrication and application of platinum screen printed electrodes have been reported, this is the first instance in which a platinum screen printed electrode is evaluated towards the sensing of hydrazine and hydrogen peroxide. The novelty of this approach is also highlighted by the fact that the electrode requires no prior pre-treatment in the form of potential cycling. Within the present study the electrochemical detection of both hydrazine and hydrogen peroxide in neutral conditions are studied through the novel application of platinum screen printed electrodes.

2.3 Results and discussion

Characterisation of the platinum screen printed electrodes

Platinum screen printed electrodes (denoted throughout as PtSPE) were fabricated as detailed in the Experimental section with a working electrode consisting of platinum ink screen printed onto an underlying graphite based screen printed electrode. Note that in this case, the expensive platinum material is parsimoniously utilised but it could be the case that the connecting legs are constructed of the same platinum material as could the counter electrode if so desired. Fig. 2.1A depicts SEM characterisation of the PtSPE revealing a non-uniform surface which consists of platinum microparticles held together with a polymeric formulation. Energy-dispersive X-ray (EDAX) analysis (see Fig. 2.1B image) was conducted on the PtSPE revealing the surface to consist of 4.00% oxygen, 8.15% carbon and 87.85% platinum. This individually determined amount of platinum is consistent with the specifications of the commercially purchased original ink formulation (see Experimental section). Note that the oxygen content arises due to the platinum being in an oxide formation and likely the carbon and oxygen content arises due to the use of a polymeric binder in the ink formulation.

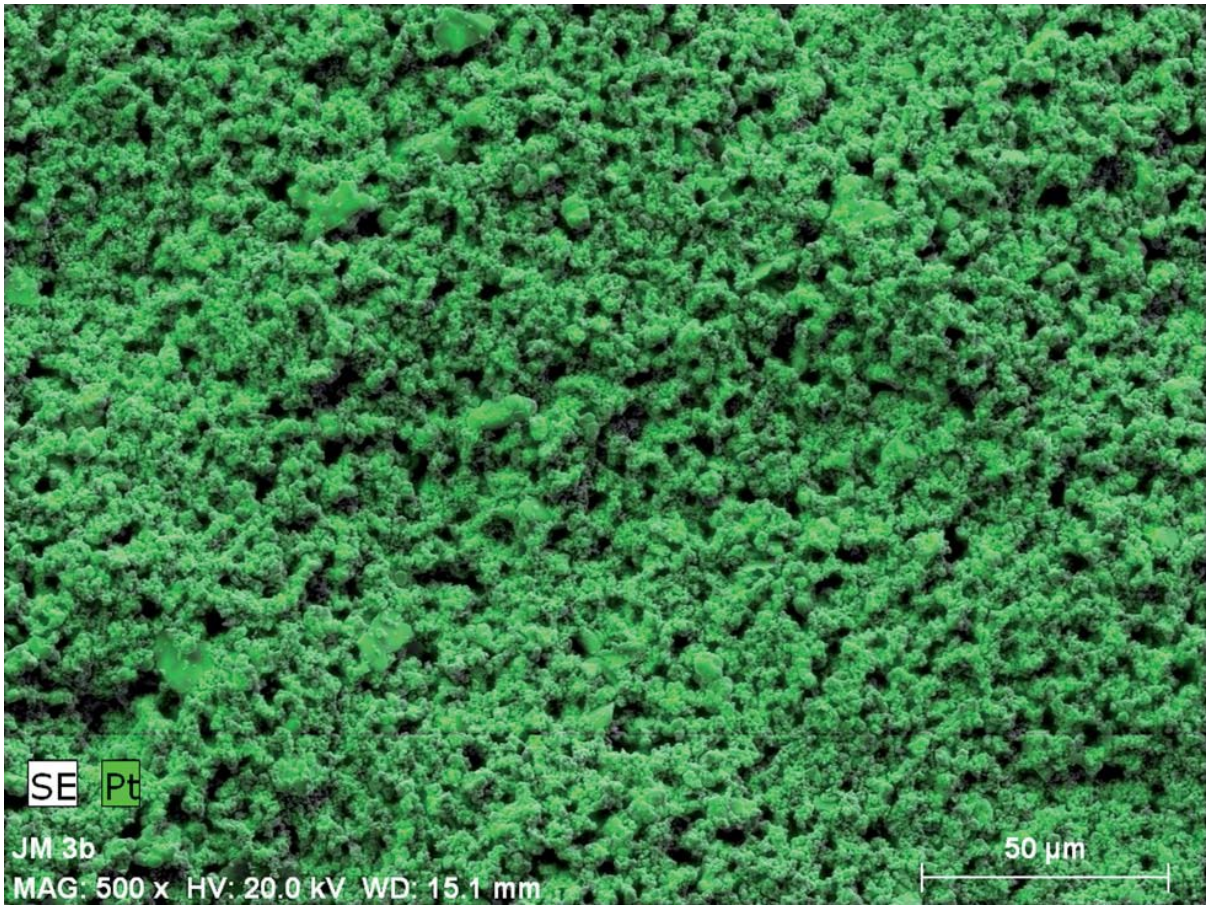

Figure 2.1A: Typical SEM image of the platinum screen printed electrode.

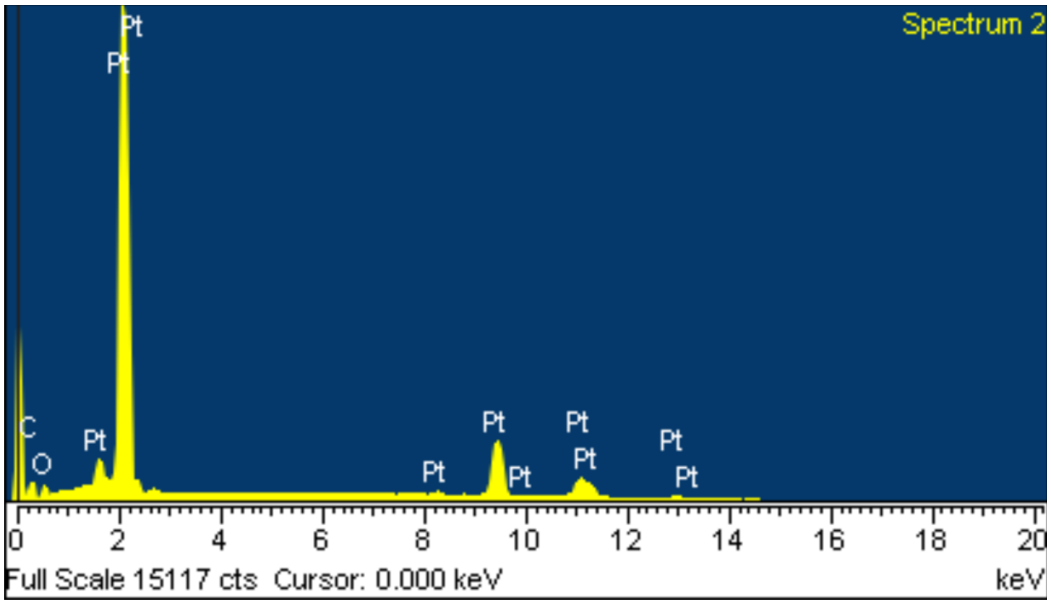

Figure 2.1B: EDAX analysis of the platinum screen printed electrode.

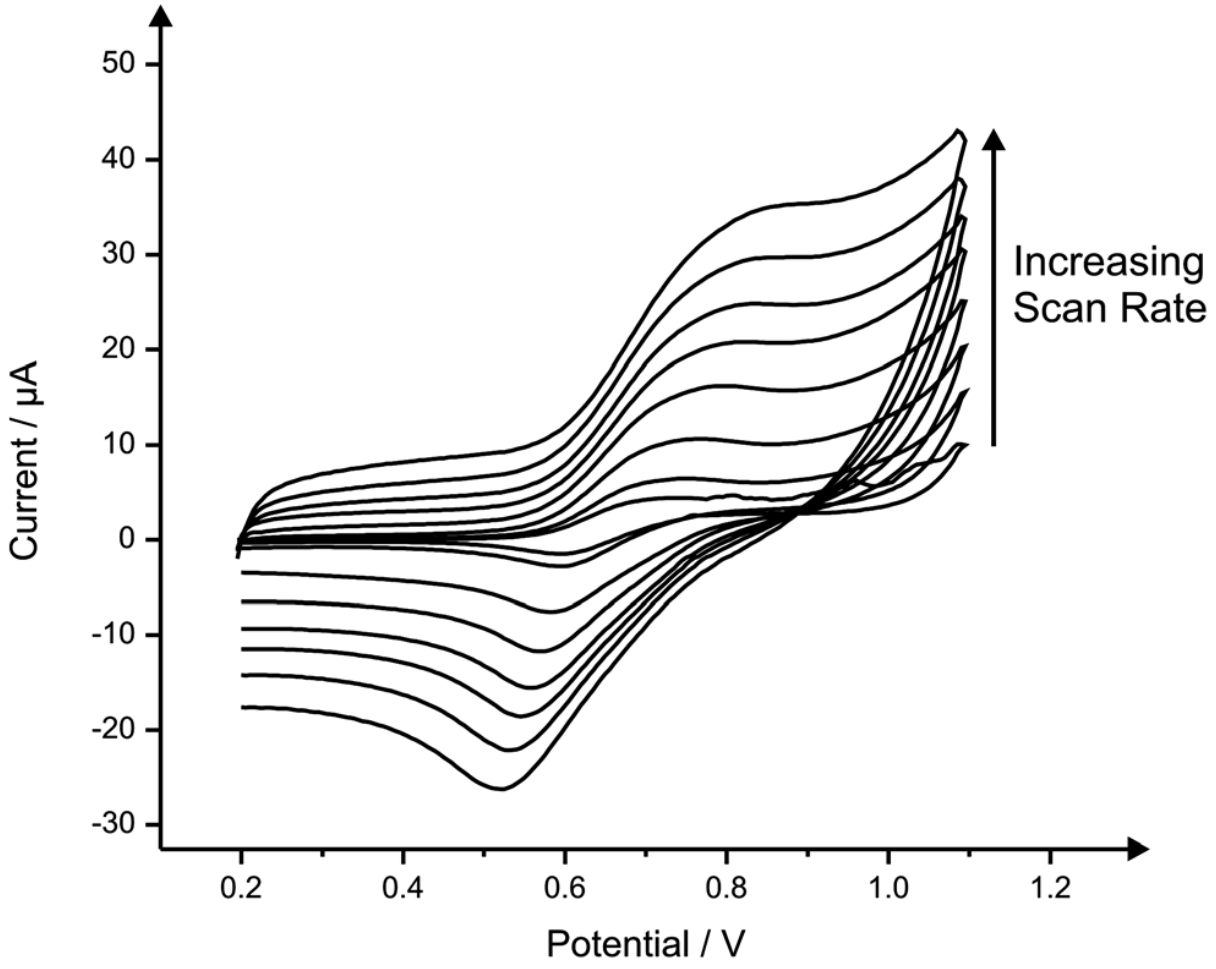

Figure 2.2: Electrochemical oxidation and reduction of 1 mM potassium hexachloroiridate in 0.1 M KCl using the PtSPEs recorded over the scan rate range of 5 to 200 mV s^{-1} (vs. Ag/AgCl).

The PtSPEs were first electrochemically characterised using the redox probe potassium hexachloroiridate. Firstly, scan rate studies were performed using the PtSPE in 1 mM potassium hexachloroiridate with 0.1M KCl (see Fig. 2.2), where observation of voltammetric peak height, plotted as peak current (I_P) against square root of the applied scan rate over the range 5-200 mV s^{-1} was found to be linear (I_p (µA) = 49.96 µA/ (µM) + 1.14 µA) confirming a diffusional process. The electron transfer rate constant, k^0, for the process was determined using the Nicholson method;[56] using a literature diffusion coefficient value of 8.3 × 10^{-6} cm^2 s^{-1} (reported in 0.2 M KCl)[57] the electron transfer rate constant was estimated to correspond to 1.4 × 10^{-3} cm s^{-1}. Such a value is relative to the rate of mass transport to the

electrode surface and using the analysis of Matsuda and Ayabe,[58] the transition between reversible and irreversible limits in terms of electron transfer can be determined by the parameter, Ψ, defined by:

$$\Psi = k^0/(FDv/RT)^{1/2} \quad (2.1)$$

where the reversible range is $\Psi \geq 15$ and quasi-reversible $15 > \Psi > 10^{-3}$. Using the electron transfer rate constant deduced (see above) along with the literature diffusion coefficient for potassium hexachloroiridate (IV), we find in our experimental case, over the range of scan rates employed, that overall the electrochemical process can be described as quasi-reversible. The electro-active area of the PtSPE can be estimated from the Equation 2.2 for quasi-reversible electrochemical processes:[3]

$$i_p = (2.99\ x10^5)n(\alpha n_a)^{1/2}ACD^{1/2}v^{1/2} \quad (2.2)$$

where n is total number of electrons transferred in the electrochemical process, D is the diffusion coefficient, α is the symmetry coefficient, n_a is the number of electrons in the rate determining step, C_0 is the bulk concentration of the analyte, A is the electrode area and v is the applied voltammetric sweep scan rate. The electrode area was consequently estimated to be 0.1 cm^2 compared to a geometric area of 0.071 cm^2; this response suggests that the platinum electrode surface is slightly porous in agreement with SEM images (see Fig. 2.1A) but is not substantially so porous that thin layer voltammetric behaviour is observed. The PtSPE electrode was also explored in 0.1 M H_2SO_4, and as shown in ESI, Fig. 2.1B, in the anodic scan, a single peak is observed at ~ -0.3 V (vs. Ag/AgCl) with a further peak seen in

the cathodic scan, which appeared at ~ -0.17 V (vs. Ag/AgCl) which can be likely attributed to the adsorption and desorption of hydrogen as observed on polycrystalline platinum surfaces. [59, 60]

Electroanalytical sensing of hydrazine

Following the characterisation of the novel platinum based sensors, their application towards the detection of the important analyte, hydrazine was trialed. Initial cyclic voltammetric measurements for the sensing of hydrazine were obtained, as shown in Fig. 2.3, where an oxidation wave corresponding to the electrochemical oxidation of hydrazine in a phosphate buffer of pH 7 was evident at a potential of +0.7 V (vs. Ag/AgCl). A reduction wave can also be observed at ~ -0.25 V (vs. Ag/AgCl), presumed to be the reduction of the oxide based platinum present within the electrode. Additions of hydrazine into the pH 7 PBS were made where the magnitude of the voltammetric peak height is observed to grow with increasing additions, as shown in Fig. 2.3. Analysis of these voltammetric profiles are presented in Fig. 2.4 where a plot of the voltammetric peak height (oxidation) versus hydrazine concentration which is seen to demonstrate linearity over the entire concentration range of 50 to 500 μM (I_p *(μA) = 0.1 μA/(μM) + 3 μA N =10*). A limit of detection (3σ) was found to correspond to 0.15 μM. The use of chronoamperometry was explored where the potential was held at a value of + 0.5 V (vs. Ag/AgCl), selected due to the observed oxidation potential of hydrazine at the PtSPE through earlier cyclic voltammetric analysis, for a period of 120 s in a phosphate buffer of ~pH 7 with additions of hydrazine being made. Fig. 2.5 demonstrates a calibration plot *(I_p (μA) = 0.02 μA/ (μM) + 0.7 μA N=8)* obtained using the PtSPE using chronoamperometric techniques, which highlights the ability of the electrochemical technique, combined with the novel PtSPE to facilitate improved sensitivity and detection of hydrazine with measurements within the concentration range 50 to 500 μM and a detection limit (3σ) calculated to be 0.12 μM.

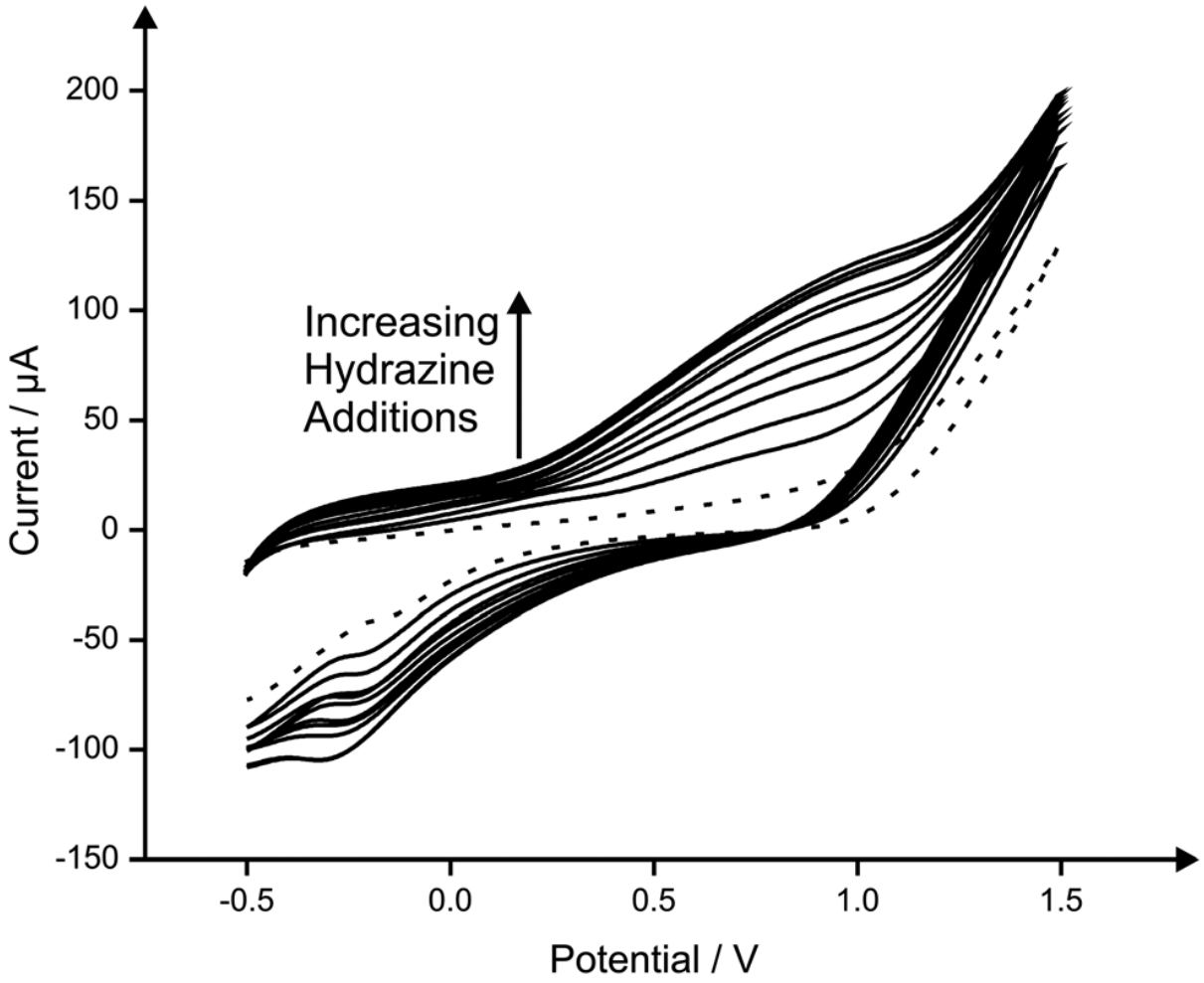

Figure 2.3: Typical cyclic voltammetric responses resulting from additions of hydrazine into a phosphate buffer using the PtSPE. Scan rate: 50 mV s^{-1}.

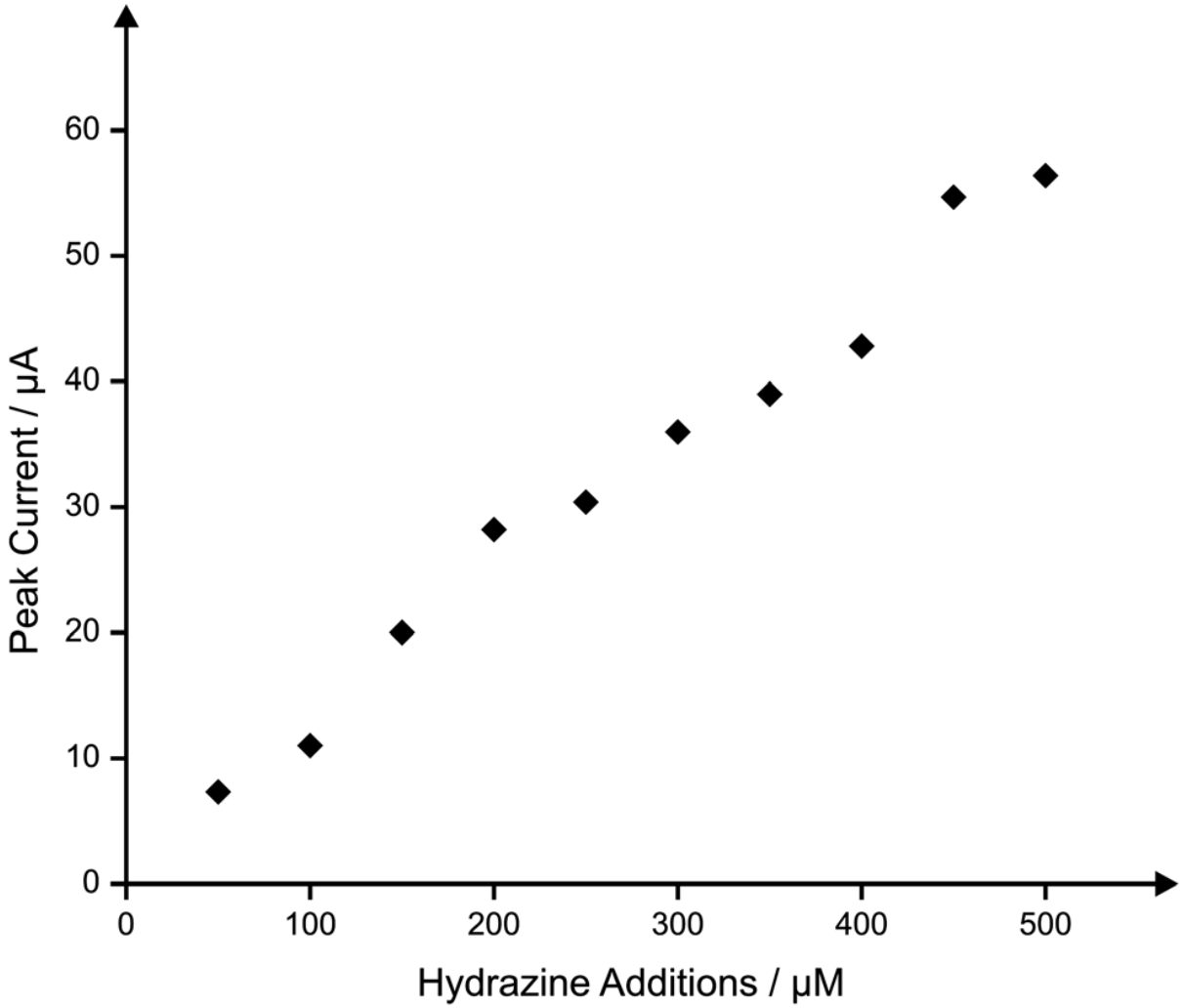

Figure 2.4: A typical calibration plot resulting from additions of hydrazine into a phosphate buffer over the range of 50 to 500 µM using the PtSPE as shown in Fig. 2.1.

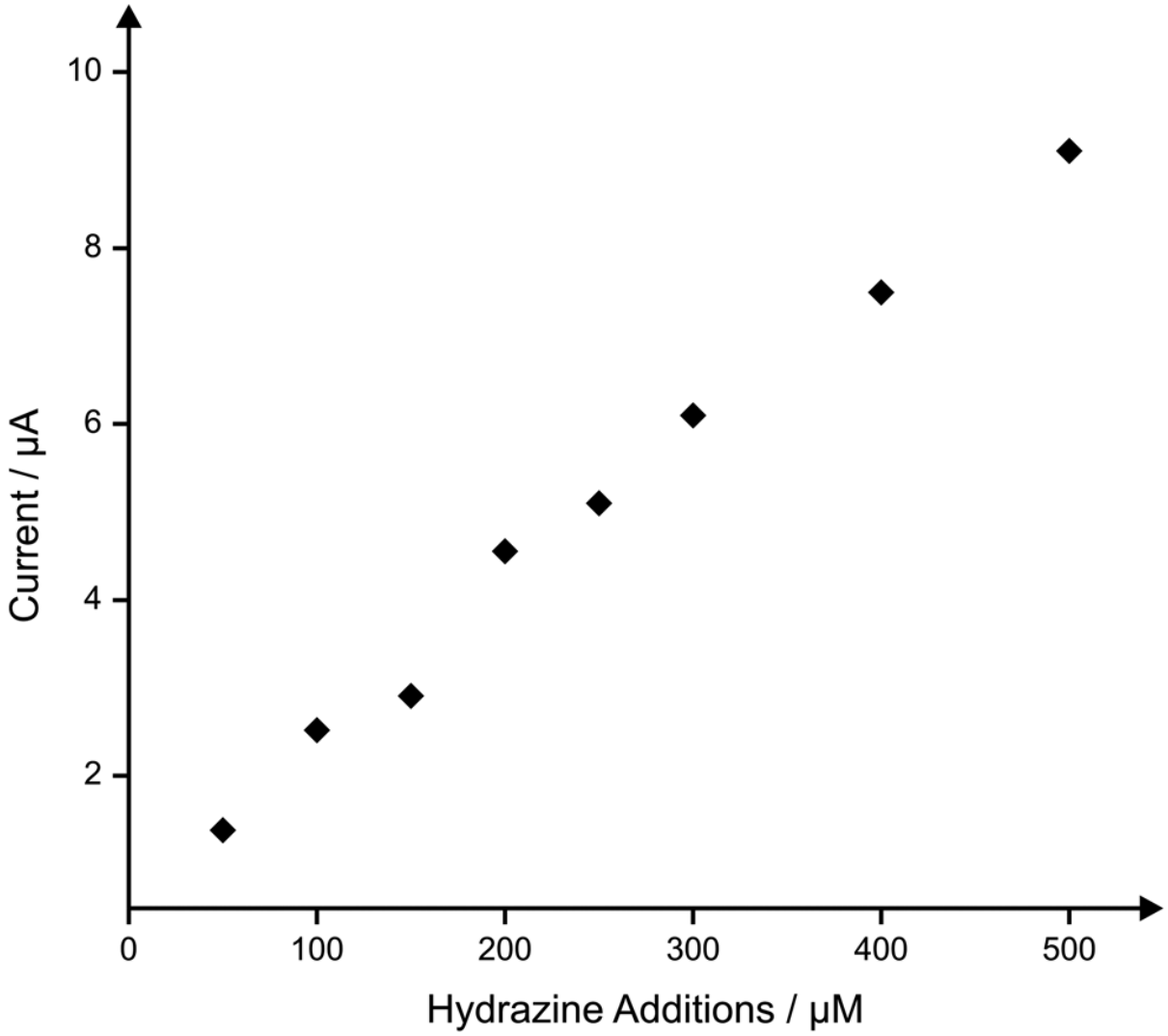

Figure 2.5: Typical chronoamperometric measurements resulting from the electrochemical oxidation of hydrazine in a phosphate buffer using a PtSPE over the range of 50 to 500 µM. Measurements were taken at a potential of 0.5 V.

In an attempt to test the applicability of the PtSPE towards the detection of hydrazine in a true sample, additions of hydrazine were made into a sample of canal water (sourced and pre-treated as reported in the Experimental section). Low level additions of hydrazine (over the range 50 to 500 µM) were made into the sample of canal water as depicted in Fig. 2.6 through a plot of peak height (µA) vs. hydrazine concentration. Though there is an apparent reduction in the sensitivity of the PtSPE towards the detection of hydrazine within canal water when compared with that in 'ideal' conditions, likely due to interferents within the

sample, it is clearly evident that the proposed PtSPE is still viable in such a potentially complex sample media.

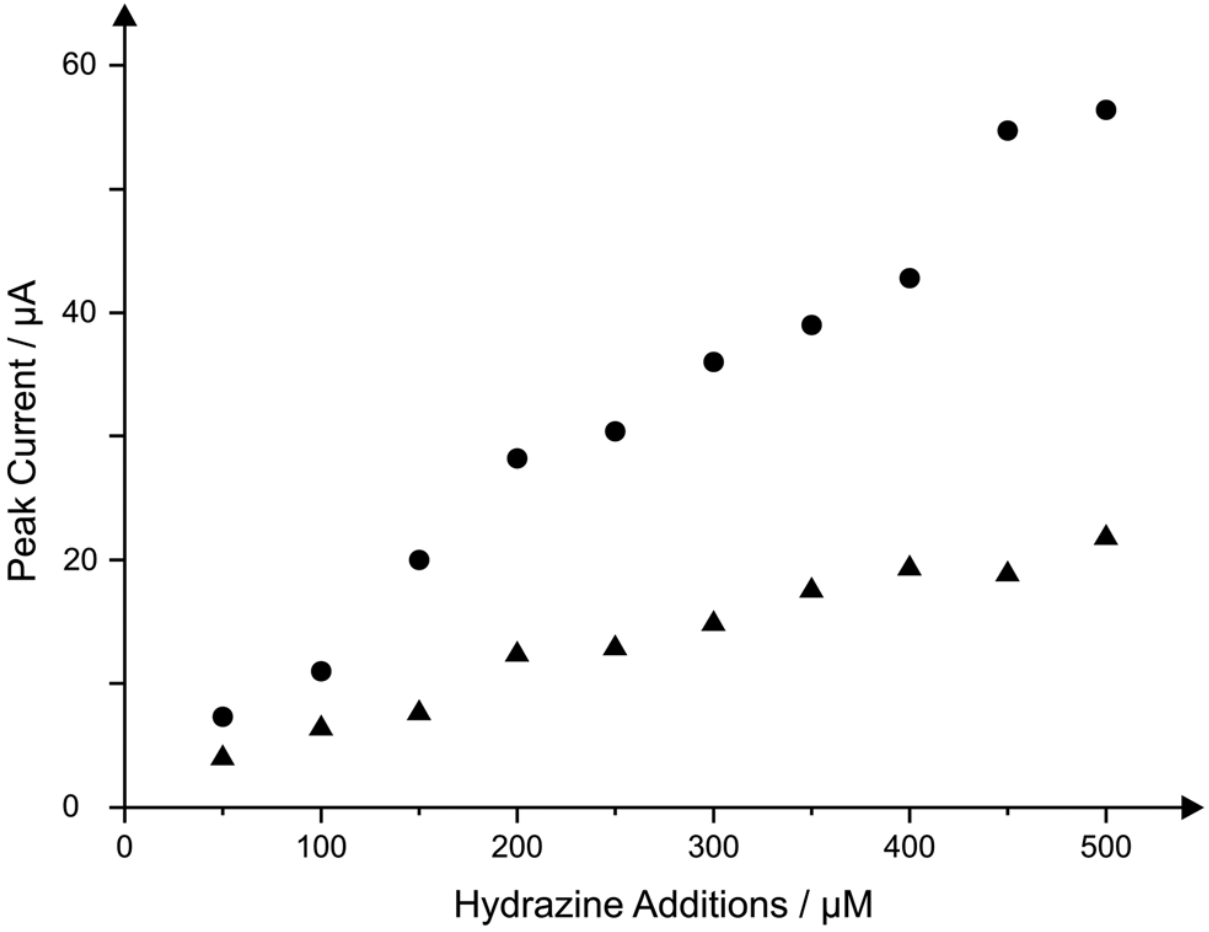

Figure 2.6: An overlay of typical responses through addition of hydrazine in 'ideal' conditions (phosphate buffer solution) (circles) and in to a canal water sample (triangles) over the range of 50 to 500 µM. Scan rate: 50 mV s^{-1}.

Both analytical responses using cyclic voltammetry and chronoamperometry are found to be competitive to previous studies relating to hydrazine such as that by Compton *et al*.[61] who report upon the sensing of hydrazine using iron (III) oxide graphite composite electrodes which is shown to boast a detection limit of 1.18 µM hydrazine; close to that determined at the PtSPE, though as with many traditional electrodes, there was a requirement for polishing between measurements. Similarly a traditional gold electrode modified through the application of an iron phthalocyanine film has been utilised for the sensing of hydrazine and

although admirable detection limits of 11 μM for hydrazine are determined extensive preparatory steps are seen to be required in order to form the electrocatalytic film upon the gold surface.[62] A low limit of detection of 1 μM was reported by Nakagaki *et al*.[49] using a carbon paste electrode modified with copper porphyrin with linearity observed over the range 5–60 μM hydrazine. Though such low operation detection (5 μM) and limits of detection are desirable, electrode preparation is in this case, somewhat of a drawback due to the extensive fabrication procedures, though the easily renewable surface offered by a paste electrode is undoubtedly an advantage of the methodology.[49] A highly novel approach towards the sensing of hydrazine was reported by Wang and co-workers,[63] with double stranded DNA being applied to a carbon paste electrode enabling part-per-billion hydrazine level detection. Though the ingenuity of the sensor and reported detection limits cannot be called in to question, as with previous studies, the requirement for modification of the electrode is an undeniable drawback, as is the requirement for reaction time waiting periods of up to 10 minutes.[63] An interesting study by Batchelor-McAuley and colleagues[64] provides a comparison between the use of palladium nanoparticle modified boron-doped diamond electrode and a palladium plated boron-doped diamond microdisc array with the nanoparticle modified electrode providing a detection limit for hydrazine of 2.6 μM and the array enhancing the detection with a low limit of detection of 1.8 μM. Although each of the studies discussed allow for the sensing of hydrazine at low μM concentrations, as is found being the case when utilising the PtSPE, many also require extensive preparatory stages or pre-treatments prior to use. Such requirements are negated through the use of the PtSPE, which is also not found to compromise the low detection limits. Interestingly, the PtSPE has an inherent advantage over that of platinum microelectrodes, where Aldous and Compton[65, 66] demonstrate that variable results can be achieved which is greatly dependant on the history of the electrode with optimal results observed at oxidised platinum surfaces; extensive

pretreatment in the form of potential cycling[65, 66] needs to be applied to ensure generation of the platinum oxide but in our case, such a step is negated since the platinum is in the form of an oxide upon the screen printed surface greatly simplifying the analytical protocol. To further test the potential utilisation of the PtSPEs towards the sensing of analytes of great interest, the sensing of the biologically important analyte, hydrogen peroxide was next pursued.

Electroanalytical sensing of Hydrogen Peroxide

First the applicability of the PtSPE was explored through cyclic voltammetric measurement in a phosphate buffer of ~pH 7 with additions of hydrogen peroxide. Fig. 2.7 highlights the successful reduction of hydrogen peroxide at ~+0.35 V (vs. Ag/AgCl) which is seen, as demonstrated through the corresponding calibration plot (Fig. 2.7, inset) to be concentration dependant and linear over the range 100 to 1000 μM *(I_p (μA) = -0.0217 μA/ (μM) - 1.3746 μA, R^2 = 0.95, N= 10)*; a limit of detection (3σ) was calculated to correspond to 0.24 μM. A redox peak couple can also be observed at ~-0.1 and 0 V (vs. Ag/AgCl) for the reduction and oxidation of the platinum species present within the PtSPE respectively.

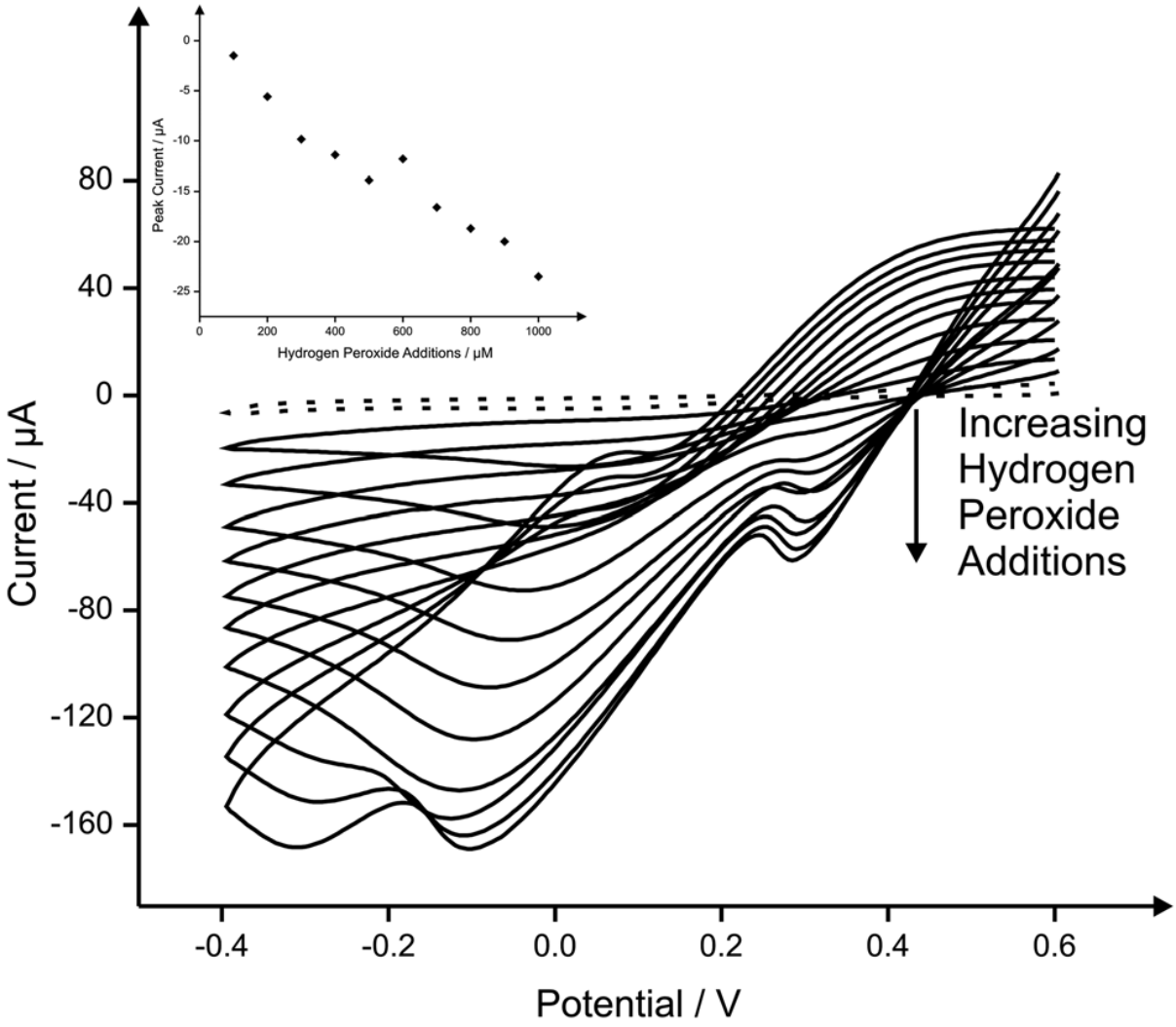

Figure 2.7: Typical cyclic voltammetric responses resulting from additions of hydrogen peroxide into a phosphate buffer using the PtSPE. Scan rate: 50 mV s^{-1}. Inset: the corresponding calibration plot over the range 100 to 1000 mM hydrogen peroxide using the peak at +0.35 V.

Note that the majority of electrochemical methods report the electrochemical oxidation of hydrogen peroxide at relatively high positive potentials which can also oxidise other substances leading to interfering currents.[67, 68] The reproducibility of the PtSPE towards hydrogen peroxide was explored with a fixed concentration of 200 µM with the peak current found to exhibit a % RSD of 4.5 (N = 4). Attention was turned towards exploring the chronoamperometric measurements for the reduction of hydrogen peroxide with the potential of the electrode being maintained at + 0.35 V (vs. Ag/AgCl) for a period of 120 seconds, with

additions of hydrogen peroxide being made as shown in Fig. 2.8. A corresponding plot of hydrogen peroxide concentration versus final current (Fig. 2.7, inset) demonstrates good linearity over the entire analytical range of 100 to 1000 μM hydrogen peroxide *(I_p (μA) = -0.005 μA/(μM) -5.40 μA, R^2 = 0.96, N=10)*, with a detection limit (3σ) found to correspond to 0.14 μM, improving on that obtained, as discussed earlier, using purely cyclic voltammetric measurements. Previous reports on the detection of hydrogen peroxide have included the use of; cobalt (II) hexacyoferrate modified glassy carbon electrode,[69] sol–gel modified glassy carbon and aluminium electrode modified with manganese hexacyanoferrate[70] allowing a detection limits of 0.06 μM, 0.5 μM and 0.2 μM respectively. Clearly the response of the PtSPE is competitive suggesting its analytical utility. As discussed in relation to the sensing of hydrazine, other electrode configurations allow for a lower limit of detection for hydrogen peroxide than that determined at a PtSPE, though none are found to offer the stability, lack of pre-treatment (in the form of techniques such as potential cycling or chemical treatment) and ease of use facilitated through the PtSPE.

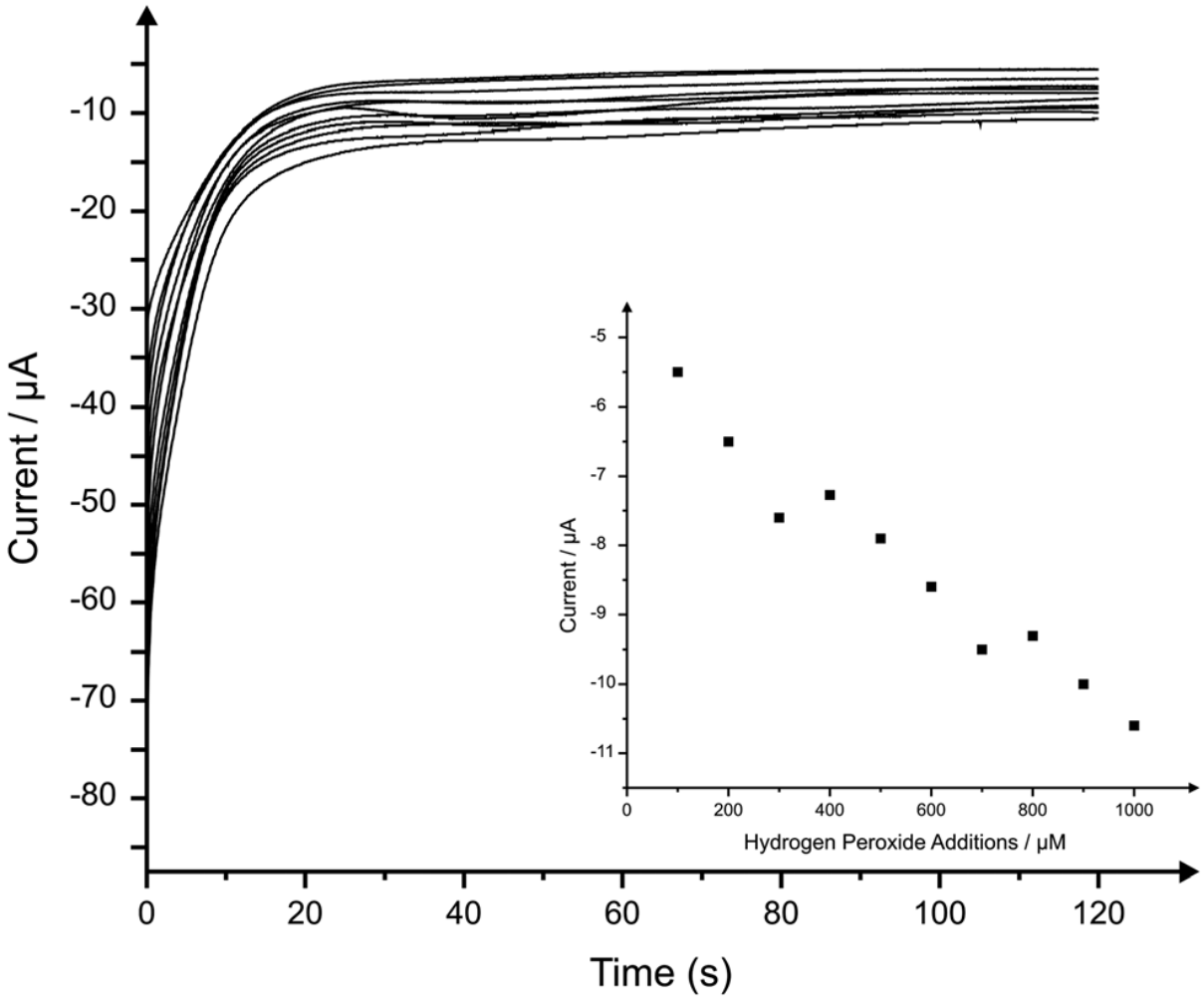

Figure 2.8: Typical chronoamperometric measurements resulting from additions of hydrogen peroxide into a phosphate buffer over the range of 100 to 1000 µM using the PtSPE. Measurements were taken at a potential of +0.35 V. Inset: the corresponding calibration plot taken when t = 120 seconds.

2.4 Conclusions

The application of novel, disposable, single shot platinum screen printed electrodes have been reported in this chapter with their analytical performances explored towards the sensing of hydrazine and hydrogen peroxide which is found to exhibit analytically useful linear ranges and limits of detection compared to existing methodologies. The added benefit is that the platinum resides as an oxide which is beneficial for hydrazine[65, 66] since the need to produce platinum oxides via extensive potential cycling on platinum electrodes is alleviated greatly simplifying the analytical protocol. Other electrode configurations can of course be made due to usefulness of the ink used.

2.5 References

1. J. P. Hart, A. Crew, E. Crouch, K. C. Honeychurch, R. M. Pemberton, *Anal. Lett.*, 2004, **37**, 789.
2. J. P. Metters, R. O. Kadara, C. E. Banks, *Analyst*, 2011, **136**, 1067.
3. R. O. Kadara, N. Jenkinson, C. E. Banks, *Sens. Actuators, B*, 2009, **138**, 556.
4. S. A. Wring, J. P. Hart, L. Bracey, B. J. Birch, *Anal. Chim. Acta*, 1990, **231**, 203.
5. L. G. I. Luiz de Mattos, T. Ruzgas, *Biosens. Bioelectron*, 2003, **18**, 193.
6. M. P. O'Halloran, G.G. Guibault, *Talanta*, 2001, **55**, 605.
7. B. S. Bilijana, R. O. Kadara, C. E. Banks, *Anal. Methods*, 2011, **3**, 105.
8. P. M. Hallam, D. K. Kampouris, R. O. Kadara, N. Jenkinson, C. E. Banks, *Anal. Methods*, 2010, **2**, 1152.
9. M. Khairy, R. O. Kadara, D. K. Kampouris, C. E. Banks, *Electroanalysis*, 2010, **22**, 1455.
10. R. O. Kadara, N. Jenkinson, C. E. Banks, *Electroanalysis*, 2009, **21**, 2410.
11. R. O. Kadara, I. E. Tothill, *Anal. Bioanal. Chem.*, 2004, **378**, 770.
12. R. O. Kadara, I. E. Tothill, *Talanta*, 2005, **66**, 1089.
13. R. O. Kadara, I. E. Tothill, *Anal. Chim. Acta*, 2008, **623**, 76.
14. Y. Lin, F. Lu, J. Wang, *Electroanalysis*, 2004, **16**, 145.
15. P. J. Lamas Ardisana, P. Queipo, F. Bolado, A. Costa Garcia, *Anal. Chim. Acta*, 2008, **615**, 30.
16. O. Dominguez-Renedo, L. Ruiz-Espelt, N. Garcia-Astorgona, M. J. Acros-Martinez, *Talanta*, 2008, **76**, 854.
17. M. C. Tsai, P. Y. Chen, *Talanta*, 2008, **76**, 533.
18. F. Kuralay, S. Campuzano, D. A. Haake, J. Wang, *Talanta*, 2011, **85**, 1330.
19. A. P. R. Garcia-Gonzalez, M. T. Fernandez-Abedul, A. Costa-Garcia, *Electrochim. Acta*, 2008, **53**, 3242.
20. M. F. Bergamini, A. L. Santos, N. R. Stradiotto, M. C. B. Zanoni, *J. Pharm. Biomed. Anal.*, 2005, **39**, 54.
21. J. Maly, J. Masojidek, A. Masci,, M. Illie, E. Cianci, V. Foglietti, W. Vastarella, R. Pilloton, *Biosens. Bioelectron*, 2005, **21**, 923.
22. S. Susmel, G. G. Guibault, C. K. O'Sullivan, *Biosens. Bioelectron.*, 2003, **18**, 881.
23. S. Laschi, I. Palchetti, M. Mascini, *Sens. Actuators, B*, 2006, **114**, 460.
24. E. Bernalte, C. M. Sanchez, C. P. Gil, *Anal. Chim. Acta*, 2011, **689**, 60.
25. P. M. Ndangili, A. M. Jijana, P. G. L. Baker, E. I. Iwuoha, *J. Electroanal. Chem.*, 2011, **653**, 67.
26. S. Campuzano, B. E. F. de Avila, J. Yuste, M. Pedrero, J. L. Garcia, P. Garcia, E. Garcia, J. M. Pingarron, *Biosens. Bioelectron*, 2010, **26**, 1225.
27. S. Zanarini, E. Rampazzo, L. D. Ciana, M. Marcaccio, E. Marzocchi, M. Montalti, F. Paolucci, L. Prodi, *J. Am. Chem. Soc.*, 2009, **131**, 2260.
28. O. A. Loaiza, S. Campuzano, M. Pedrero, P. Garcia, J. M. Pingarron, *Analyst*, 2009, **134**, 34.
29. V. Bhalla, X. Zhao, V. Zazubovich, *J. Electroanal. Chem.*, 2011, **657**, 84.
30. T. Garcia, M. Revenga-Parra, B. Sobrinod, A. Carrecedo, C. Alonso, E. Lorenzo, F. Pariente, *Biosens. Bioelectron*, 2011, **27**, 40.
31. O. A. Loaiza, S. Campuzano, M. Pedrero, P. Garcia, J. M. Pingarron, *Electroanalysis*, 2008, **20**, 1397.
32. S. C. C. Escamilla-Gomez, M. Pedrero, J. M. Pingarron, *Biosens. Bioelectron*, 2009, **24**, 3365.
33. S. C. M. Gamella, C. Parrado, A. J. Reviejo, J. M. Pingarron, *Talanta*, 2009, **78**, 1303.
34. O. A. Loaiza, S. Campuzano, M. Pedrero, P. Garcia, J. M. Pingarron, *Anal. Chem.*, 2008, **80**, 8239.
35. S. C. V. Escamilla-Gomez, M. Pedrero, J. M. Pingarron, *Talanta*, 2008, **77**, 876.
36. C. M. Welch, M. E. Hyde, O. Nekrassova, R. G. Compton, *Phys. Chem. Chem. Phys.*, 2004, **6**, 3153.
37. J. B. Vincent, *J. Trace Elem. Med. Biol.*, 2003, **16**, 227.
38. L. Lin, N. S. Lawrence, S. Thongngamdee, J. Wang, Y. Lin, *Talanta*, 2005, **65**, 144.

39. L. del Torno-de Roman, M. A. Alonson-Iomillo, O. Dominguez-Renedo, C. Merino-Sanchez, M. P. Merino-Amayuelas, M. J. Arcos-Martinez, *Talanta*, 2011, **86**, 324.
40. P. Dutronc, B. Carbonne, F. Menil, C. Lucat, *Sens. Actuators, B*, 1992, **6**, 279.
41. D. R. M. S. D. Zelnick, P. C. Stepaniak, *Aviat., Space Environ. Med.*, 2003, **74**, 1285.
42. J. W. Mo, B. Ogoreve, X. Zhang, B. Pihlar, *Electroanalysis*, 2000, **12**, 48.
43. S. Garrod, M. E. Bollard, A. W. Nicholls, S. C. Connor, J. Connelly, J. K. Nicholson, E. Holmes, *Chem. Res. Toxicol.*, 2005, **18**, 115.
44. J. Wang, Z. Lu, *Electroanalysis*, 1989, **1**, 517.
45. M. Ebadi, *Can. J. Chem.*, 2003, **81**, 161.
46. R. Gilbert, R. Rioux, *Anal. Chem.*, 1984, **56**, 106.
47. A. Safavi, A. A. Ensafi, *Anal. Chim. Acta*, 1995, **300**, 307.
48. S. M. Golabi, H. R. Zare, *Electroanalysis*, 1999, **11**, 293.
49. S. V. Guerrra, L. T. Kubota, C. L. Xavier, S. Nakagaki, *Anal. Sci.*, 1999, **15**, 1231.
50. J. W. White, M. H Subers, A. I. Schepartz, *Biochimica et Biophysica Acta (BBA) - Specialized Section on Enzymological Subjects*, 1963, **73**, 57.
51. N. Kiba, T. Tokizawa, S. Kato, M. Tachibana, K. Tanai, H. Koizumi, E. Edo, E. Yonezawa, *Anal. Sci.*, 2003, **19**, 823.
52. E. C. Hurdis, H. Romeyn, *Anal. Chem.*, 1953, **26**, 320.
53. X. M. Miao, R. Yuan, Y. Q. Chai, Y. T. Shi, Y. Y. Yuan, *J. Electroanal. Chem.*, 2008, **612**, 157.
54. C. M. Welch, C. E. Banks, A. O. Simm, R. G. Compton, *Anal. Bioanal. Chem.*, 2005, **382**, 12.
55. C. Batchelor-McAuley, Y. Du, G. G. Wildgoose, R. G. Compton, *Sens. Actuators, B*, 2008, **135**, 230.
56. R. S. Nicholson, *Anal. Chem.*, 1965, **37**, 1351.
57. J. J. Watkins, H. S. White, *Langmuir*, 2004, **20**, 5474.
58. H. Matsuda, Y. Ayabe, *Z. Elektrochem.* , 1955, **59**, 494.
59. F. C. Anson, J. J. Lingane, *J. Am. Chem. Soc.*, 1957, **79**, 4901.
60. M. Lj. Smiljanic, I. Lj. Srejic, V. M. Marinovic, Z. Lj. Rakocevic, S. B. Strbac, *Hemijska Industrijia*, 2011.
61. B. Sljukic, C. E. Banks, A. Crossley, R. G. Compton, *Electroanalysis*, 2006, **18**, 1757.
62. K. I. Ozoemena, T. Nyokong, *Talanta*, 2005, **67**, 162.
63. J. Wang, M. Chicharro. G. Rivas, X. Cai, N. Dontha, P. A. M Farias, H. Shiraishi, *Anal. Chem.*, 1996, **68**, 2251.
64. C. Batchelor-McAuley, C. E. Banks, A. O. Simm, T. G. J. Jones, R. G. Compton, *Analyst*, 2006, **131**, 106.
65. L. Aldous, R. G. Compton, *Phys. Chem. Chem. Phys.*, 2011, **13**, 5279.
66. R. G. C. L. Aldous, *ChemPhysChem*, 2011, **12**, 1280.
67. C. Malitesta, F. Palmisano, L. Torsi, P. G. Zambonin, *Anal. Chem.*, 1990, **62**, 2735.
68. Y. Li, R. Lenigk, X. Wu, B. Gruendig, S. Dong, R. Renneberg, *Electroanalysis*, 1998, **10**, 671.
69. M. S. Lin, B. I. Jan, *Electroanalysis*, 1997, **9**, 340.
70. A. Eftekhari, *Talanta*, 2001, **55**, 395.

CHAPTER 3: SCREEN PRINTED PALLADIUM ELECTROANALYTICAL SENSORS

3.1 Abstract

This chapter presents the first known fabrication of palladium screen printed macro electrodes were reported which are electrochemically characterised and their potential usefulness in analytical applications explored towards the sensing of formaldehyde, hydrazine and sulphuric acid (protons) with limits of detection (3σ) of 1.61 mM, 3.95 µM and 41.54 µM determined for each of the analytes respectively. The further exciting application of the palladium screen printed sensors towards the sensing of both hydrogen and methane gas is also explored with successful determination of each being successfully described. Such applications demonstrate the plethora of potential uses for screen printed sensors, particularly those fabricated utilising palladium, giving rise to the niche market of sensors capable for utilisation away from the laboratory and within the field.

3.2 Introduction

Since its discovery in 1803, palladium has remained a highly expensive yet expedient material. Palladium, like other platinum-group metals, exhibits high catalytic activity towards several electrochemical processes, such as the hydrogen evolution reaction (HER), hydrogen absorption, and reduction of simple organic compounds.[1-12] The key unique attribute yielded through palladium is the ability of palladium to absorb hydrogen[13] which can be accomplished under both gas-phase and electrochemical conditions.[12]

One well documented and explored application of palladium is within the field of fuel cell development.[14-19] The activity for the oxygen reduction reaction (ORR) of palladium is only slightly lower than that of platinum, and through the formation of an alloy utilising a suitable metal, such as cobalt or iron, the ORR activity of palladium can improve on that of platinum. Conversely, the activity for the hydrogen oxidation reaction (HOR) of palladium is considerably lower than that of platinum, however through the addition of a very small amount (~ 5 %) of platinum such problems can be overcome ensuring that the HOR activity of palladium attains that of pure platinum.[14]

Additionally, palladium has been reported within the literature for the beneficial sensing of key analytes. For example, previous studies have reported the use of palladium for the sensing of analytes such as hydrogen peroxide.[20] A thin-film composite metal electrode comprising gold and palladium fabricated by thermally evaporating a layer of gold/palladium through a copper mask onto a plastic substrate has been reported allowing the oxidation of hydrogen peroxide at a facile potential.[20]

Further elegant work has reported on the utilisation of palladium nanoparticles dispersed upon a carbon based screen printed electrode employed for the sensing of oxygen dissolved in a phosphate buffer solution.[21] The activated screen-printed carbon electrodes

modified with palladium nanoparticles were found to be effective for oxygen reduction reaction (ORR) and found to offer comparable sensitivity to a commercially available dissolved oxygen meter in both laboratory-based samples and also ground and tap water samples.[21]

Highly novel and economical screen printed sensors have been fabricated by Wang *et al*[22] where expensive metal particles including nickel, cobalt, copper and palladium are dispersed within a carbon based ink through doping of the carbon ink with given metal. This therefore enables the sensors to possess the electro-catalytic behaviour of the metal based materials whilst maintaining the relatively low cost nature of the carbon based sensor. The group found that the dispersed metal particles lead to a marked decrease in the oxidation potential for carbohydrates, amino acids, aldehydes or alcohols.[22] Expanding on this work, Wang and co-workers[23] demonstrated the functionality of the palladium-doped carbon screen printed sensors for the sensing of formaldehyde, relying on the strong electro-catalytic action of the dispersed palladium particles contributing to the reduction of formaldehyde. The low detection limit of 2 μM is accompanied by a wide linear range and high selectivity, with the ease of development to form a single-use sensor for the on-site environmental and industrial monitoring of formaldehyde being alluded to.[23] A further example of the potential benefits of incorporating dispersed metal particle within an a low cost economical screen printing ink such as graphite is once more provided by Wang *et al* reporting once more on the 'strip-based' sensors, in this instance coupled with a permi-selective polyphenol film.[24] The work demonstrated that palladium-dispersed carbon inks can be used to enhance greatly the performance of disposable amperometric strips for the sensing of glucose. It is shown that the coupling of the efficient electro-catalytic action of the palladium particles with the permi-selective function of the polyphenol film results in a highly selective and sensitive response validated through a limit of detection (3σ) of 0.1 mM glucose.[24] From inspection of the

literature a true screen printed palladium electrode is yet to be realised, that is, an electrode comprising entirely of palladium that can be easily mass produced using a palladium polymeric paste.

Consequently, in this chapter the first known fabrication of screen printed electrodes with a working electrode comprising micron-sized palladium particles which are held together using a polymeric binder is presented. The electrodes are fabricated in such a way that the expensive palladium material is economically utilised through underlying carbon based tracks being incorporated within the senor. The use of screen printing techniques allows for the formation of a working electrode surface which is consistent across the surface whilst ensuring that a well-defined and uniform working electrode; a factor which is essential to allow for excellent reproducibility between sensors. The palladium screen printed sensors are characterised electrochemically and consequently explored as sensors for the determination of formaldehyde, hydrazine, sulphuric acid and hydrogen gas.

3.3 Results and Discussion

Characterisation of Palladium Screen Printed Macro Electrodes

Palladium screen printed macroelectrodes (denoted throughout as PdSPE) were fabricated as detailed in the Experimental Section with a working electrode comprising palladium ink printed onto an underlying graphite based screen printed electrode. Note that in this configuration, the palladium material is economically utilised rather than the connecting legs being constructed of the same material. Figure 3.1 depicts SEM analysis of the electrode surface where close inspection reveals a potentially porous structure, which upon magnification is revealed to consist of palladium microparticles held together with a polymeric formulation. Energy-dispersive X-ray (EDAX) analysis was performed on the

PdSPE surface with typical values revealing the surface to consist of 4.86 % oxygen, 11.90 % carbon and 83.24 % palladium.

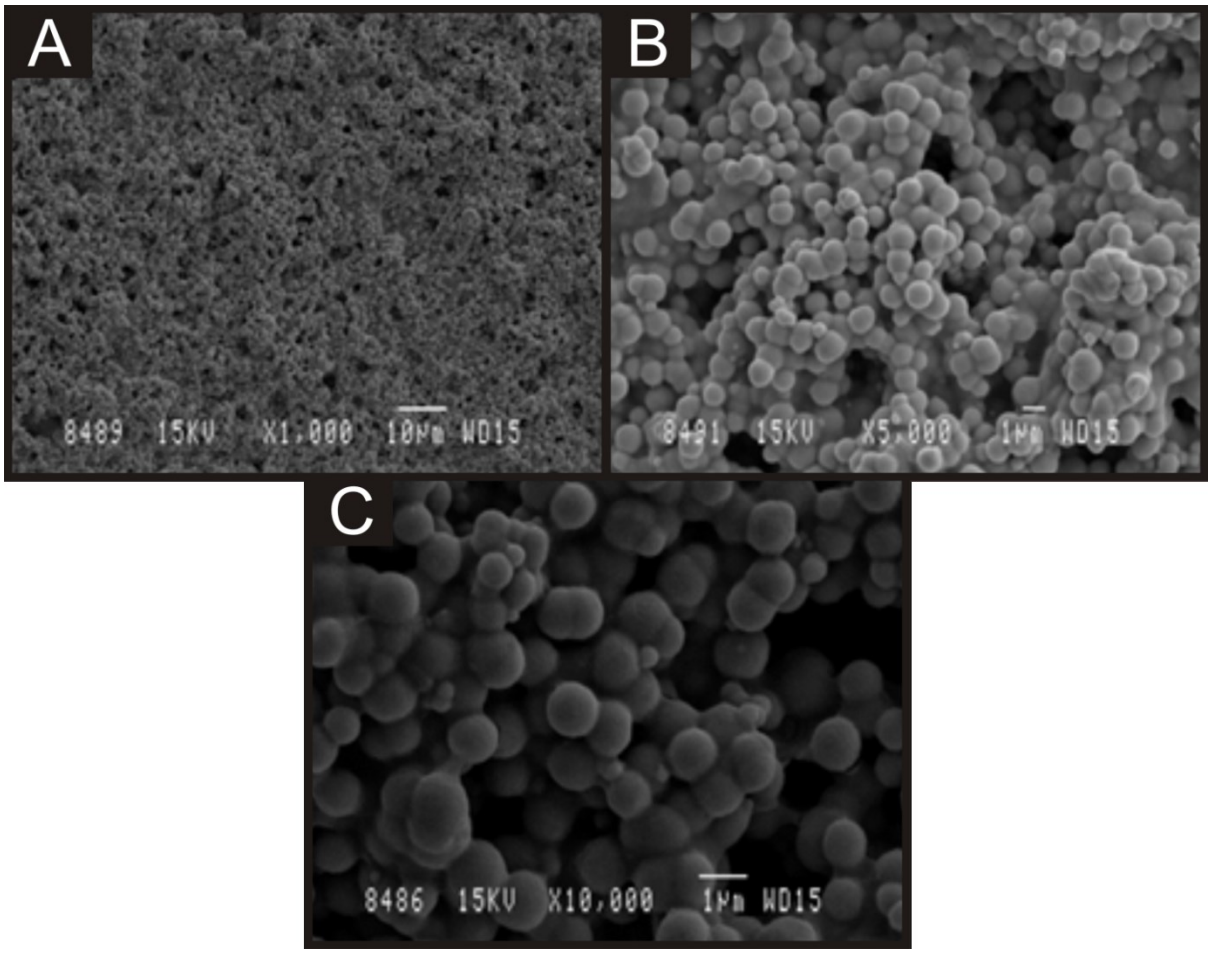

Figure 3.1: Typical SEM images of the palladium screen printed macro electrode at increasing magnifications of: x1000 (A), x5000 (B) and x10000 (C).

The PdSPEs were electrochemically characterised using the redox probe hexaammine-ruthenium (III) chloride. Firstly, scan rate studies were performed using the PdSPE in 1 mM hexaammine-ruthenium (III) chloride with 0.1 M KCl (see figure 3.2), where observation of voltammetric peak height, plotted as peak current (I_P) against square root of the applied scan rate over the range 5 – 200 mVs^{-1} was found exhibit a linear response (I_p *(µA) = -4.714 µA/ (µM) + 13.42 µA)* confirming a diffusional process.

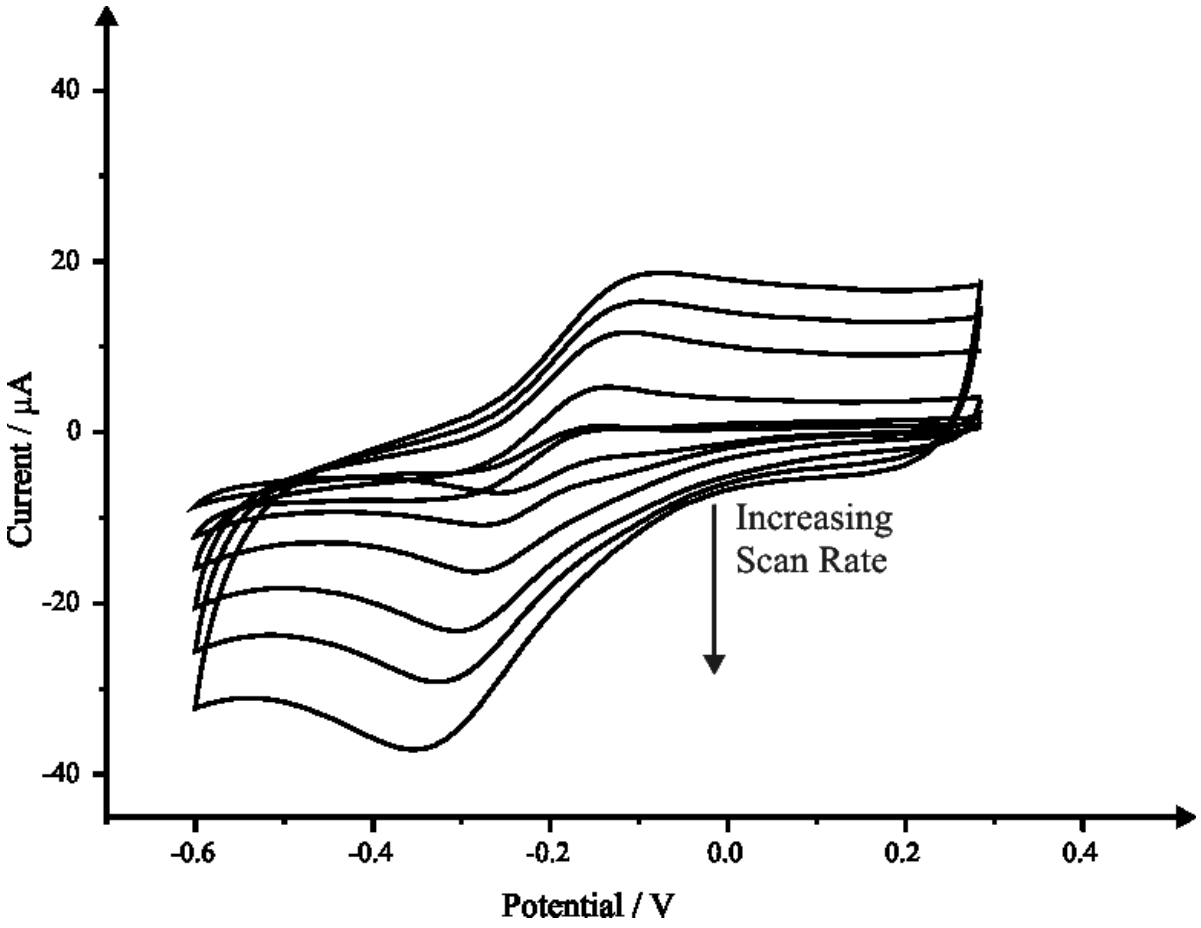

Figure 3.2: Electrochemical signatures obtained in 1 mM hexaammine-ruthenium (III) chloride in 0.1 M KCl using the PdSPEs recorded over the scan rate range of 5 to 200 mVs^{-1} (vs. Ag/AgCl).

The heterogeneous electron transfer rate constant, k^0, was estimated at the PdSPE when studied using the outer-sphere electron transfer probe hexaammine-ruthenium (III) chloride. The Nicholson method is routinely used to estimate the observed standard heterogeneous electron transfer rate for quasi-reversible systems using the following equation[25] (see eq. 1.13) where ψ is the kinetic parameter, D, is the diffusion coefficient, n, is the number of electrons involved in the process, F, is the Faraday constant, υ, the scan rate, R, the gas constant, and T the temperature. The kinetic parameter, ψ is tabulated as a function of peak-to-peak separation (ΔE_P) at a set temperature (298 K) for a one-step, one electron process (where α = 0.5). The function of $\psi(\Delta E_P)$, which fits Nicholson's data, for practical usage (rather than producing a working curve) is given by:[26]

$$\psi = (-0.6288 + 0.021X) / (1 - 0.017X) \quad (3.1)$$

where $X = \Delta E_P$ is used to determine ψ as a function of ΔE_P from the experimentally recorded voltammetry. From this, a plot of ψ against $[\pi Dn\upsilon F / (RT)]^{-1/2}$ is produced graphically (see Equation 1.13) allowing the standard heterogeneous rate transfer constant, k^o to be readily determined. Using this approach, the heterogeneous electron transfer rate constant, k^0 of 3.69 x 10^{-3} cm $s^{-1}$was determined at the PdSPE. The electrochemically active area of the PdSPE was estimated using the following equation for quasi-reversible electrochemical processes at 298 K where n is total number of electrons transferred in the electrochemical process, D is the diffusion coefficient, C_0 is the bulk concentration of the analyte, A is the electrode area and υ is the applied voltammetric sweep scan rate. The electrochemically active area was estimated to correspond to 0.12 (± 0.04) cm^2 compared to a geometric area of 0.071 cm^2 in agreement with observations from figure 3.1 which highlights the slightly porous nature of the electrode surface.

Electroanalytical Applications of the Palladium Screen Printed Electrode

The analytical performance of the PdSPE was next examined towards the electrochemical sensing of formaldehyde. Formaldehyde, a carcinogen to humans, is an automotive exhaust gas and an important chemical in the manufacturing of a variety of consumer products and it may be the main in-door pollutant especially when the house is freshly fabricated.[27] As a reported environmental pollutant, it has been extensively investigated and continues to be of interest to analyst.[27-31] Many formaldehyde-assessment methods have been developed in recent years, for example, Spectrophotometry, High Performance Liquid Chromatography, Gas Chromatography, and Polarography.[27, 32-34] Importantly however, these existing methods require the inclusion and use of various toxic reagents and/or expensive and bulky instrumentation for example, High-Performance Liquid Chromatography as mentioned. Therefore, clearly, such techniques are impractical for real time 'field' analysis owing to the requirement of apparatus set-up, a sterile environment, not to mention difficult logistics. Evidently, a simple and sensitive method for the determination of trace amounts of formaldehyde is needed.

Cyclic voltammetric measurements were first undertaken using the PdSPE in 3.5 mM formaldehyde and 0.1 M KOH which was selected based on previous literature.[35, 36] The electrochemical oxidation of formaldehyde was found to occur at ~ - 0.09 V (*vs*. Ag/AgCl) with the effect of increasing scan rate over the range 5 to 150 mVs^{-1} explored. Through a plot of the square root of scan rate ($v^{0.5}$) versus voltammetric peak current (I_P) a linear response (I_p *(μA) = 6.26 μA/ (μM) + 35.43 μA;* R^2 *= 0.98)* was observed confirming the electrochemical reaction is diffusional in nature.

The analytical utility of the PdSPE was trialed towards formaldehyde sensing with additions made over the range 2.5 to 6.5 mM into 0.1 M KOH. The previously discussed peak

resulting from the electrochemical oxidation of formaldehyde is seen to increase in magnitude correlating with concentration as depicted in figure 3.3A. Figure 3.3B shows a typical calibration plot (peak height / μA versus formaldehyde concentration / mM), which although not showing uniform linearity over the analytical range ($Ip/\mu A = 19.68\ \mu A/\mu M - 27.84\ \mu A;\ R^2 = 0.92,\ N = 9$), does demonstrate a distinct positive analytical correlation between the observed peak height (I_P) and formaldehyde concentration. A limit of detection (3σ) using cyclic voltammetry for the sensing of formaldehyde was found to correspond to 1.61 mM. When benchmarked against existing electrochemical methods reported for the sensing of formaldehyde, it is evident that other systems are capable of offering lower limits of detection towards formaldehyde.[23, 27, 37-39] Critically, of the reports within the literatures describing the sensing of formaldehyde, only that by Wang *et al*[23] requires no extensive preparatory step through the screen printing of palladium-doped carbon strips allowing for a limit of detection of 2 μM.[23] Ultra-low, highly admirable detection limits are reported at other configurations. For example the utilisation of a palladium over layer on gold nanoparticles electrodeposited upon a carbon ionic liquid electrode (3 μM),[37] the electro-deposition of a nanostructured platinum–palladium alloy upon a Nafion film-coated glassy carbon electrode (3 μM),[27] a nanoporous palladium-modified TiO_2 electrode, prepared by the hydrothermal process (23 μM),[38] the response observed at the PdSPE is also comparable to nanoparticle modified electrodes which are found to exhibit mM linear ranges.[36-38]

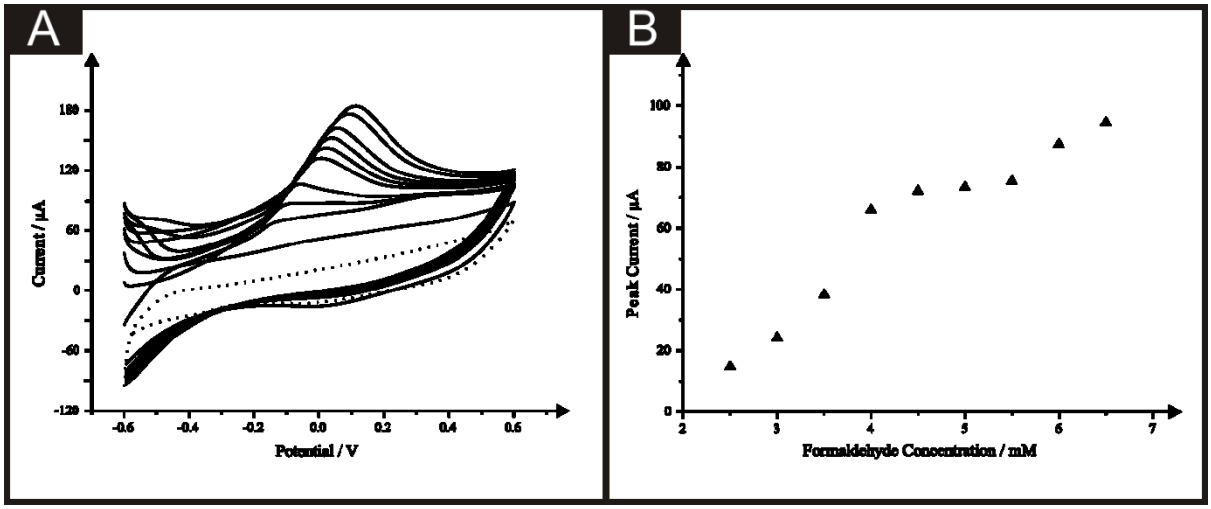

Figure 3.3: A) Typical cyclic voltammetric responses resulting from additions of formaldehyde into a 0.1 M KOH buffer (dotted line is the response in the absence of formaldehyde) using the PdSPE. Scan rate: 50 mVs^{-1}. **B)** A typical corresponding calibration plot resulting from analysis of the cyclic voltammetric response presented in **(A).**

Next, hydrazine was selected as a model analyte to further test the analytical performance of the palladium-based screen printed sensor due to extensive reports within the literature of the electro-catalytic activity of palladium towards the electrochemical sensing of hydrazine.[40-43] Consequently, additions of hydrazine were made into a pH 7 phosphate buffer solution over the concentration range of 200 to 1000 µM; the pH 7 buffer was utilised throughout as is in-line with previous literature reports allowing a direct comparison to be made.[40, 44, 45] Figure 3.4A shows the cyclic voltammograms resulting from increasing hydrazine concentrations made into the pH 7 buffer. The electrochemical oxidation of hydrazine is evident at the potential of ~ - 0.05 V (*vs*. Ag/AgCl) with the peak increasing in magnitude upon increasing hydrazine concentrations. A clear linear relationship ($I/\mu A = 1.75 \times 10^{-2}\ \mu A/\mu M - 1.51\ \mu A$; $R^2 = 0.95$, $N = 17$) between the hydrazine concentration in solution and the recorded peak height (I_P) is depicted in figure 3.4B, with the high reproducibility of the palladium-based screen printed sensors being highlighted through the incorporation of

error bars (standard deviation). The limit of detection (3σ) for hydrazine was determined to equate to 3.95 μM.

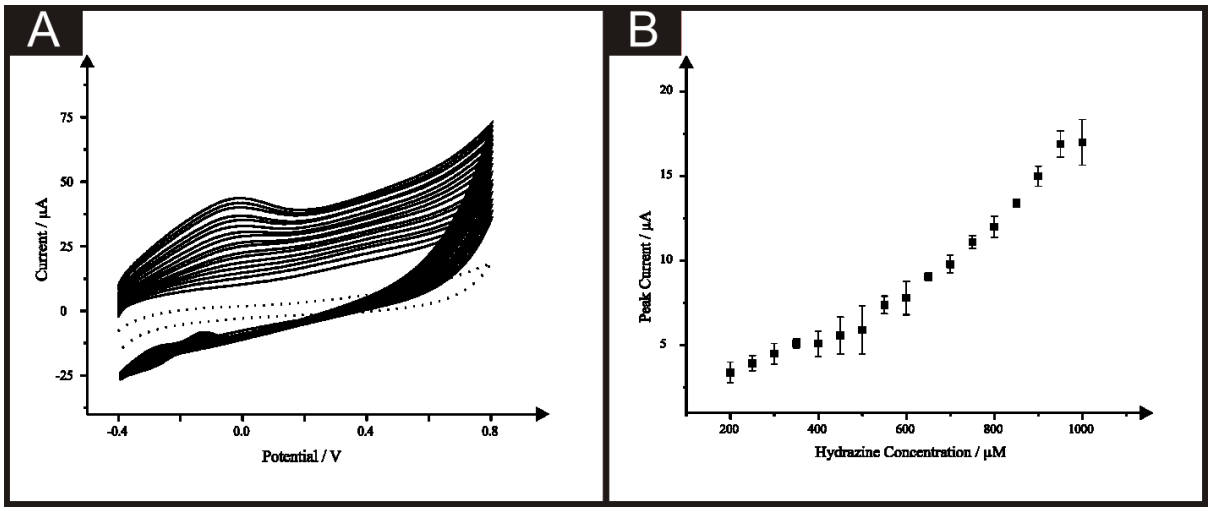

Figure 3.4: A) Typical cyclic voltammagrams resulting from additions of hydrazine (200 – 1000 μM) into a pH 7 phosphate buffer solution (dotted line is the response in the absence of hydrazine). Scan rate: 50 mVs^{-1}. **B)** The corresponsing calibration plot resulting from analysis of the cyclic voltammetric shown in **(A)**.

Such a limit of detection compares well with existing reports within the literature utilising well-documented palladium nanoparticles for the sensing of hydrazine. Example of such work include that of Compton *et al*[40] who report a palladium nanoparticle modified boron-doped diamond electrode offering a limit of detection of 2.6 μM, but also the use of a palladium plated boron-doped diamond array which allowed for the improved limit of detection of 1.8 μM.[40] Further work by Compton *et al*[46] discusses the use of mixture of palladium and carbon black nanoparticle modified glassy carbon electrodes which were determined to be slightly less sensitive than the studies at boron-doped diamond electrodes offering a limit of detection of 8.8 μM for hydrazine.[46] Clearly, such limits of detection are comparable to existing literature reports yet have the further advantage of the alleviation of any pre-treatment or conditioning steps associated with the deposition or formation of the nanoparticle based sensors. It is however important to note, that in some instances the

incorporation of nanoparticles has been found to offer substantial improvements towards the detection of hydrazine. One such example is that utilising a glassy carbon electrode modified with palladium nanoparticle decorated multiwalled carbon nanotubes, which was reported to facilitate a limit of detection of 16 nM for hydrazine.[47]

Finally the potential use of the PdSPE in gas sensors was studied, in particular the voltammetric response in sulphuric acid and for sensing protons and towards the sensing of hydrogen gas. The hydrogen–palladium system is an important and complex topic of interest,[1, 48-56] with the absorption of molecular hydrogen by palladium is of vast practical interest.[13] Hydrogen atoms have a high mobility within the lattice and diffuse rapidly through the metal. This process is highly specific to H_2 and D_2, and palladium metal is impervious to all other gases, a fact which is utilised in the separation of hydrogen from mixed gases.[13, 56] The dissolution and adsorption of hydrogen has been studied in sulphuric acid on (smooth) palladium electrodes with the following sequence of processes reported:[48]

$$H^+ + e^- \rightleftharpoons H_{ad} \quad (3.2)$$

$$H_{ad} \rightleftharpoons H_{dis,s} \quad (3.3)$$

$$H_{dis,s} \rightleftharpoons H_{dis,b} \quad (3.4)$$

where H_{ad} is an adsorbed hydrogen atom, $H_{dis,s}$ is a dissolved hydrogen atom directly below the surface, and $H_{dis,b}$ denotes H atoms below the first atomic layers of palladium atoms from the surface.[48] Equation 3.2 describes the Volmer reaction, while Equation 3.3 is shows one without charge transfer for the transition from the adsorbed state into a dissolved state directly below the surface, that is, in the bulk of the palladium metal.[48]

First, the PdSPE was utilised in a solution of 3 M H_2SO_4, with the cyclic voltammetric measurement being recorded. Figure 3.5 depicts a typical response revealing a clear cathodic peak corresponding to the electrochemical reduction of Pd^{2+} to Pd^0,[48] apparent at ~ + 0.33 V (*vs*. Ag/AgCl) while an anodic peak is evident at ~ - 0.01 V (vs. Ag/AgCl). Next the voltammetric response of the PdSPE through holding the potential negative at - 0.8 V (*vs*. Ag/AgCl) in 1 mM H_2SO_4 in 0.1 M sodium sulphate was sought as is depicted in figure 3.6. Clearly, after holding the potential up to 30 seconds a large single voltammetric peak is observed at a potential of ~ - 0.2 V (*vs*. Ag/AgCl) which continues to increase in magnitude upon the lengthening of the holding time. The application of the negative potential electrochemically reduces protons to hydrogen gas with the voltammetric anodic scan oxidising this back to H^+. Importantly, only a single oxidative current is observed, likely as a result of the palladium surface upon the PdSPE residing as a bulk form, rather than two oxidation voltammetric peaks as has been reported through utilisation of nanoparticle sized palladium.[56] The effect of H_2SO_4 concentration was also studied with additions of H_2SO_4 being made into a 0.1 M sodium sulphate buffer solution over the concentration range of 100 to 1000 μM. Shown in figure 3.7A are the resultant linear sweep voltammograms arising from the additions of H_2SO_4, where the oxidation peak at ~ - 0.35 V (*vs*. Ag/AgCl) increases in magnitude with increasing additions of H_2SO_4. The corresponding calibration plot of peak height (I_P) versus concentration (μM) (figure 3.7B) demonstrates the linearity offered by the PdSPE over the concentration range studied ($I/\mu A = 1.02 \times 10^{-1}\ \mu A/\mu M - 19.07\ \mu A;\ R^2 = 0.98,\ N = 9$). The limit of detection (3σ) when utilising the PdSPE for the sensing of H_2SO_4 was determined to correspond to 41.54 μM.

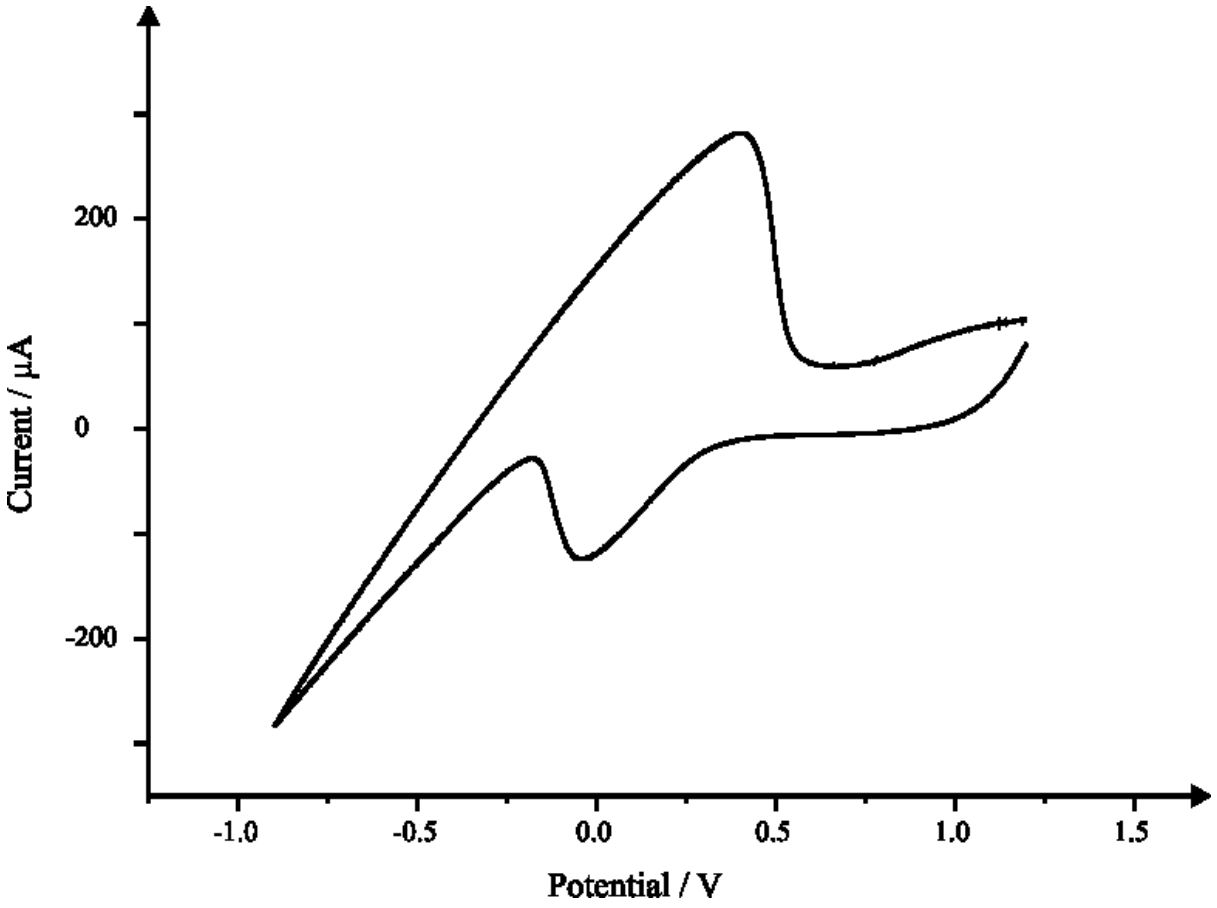

Figure 3.5: A cyclic voltammetric signature obtained in 3 M H_2SO_4 using the PdSPE. Scan rate: 50 mVs^{-1}.

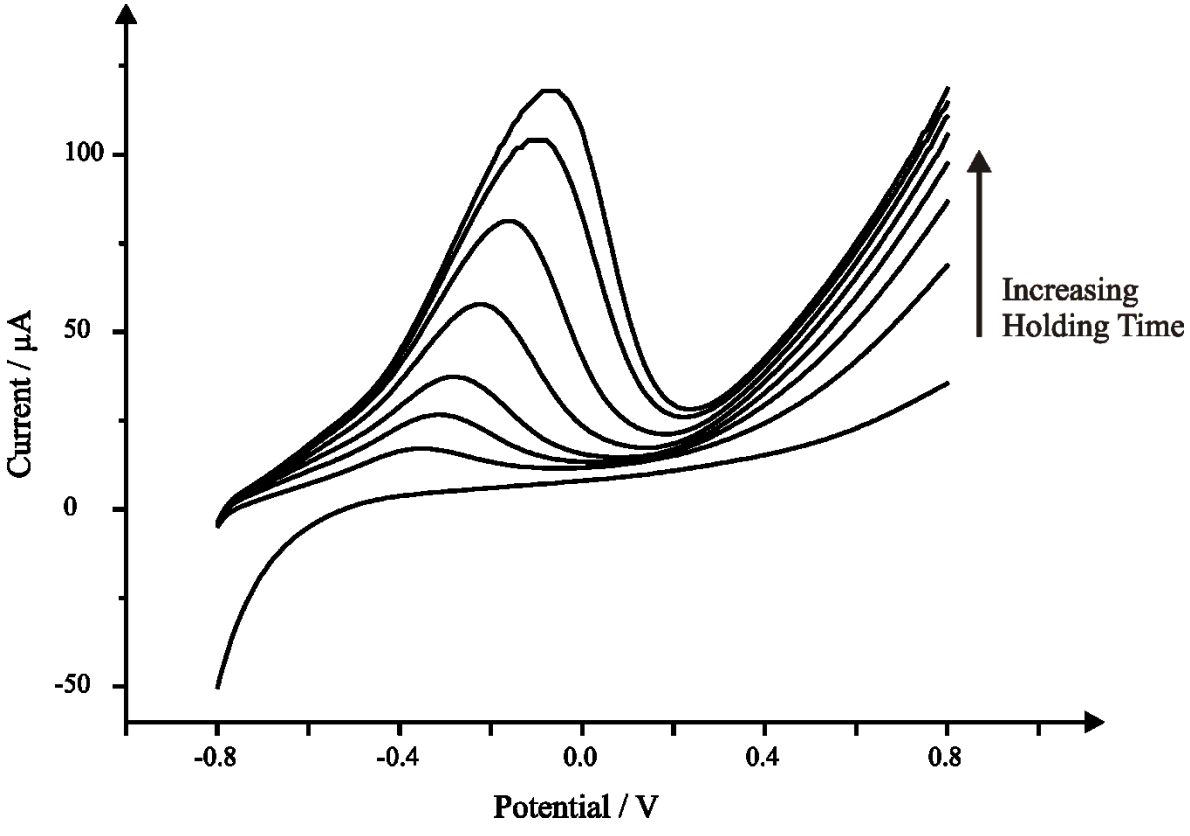

Figure 3.6: Linear sweep voltammograms from holding a PdSPE in 10 mM H_2SO_4 at - 0.8 V (vs. Ag/AgCl) for 1, 30, 60, 90, 120, 180, 240 and 300 seconds. Scan rate: 50 mVs^{-1}.

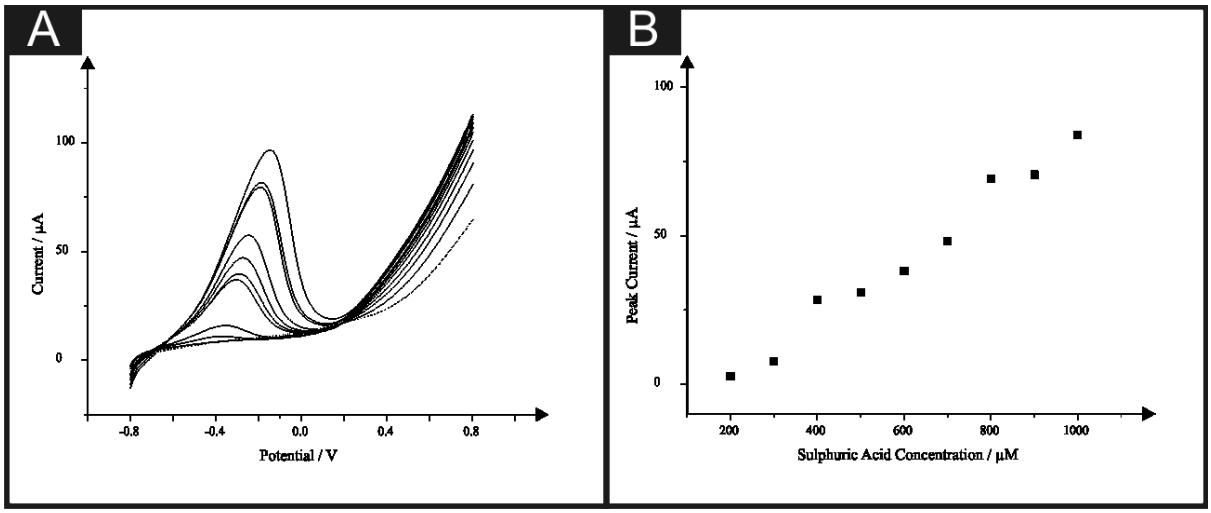

Figure 3.7: A) Typical cyclic voltammetric responses resulting from additions of sulphuric acid (200 – 1000 µM) into a 0.1 M sodium sulphate buffer using the PdSPE (first held at - 0.8 V (vs. Ag/AgCl) for 30 seconds) (dotted line is the response in the absence of suphuric acid). Scan rate: 50 mVs^{-1}. **B)** A typical calibration plot corresponding to additions of sulphuric acid into a 0.1 M sodium sulphate buffer using the PdSPE arising fron the voltammetric responses shown in **(A)**.

Next the potential application of the PdSPE towards the sensing of hydrogen gas was explored in 0.1 M sodium sulphate with first, a blank cyclic voltammogram performed and then following the introduction of hydrogen gas into the solution at time intervals of 30 seconds. After each period of bubbling, the cyclic voltammetric signature was recorded using the PdSPE. As is shown in figure 3.8A, the introduction of hydrogen gas gives rise to a large easily quantifiable oxidative current present at ~ - 0.1 V (*vs*. Ag/AgCl); the process involves the electrochemical oxidation of hydrogen gas to protons. An initial rise is observed in the response which then plateaus as shown in figure 3.8B; such a plateauing effect has previously been reported for the case of palladium nanoparticle modified electrodes.[56]

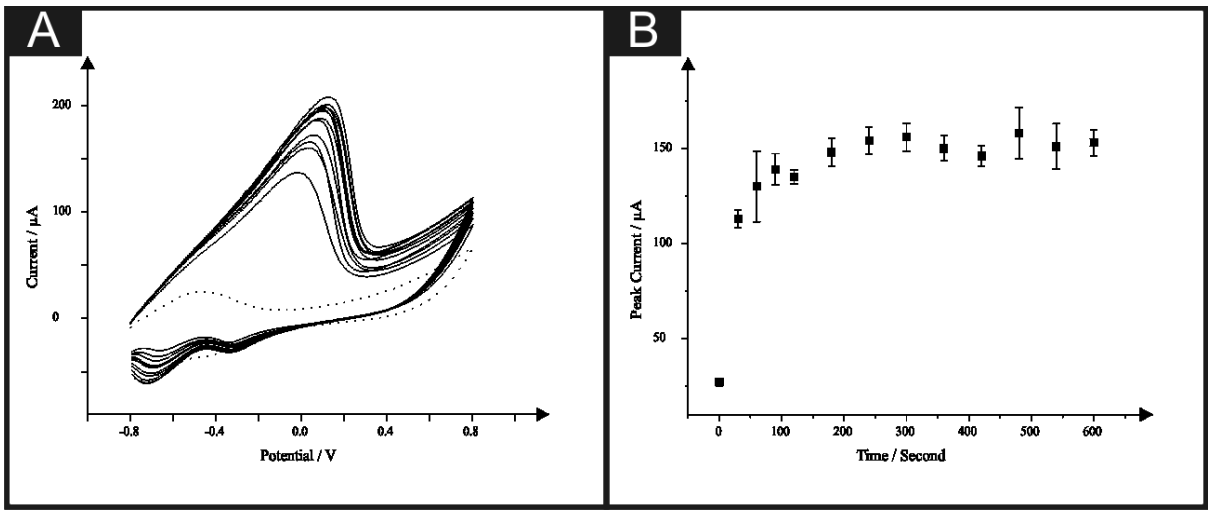

Figure 3.8: A) Typical cyclic voltammetric responses resulting from bubbling of hydrogen gas (0 – 600 seconds) into a 0.1 M potassium chloride solution using the PdSPE (dotted line is the response in the absence of hydrogen). Scan rate: 50 mVs^{-1}. **B)** A typical calibration plot corresponding to the bubbling time of hydrogen gas into 0.1 M potassium chloride using the PdSPE arising from the voltammetric responses shown in **(A)**.

Finally, the screen printed palladium sensors were trialled towards the sensing of methane gas. Methane gas is highly volatile when mixed with air and can cause explosions due extreme flammability posing a serious risk to human life and infrastructure. The displacement of oxygen by methane gas resulting in asphyxiation in cramped or inadequately ventilated areas is also of great risk. Methane is also known to pose a great risk to the wider society and environment as a whole being around a 20 times more potent greenhouse gas than carbon dioxide.[57] Thus, the development of a reliable and cost effective methane gas sensor through the oxidation of methane at ambient conditions could potentially allow for the opportunity to develop a fast and safe method for the detection of methane.[58]

As is demonstrated in figure 3.9, the blank solution of 0.5 M H_2SO_4, under the prescribed parameters, was revealed to exhibit solely a reduction peak at ~ - 0.05 V (*vs*. Ag/AgCl) presumed to be the reduction of the palladium oxide. Interestingly, upon saturation of the blank solution with methane through the bubbling of the gas for 5 minutes, a large oxidation current ~ + 0.96 V (*vs*. Ag/AgCl) is observed with a relatively small increase in

reduction current through utilisation of the PdSPE. It has been suggested, in the case of palladium nanoparticles modified C_{60} that the reaction mechanism may be described as follows:[58]

$$CH_4 + PdO \rightarrow CH_3OH + Pd \text{ (or } CH_4 + PdO_2 \longrightarrow CH_3OH + PdO) \quad (3.5)$$

$$CH_3OH + PdO \rightarrow HCHO + H_2O + Pd \text{ (or } CH_3OH + PdO_2 \longrightarrow HCHO + H_2O + PdO) \quad (3.6)$$

The broad oxidation peak observed in the presence of methane gas can be attributed to the multi-step process occurring described by Equations 3.5 and 3.6. The shift in the potential of the reduction peak in comparison to that within the literature which occurs at a slightly more negative potential[58] can be attributed to the PdSPE consisting of palladium microparticles rather than nanoparticles, hence a greater overpotential is required at a micron-sized palladium particles over the nano-sized counterparts for the electrochemical reduction of the palladium oxide to occur. Clearly, the palladium-based screen printed sensor holds great promise for the monitoring of methane, with such beneficial applications being further amplified through the compact and disposable nature and ease of use of screen printed electrodes.

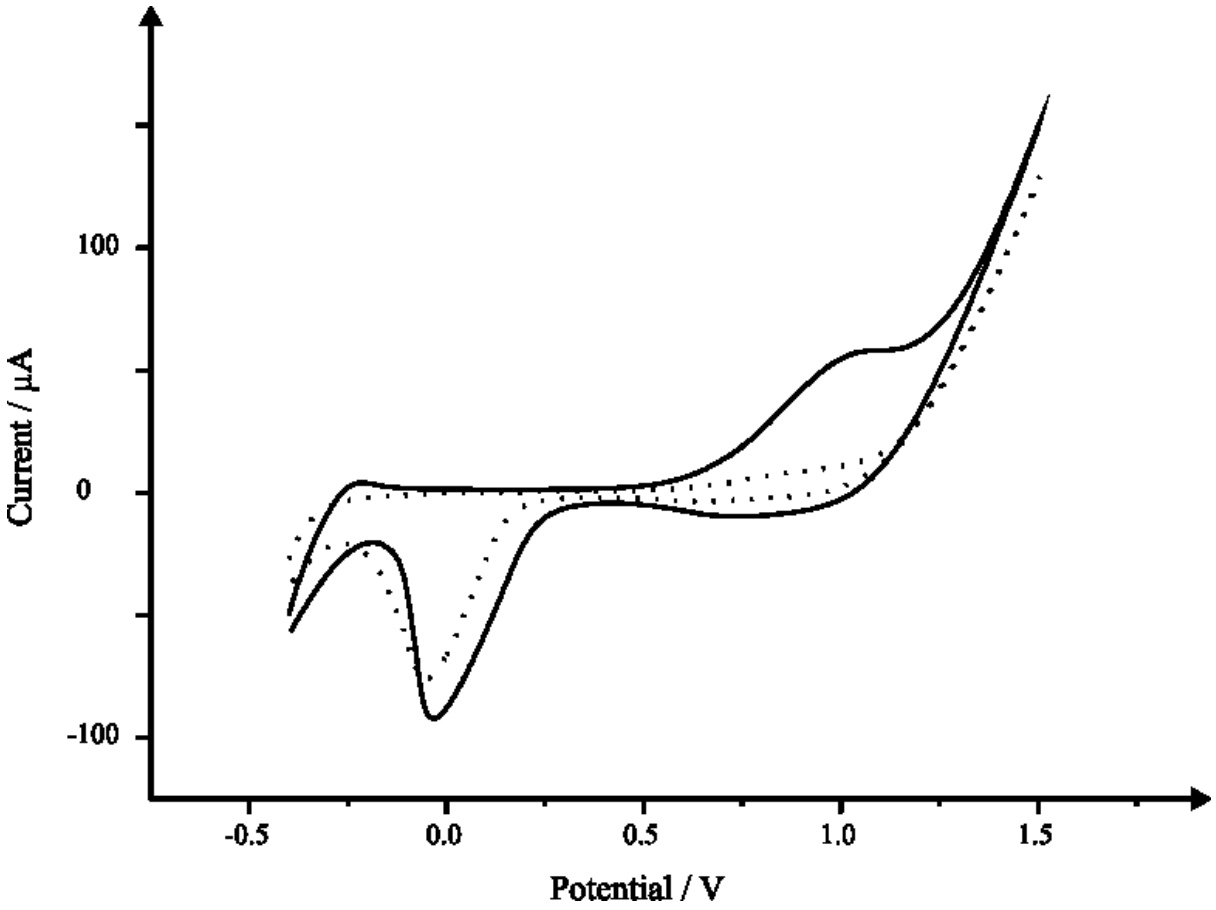

Figure 3.9: Cyclic voltammograms recorded in 0.5 M H_2SO_4 before (dotted line) and after being saturated (solid line) with methane gas using the PdSPE. Scan rate: 50 mVs^{-1}.

3.4 Conclusion

This chapter has reported the application of novel, disposable, single-shot palladium screen printed macro electrodes and evaluated their analytical performance towards the sensing of formaldehyde, hydrazine, sulphuric acid (protons) and hydrogen. Favourable analytical sensing of both formaldehyde and hydrazine has been demonstrated with the palladium screen printed sensor exhibiting good reproducibility throughout. Excitingly we have determined the potential for the screen printed sensor to be utilised for the qualitative measurement of two *key* gaseous analytes; hydrogen and methane demonstrating the truly wide scope for the potential applications of not only palladium based sensors, but those fabricated through the application of screen printing technologies.

3.5 References

1. M. Elam, B. E. Conway, *J. Electrochem. Soc.*, 1988, **135**, 1678.
2. J. Simonet, *J. Electroanal. Chem.*, 2005, **583**, 34.
3. C. Iwakura, T. Ito, H. Inoue, *J. Electroanal. Chem*, 1999, **463**, 116.
4. C. Iwakura, T. Abe, H. Inoue, *J. Electrochem. Soc.*, 1996, **143**, L71.
5. S. J. C. Celghorn, D. Pletcher, *Electrochim. Acta*, 1993, **38**, 425.
6. M. W. Breiter, *Electrochim. Acta*, 1962, **8**, 973.
7. U. Muller, A. Dulberg, A. Stoyanova, H. Baltruschat, *Electrochim. Acta*, 1997, **42**, 2499.
8. T. R. Blackburn, P. C. Campbell, *J. Electroanal. Chem*, 1964, **8**, 145.
9. V. Solis, T. Iwasita, A. Pavese, W. Vielstich, *J. Electroanal. Chem.*, 1988, **255**, 155.
10. M. C. Arevalo, J. L. Rodriquez, E. Pastor, *J. Electroanal. Chem.*, 1999, **472**, 71.
11. Y. Gimeno, A. H. Creus, S. Gonzalez, R. C. Salvarezza, A. J. Arvia, *Langmuir*, 2001, **13**, 1857.
12. M. Grden, M. Lukaszewski, G. Jerkiewicz, A Czerwinski, *Electrochim. Acta*, 2008, **53**, 7583.
13. F. A. Lewis, *Academic Press, London/ New York*, 1967.
14. E. Antolini, *Energy Environ. Sci.*, 2009, **2**, 915.
15. Y. Zhu, Z. Khan, R. I. Masel, *J. Power Sources*, 2005, **139**, 15.
16. B. Tao, F. Miao, P. K. Chu, *Electrochim. Acta*, 2012, **65**, 149.
17. F. Miao, B. Tao, L. Sun, T. Liu, J. You, L. Wang, P. K. Chu, *J. Power Sources*, 2010, **195**, 146.
18. S. P. Jiang, Y. Ye, T. He, S. B. Ho, *J. Power Sources*, 2008, **185**, 179.
19. H. Q. He, L. Zhang, A. Babaei, X. Wang, S. P. Jiang, *J. Alloys Compd.*, 2011, **509**, 9708.
20. D. A. Johnston, M. F. Cardosi, D. H. Vaughan, *Electroanalysis*, 1995, **7**, 520.
21. C. C. Yang, A. S. Kumar, J. M. Zen, *Electroanalysis*, 2006, **18**, 64.
22. J. Wang, *Electroanalysis*, 1995, **7**, 1032.
23. J. Wang, M. Pedrero, X. H. Cai, *Analyst*, 1995, **120**, 1969.
24. J. Wang, O. Chen, *Analyst*, 1994, **119**, 1849.
25. R. S. Nicholson, *Anal. Chem.*, 1965, **37**.
26. I. Lavagnini, R. Antiochia, F. Magno, *Electroanalysis*, 2004, **16**, 505.
27. Z. L. Zhou, T. F. Kang, Y. Zhang, S. Y. Cheng, *Microchim. Acta*, 2009, **164**, 133.
28. J. Wang, P. V. A. Pamidi, G. Cepria, *Anal. Chim. Acta*, 1996, **330**, 151.
29. F. Vianello, A. Stefani, M. L. Di Paolo, A. Rigo, A. Lui, B. Margesin, M. Zen, M. Scarpa, G. Soncini, *Sens. Actuators, B*, 1996, **37**, 49.
30. Y. Herschkovic, I. Eshkenazi, C. E. Campbell, J. Rishpon, *J. Electroanal. Chem.*, 2000, **491**, 182.
31. L. Zhang, J. F. Hu, P. Song, H. W. Qin, X. D. Liu, M. H. Jiang, *Physica B*, 2005, **370**, 259.
32. G. R. Mohlmann, *Appl. Spectrosc.*, 1985, **39**, 98.
33. B. Mann, M. L. Grajeski, *J. Chromatogr.*, 1987, **386**, 149.
34. T. Dumas, *J. Chromatogr.*, 1982, **247**, 289.
35. Y. Zhang, M. Zhang, Z. Cai, M. Chen, F. Cheng, *Electrochim. Acta*, 2012, **68**, 172.
36. A. Safavi, N. Maleki, F. Farjami, E. Farjami, *J. Electroanal. Chem.*, 2009, **626**, 75.
37. A. Safavi, F. Farjami, *Electroanalysis*, 2011, **23**, 1842.
38. Q. Yi, F. Niu, W. Yu, *Thin Solid Films*, 2011, **519**, 3155.
39. G. P. Jin, J. Li, X. Peng, *J. Appl. Electrochem.*, 2009, **39**, 1889.
40. C. Batchelor-McAuley, C. E. Banks, A. O. Simm, T. G. J. Jones, R. G. Compton, *Analyst*, 2006, **131**, 106.
41. F. Li, B. Zhang, S. Dong, E. Wang, *Electrochim. Acta*, 1997, **42**, 2563.
42. N. Maleki, A. Safavi, E. Farjami, F. Tajabadi, *Anal. Chim. Acta*, 2008, **611**, 151.
43. J. Liu, W. Zhou, T. You, F. Li, E. Wang, S. Dong, *Anal. Chem.*, 1996, **68**, 3350.
44. J. P. Metters, F. Tan, R. O. Kadara, C. E. Banks, *Anal. Methods*, 2012, **4**, 1272.
45. J. P. Metters, F. Tan, R. O. Kadara, C. E. Banks, *Anal. Methods*, 2012, **4**, 3140.
46. J. Panchompoo, L. Aldous, C. Downing, A. Crossley, R. G. Compton, *Electroanalysis*, 2011, **23**, 1568.
47. B. Haghighi, H. Hamidi, S. Bozorgzadeh, *Bioanal. Chem.* , 2010, **398**, 1411.

48. M. W. Breiter, *J. Electroanal. Chem.*, 1980, **109**, 253.
49. G. Mengoli, M. Fabrizio, C. Manduchi, G. Zannoni, *J. Electroanal. Chem.*, 1993, **350**, 57.
50. H. L. L. D. J. Guo, *J. Coll. Int. Sci.*, 2005, **286**, 274.
51. J. Horkans, *J. Electroanal. Chem.*, 1980, **106**, 245.
52. M. Enyo, *J. Electroanal. Chem.*, 1982, **134**, 75.
53. R. V. Bucur, F. Bota, *Electrochim. Acta*, 1981, **26**, 1653.
54. J. McBreen, *J. Electroanal. Chem.*, 1990, **287**, 279.
55. L. D. Burke, J. K. Casey, *J. Appl. Electrochem.*, 1993, **23**, 573.
56. C. Batchelor-McAuley, C. E. Banks, A. O. Simm, T. G. J. Jones, R. G. Compton, *ChemPhysChem*, 2006, **7**, 1081.
57. Q. Schiermeier, *Nature*, 2006, **439**, 128.
58. J. Li, J. Zhang, Y. Shou, S. Shuang, C. Dong, M. M. D. Choi, *Electrochim. Acta*, 2012, **76**, 288.

CHAPTER 4

ELECTROANALYTICAL PROPERTIES OF SCREEN PRINTED SHALLOW RECESSED ELECTRODES.

4.1 Abstract

This chapter reports the fabrication of novel carbon based screen printed disc-shaped recessed electrodes (250 µm radius) which are electrochemically characterised and contrasted to other screen printed sensors previously reported upon within the literature. In these circumstances, the electrode is fabricated entirely through screen printing and the electrode geometry is defined by the dielectric (inert polymer) producing shallow recessed electrodes. In comparison to co-planar carbon screen printed electrodes, the shallow recessed screen printed electrodes exhibit a greater current density over the former. The potential electroanalytical applications of these carbon based disc-shaped shallow recessed electrodes are explored through the sensing of NADH and nitrite exhibiting analytically relevant limits of detection (3σ) of 5.2 and 7.28 µM respectively. Additionally, the electroanalytical sensing of nitrite is further trialled in a canal water sample demonstrating the robust nature of the sensors analytical performance. Furthermore we explore the potential improvement of the shallow recessed electrodes through the fabrication of pentagon-shaped carbon based shallow recessed electrodes, which are compared and contrasted with shallow recessed disc electrodes towards the electroanalytical sensing of manganese (II); this to be the first example of such an electrode geometry. In comparison of the observed current density the disc-shaped shallow recessed electrode offers greater sensitivity over co-planar screen printed electrode, whilst in addition to this, a pentagon-shaped recessed electrode offers improved sensitivity over even that of the disc-shaped shallow recessed screen printed electrode. The ultra-low nM sensing of manganese (II) is shown to be possible at both the disc and pentagon shallow recessed electrodes exhibiting limits of detection (3σ) found to correspond to 63 and 36 nM

respectively. Both the disc and pentagon-shaped shallow recessed screen printed electrodes are determined to offer greater analytical sensitivity as determined within this study and in comparison with previous literature using graphitic electrodes. The fabrication methodology of the shallow recessed electrodes is shown to be generic in nature such that the underlying carbon layer, which defines the composition of the shallow recessed working electrode, can be replaced with electrocatalytic surfaces. This is demonstrated with the fabrication of platinum disc-shaped shallow recessed screen printed electrodes, which are electrochemically characterised and explored towards the sensing of hydrazine and hydrogen peroxide displaying limits of detection (3σ) of 26.3 and 44.3 μM respectively, which are found to be analytically useful.

4.2 Introduction

Electrochemists are forever exploring new approaches to improve mass transport of the target analyte towards the electrode surface which consequently influences the observed electrochemical response. One such approach to improve mass transport is to use microelectrodes which have unique features of high mass flux, low ohmic drop, steady-state currents and minimal stirring dependence characteristics which are highly important with regard to the development of practical electrochemical sensors.[1] The advantages offered by an electrochemical sensor which incorporates a microelectrode and consequently steady-state behaviour are: greater analytical sensitivities, increased current densities, and improved signal-to-noise ratios[2] which ultimately lead to enhancements in the electroanalytical performance towards the target analyte.[3, 4] Various approaches have been reported for the fabrication of microelectrodes such as photolithography and sealing wires within glass. Another approach is the screen printing of microelectrodes which have the advantage of reproducibility, simplicity and ability to produce *en mass* at a low production cost; recently, Kadara and co-workers have reported the fabrication of screen printed microelectrodes, producing microelectrodes with radii of 60 to 100 μm.[5] Related to microelectrodes are recessed electrodes, which reach steady-state responses faster than their co-planar counterparts due to the confinement of the diffusion layer by the recess.[4, 6, 7] Thus it is easier and faster to achieve a sigmoidal response at a recessed microelectrode configuration over a coplanar microelectrode configuration which has the same disc size and geometry.[8]

Varying fabrication approaches have been reported for the fabrication of recessed electrodes. One approach towards screen printed microelectrode arrays has reported the coating of screen printed electrodes with polymeric films. These are then subjected to sonochemical ablation producing a random ensemble of microelectrodes, albeit with a large size distribution,[4] which are also irregularly shaped and distorted which is likely to hamper

the reproducibility between sensors from the same batch.[9, 10] Another approach is the screen printing of a carbon layer onto which an inert material is placed, which is laser ablated to produce micron sized holes which expose the underlying screen printed carbon surface.[11] However, problems may be encountered between sealing the patterned material to the carbon layer leading to leakages of the solution media resulting in loss of microelectrode behaviour and giving irreproducible results within and between batches. Other approaches involve patterning inert material *in situ* but this can change the microstructure of the underlying carbon surface, ultimately affecting the electrochemical performance of the sensor. Note in these examples, since the dielectric (inert polymer) layer defines the working electrode geometry, shallow recessed electrodes will be realised. As noted above, this can provide beneficial enhancements in mass transport. Consequently, in this chapter, the fabrication of carbon based shallow recessed screen printed electrodes are presented, one disc shaped with a working electrode of 250 μm radii, the other a pentagon with a working electrode width of 50 μm where in both configurations the screen printed dielectric (inert polymer) layer defines the working electrode geometry. The shallow recessed screen printed electrodes were first optically and electrochemically characterised, and consequently trialled towards the detection of two key analytes of interest, NADH and nitrite. We demonstrate that this can be extended to other electrodes of various surface materials, such as in the case of platinum discshaped shallow recessed screen printed electrodes which are explored towards the sensing of analytically useful analytes. The concept could easily be extended to other metallic surfaces such as gold, palladium, copper and so-on, and is only limited by the availability of commercially available inks.

4.3 Results and Discussions

Disc-shaped shallow screen printed recessed electrodes Disc-shaped recessed screen printed electrode (drSPE) were first fabricated as described in the Experimental section, by primarily printing a carbon layer with contacts and contact pad onto a plastic substrate (see Fig. 4.1A). Following curing in an oven, an insulating dielectric layer was screen printed over the initial carbon layer. The dielectric (inert polymer) defines the microelectrode size exposing the screen printed carbon surface below. The advantage of this technique over previous reports is that the dielectric is cured in the oven which allows efficient bonding of the insulating dielectric to the underlying carbon surface. Note that an additional carbon counter and a silver/ silver chloride reference electrodes are also incorporated onto this electrochemical sensing platform for ease of use (see Fig. 4.1A). Fig. 4.1 shows the overall configuration of the drSPE forming the single-shot, disposable 3 electrode system, consisting of a carbon recessed working electrode (250 ± 6 μm radius), carbon counter electrode and silver/silver chloride reference electrode, which are all housed upon the same sensor. Fig. 4.1B is an optical microscope image obtained at the drSPE which shows that a well-defined recessed electrode is present, though it is also clear that some migration of the non-conductive dielectric layer occurs during fabrication resulting in a non-uniform disc shape.

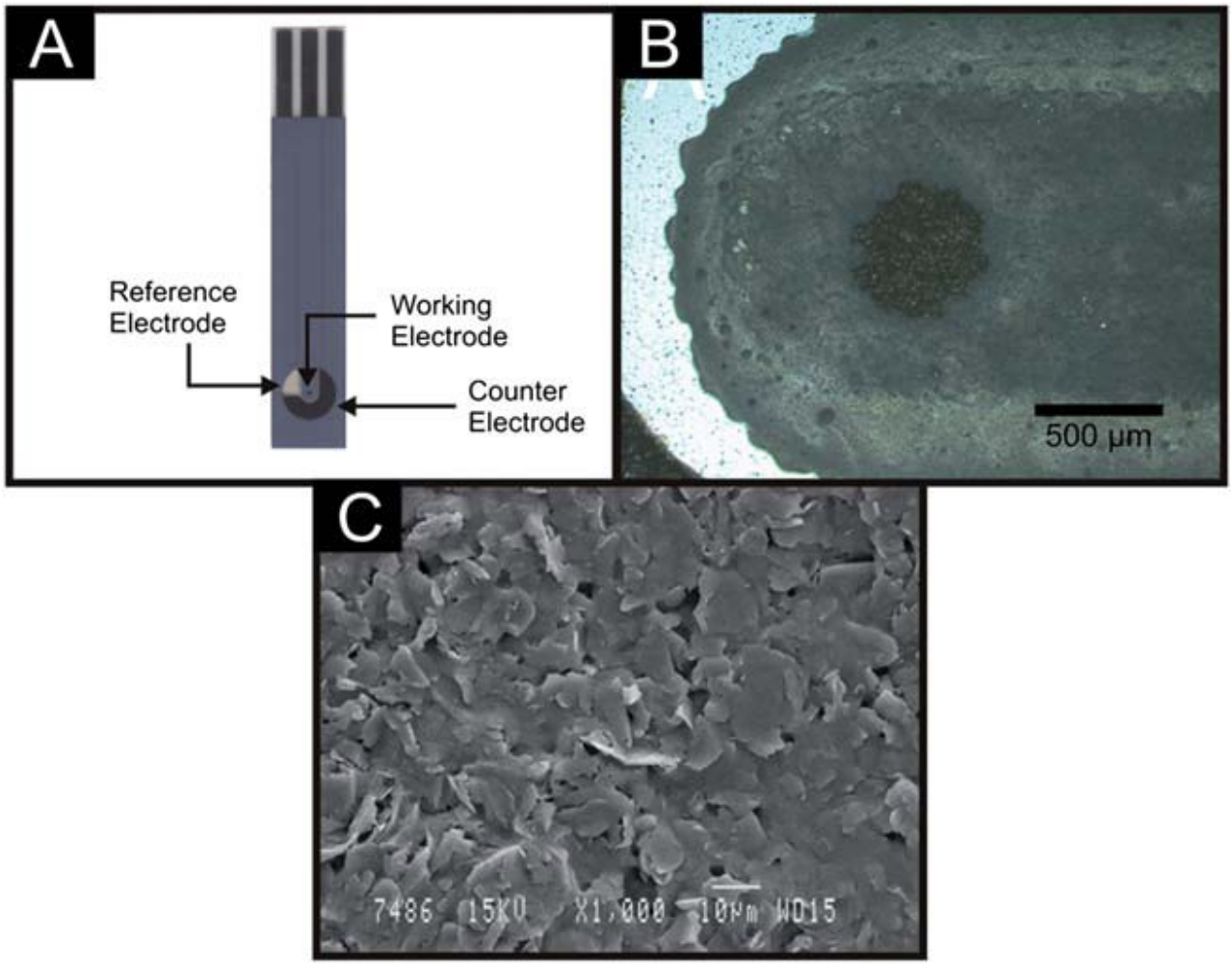

Figure 4.1: A single recessed screen printed electrode (drSPE; working area: 500 µm) **(A)**, an image of the drSPE obtained using an optical microscope (x5 magnification) **(B)**, SEM analysis of the drSPE working electrode (x1000 magnification) **(C)**.

Also presented in Fig. 4.1C is the SEM image obtained at the carbon based drSPE examining the working electrode area depicting a typical carbon–graphite structure as previously reported.[12] Since the dielectric defines the working electrodes geometry, the resulting electrode is naturally recessed with a depth of 4 microns, as reported similarly by Kadara *et al*. for a screen printed recessed array.[13] Electrochemical characterisation of the rSPE's was carried out using the common redox probe hexaammine-ruthenium (III) chloride. First, the effect of scan rate in 1 mM hexaammine ruthenium(III) chloride was studied at the drSPE as shown in Fig. 4.2, where it is readily evident that at slow scan rates a steady-state type

response is observed where upon faster scan rates, the voltammetric profile becomes peak shaped. Such responses are expected at a shallow recessed electrode where steady-state behaviour is reached faster than their non-recessed counterparts due to confinement of the diffusion layer by the recess.[14]

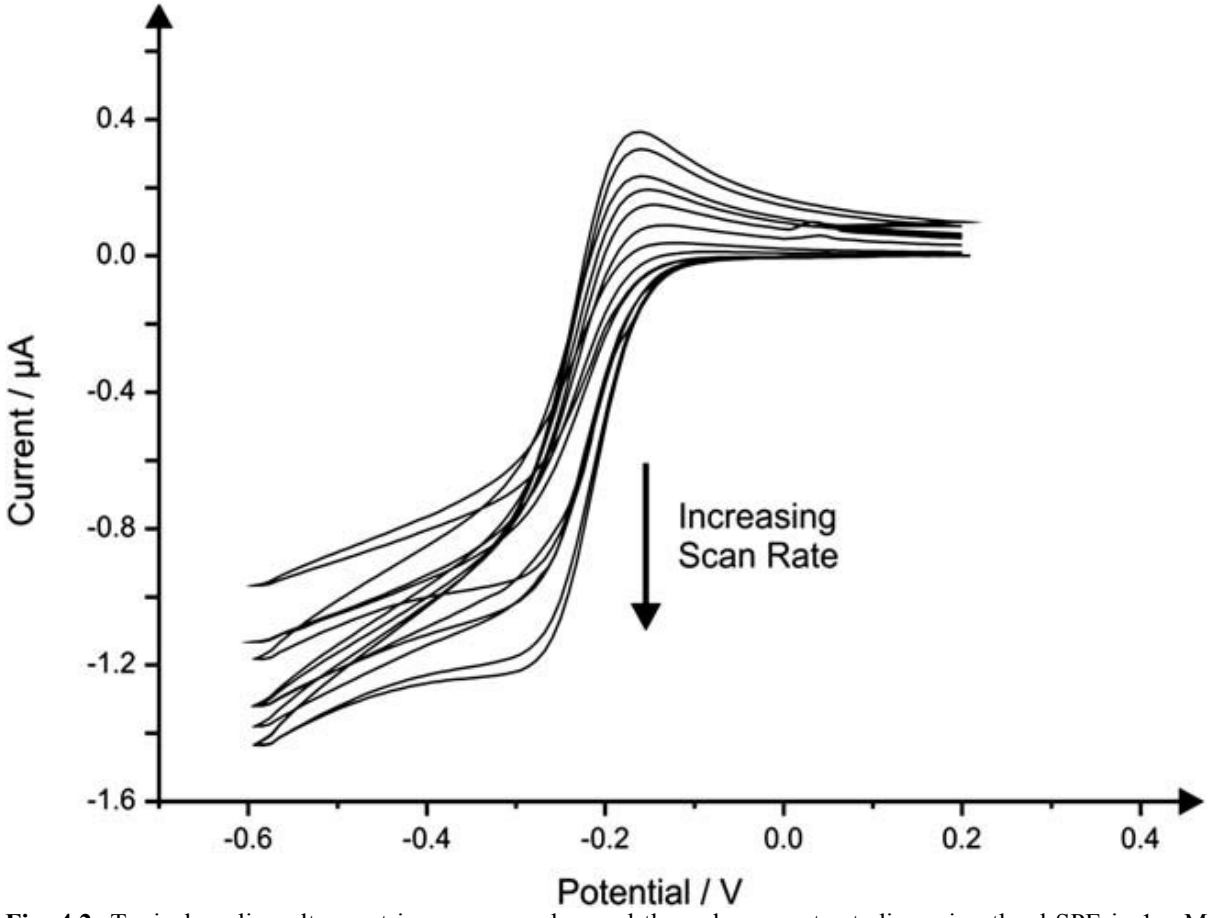

Fig. 4.2: Typical cyclic voltammetric responses observed through scan rate studies using the drSPE in 1 mM hexaammine-ruthenium (III) chloride/0.1M KCl. Scan rates: 5–200 mV s^{-1}.

In addition the effect of scan rate (*viz*. Fig. 4.2) through observation of the voltammetric peak height, plotted as peak current (I_P) against square root of the applied scan rate over the range 5-200 mV s^{-1} was found to be linear ($I_P/\mu A$ = *-0.0269 µA/(µM) + 1.0737 µA*) confirming a diffusional process. The expected limiting current (I_L^{Recess}) at a shallow recessed electrode can be estimated from:[15, 16]

$$I_L^{Recess} = 4\pi nFDC\left(\frac{r^2}{4L + \pi r^2}\right) \quad (4.1)$$

where, n is the number of electrons involved in the redox reaction, F and D represent the Faraday constant and the diffusion coefficient (9.1 x 10^{-6} cm^2 s^{-1})[17-19] respectively, r the radius of the microdisc (cm), C the bulk concentration (mol cm^{-3}) and L is the depth of the electrode recession (cm). The theoretically expected current observed at the drSPE can be estimated from equation (4.1) to correspond to 1.46 μA which agrees well with the experimentally observed value in 1 mM hexaammine-ruthenium(III) chloride in 0.1 M KCl of 7.69 μA (at 5 mV s^{-1}). This deviation between the experimental and calculated value is likely due to the electrode geometry being departed from that of a true microelectrode. Another useful approach is to explore the concept of fabricating recessed microelectrode arrays.[4]

During the fabrication process, the electrodes are produced upon a single sheet and are individually cut prior to use. One approach is to cut these in such a way that, say, three recessed electrodes are kept together to form a single sensor strip which comprises three recessed electrodes in an array. The potential application of an array comprising differing numbers of the drSPE (N = 3 and 5) was explored, initially through the characterisation of the arrays once again in 1 mM hexaammine-ruthenium (III) chloride to allow for comparison. Little improvement (peak current) was observed through the implementation of an array of increasing working electrode numbers in terms of current density plots. In order for the array to function properly, that is, ensure diffusional interaction between working electrodes is negligible, a minimum geometric distance between working electrodes is required, defined as $d_{required}$;[14]

$$d_{required} = 10.86 + 6.218 \exp\left(-\frac{L+0.0888}{0.222}\right) + 9.435 \exp\left(-\frac{L+0.0888}{0.492}\right) \qquad (4.2)$$

where $L = L_{recess}/r$ and where L is in the range $0 \leq L \leq 5$. Thus, the $d_{required}$ is found to correspond to 22.35, where $d_{required}$ is measured in units of r, resolving the $d_{required}$ to be 5.59

mm. In our experimental case, the centre-to-centre distance corresponds to 6 mm which is not significantly larger than $d_{required}$, the minimum distance between working electrodes, and hence an overlap of the diffusional zones of each of the shallow recessed working electrodes occurs which is in line with our experimental observations. Another approach would be to 'miss-out' every other working electrode, but the overall sensor size would then become excessive. Consequently, the decision was made to utilise the single drSPE only for further electroanalytical applications.

Next the drSPE was explored towards the sensing of the key analyte NADH; an analyte of great interest because it is used prolifically as the basis of over 300 biosensors.[20-24] For example, NADH-dependent dehydrogenases catalyse the oxidation of compounds such as ethanol and lactic acid.[25] The electroanalytical sensing of NADH was first explored with cyclic voltammetry using the drSPE. Fig. 4.3 depicts typical cyclic voltammetric responses resulting from additions of NADH into a solution of pH 7 phosphate buffer over the range 10 to 90 μM. Clearly an oxidation wave is observed upon addition of NADH into the phosphate buffer at ~+0.45 V (vs. Ag/AgCl). Note that a wave is observed at the drSPE rather than a well-defined peak which is commonly observed at co-planar electrodes due to the change in mass transport characteristics occurring at the drSPE. Upon increasing concentration of NADH using the drSPE an increase in the peak height (μA) for the oxidation of NADH (+0.45 V (vs. Ag/AgCl)) can be observed over the entire analytical range whilst demonstrating linearity ($I/\mu A = 4.73 \times 10^{-4}\ nA/\mu M - 3.09 \times 10^{-3}\ \mu A;\ R^2 = 0.99,\ N = 9$) throughout (see Fig. 4.3B). The response obtained for the detection of NADH was further compared and contrasted towards that of a more traditional graphite based screen printed co-planar macro electrode, with a working electrode area of 3 mm in diameter (previously reported in ref. [6, 12, 26]), over the previously studied analytical range (10 to 90 μM) using current density plots. As is shown in Fig. 4.4, a comparison of current density plots for the

drSPE and traditional macro electrode demonstrates the much greater current per cm^2 realised at the drSPE opposed to that obtained at the more traditional co-planar macro electrode. Comparison of the slopes for the two contrasting calibration plots for the sensing of NADH provides an insight into the much improved sensitivity towards the detection of NADH offered through the utilisation of the drSPE, with typical slopes obtained for the drSPE and traditional macro electrode being 6.6 and 2.42 x 10^{-4} μA M^{-1} respectively. Such values demonstrate the drSPE's enhanced efficiency per area of electrode in comparison to that of the traditional macro electrode. Returning to the drSPE, the limit of NADH detection (3σ) at the drSPE was determined to correspond to 5.2 μM. Such a detection limit highlights the analytical applicability of the drSPE, when compared to previous studies utilising differing electrode configurations, for example chemically reduced graphene oxide modified glassy carbon electrode has been used for the sensing of NADH with a reported limit of detection of 10 μM.[27]

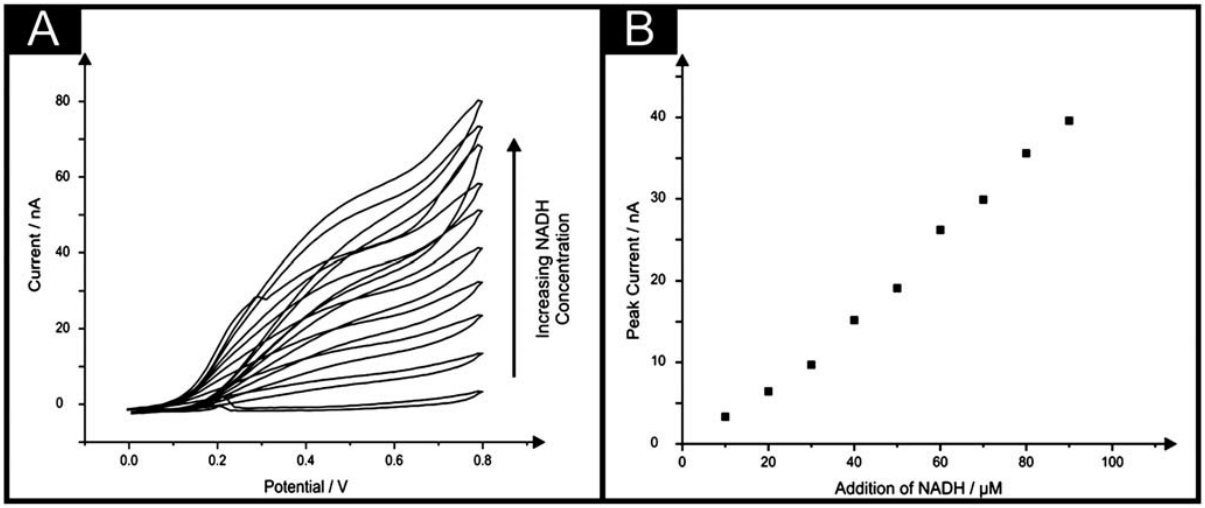

Fig. 4.3: Typical cyclic voltammetric responses **(A)** and the corresponding calibration plot **(B)** resulting from additions over the range 10 to 90 μM of NADH into a phosphate buffer (pH 7) using the drSPE. Scan rate: 50 mV s^{-1}.

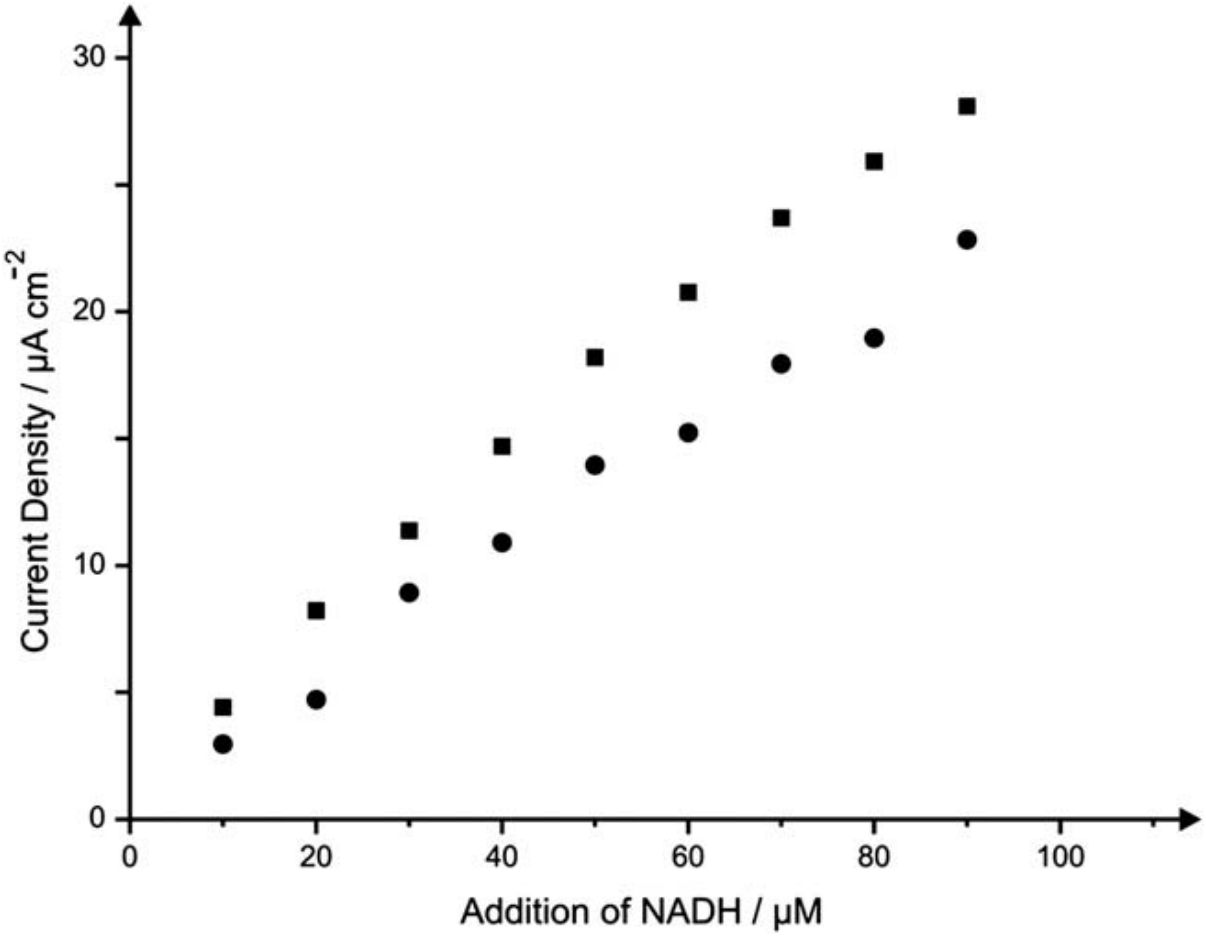

Fig. 4.4: An overlay of typical current density calibration plots resulting from cyclic voltammetric measurement of additions of NADH into a phosphate buffer over the range of 10 to 90 µM using the drSPE (squares) versus a standard 3 mm diameter co-planar SPE (circles).

Lower limits of detection have however been reported recently, for example at a graphite screen printed microband where a limit of detection of 0.48 µM has been reported![28] A detailed listing of NADH detection at various electrode configurations has been recently compiled.[28] Although many of the reported techniques do offer lower limits of NADH detection, it is worth noting that it is also a requirement that laborous pre-treatment and preparation of the electrodes is also often required, a hurdle negated through the use of the drSPE. Upon finding that the drSPE offered competitive limits of detection for the sensing of NADH, and furthermore, improved sensitivity over a traditional macro electrode, the applicability of the drSPE towards analytical sensing of nitrite was undertaken. The excess uptake of nitrite can cause gastric cancer[29] and it is therefore necessary to develop a reliable

and sensitive sensor to detect nitrite in food, drinking water and environmental samples. Several techniques have been developed for nitrite determination, including spectrophotometry,[30] chemiluminescence,[31] chromatography[32] and capillary electrophoresis.[33] However, these methodologies usually have tedious detection procedures and therefore are time-consuming. Compared to these methods, the electrochemical methods can provide cheaper, faster and real-time analysis and thus have attracted more attention.[34] As is clear from Fig. 4.5, cyclic voltammetric measurement of nitrite added to a pH 7 phosphate buffer at the drSPE results in an oxidation wave at ~+0.6 V (vs. Ag/AgCl). Consequently the sensing of nitrite over the range 100 to 1000 μM in a pH 7 phosphate buffer was trialed at a drSPE; pH 7 was selected for analysis as it is the most likely pH value in which nitrite sample would be encountered.[35] Fig. 4.5 shows typical cyclic voltammograms for the sensing of nitrite over the analytical range, with the corresponding calibration plot (I/μA = 1.2 x 10^{-3} μA/μM - 1.46 x 10^{-2} μA; R^2 = 0.99, N = 10). As is evident excellent linearity is possible through the utilisation of the drSPE over the entire analytical range. The sensing of nitrite at both the drSPE and a traditional macro screen printed sensor was compared and contrasted through the comparison of current density plots for both electrodes resulting from additions of nitrite over the range 100 to 1000 μM. As shown in Fig. 4.6, a comparison of current density plots for the drSPE and traditional macro electrode demonstrates the much greater current per cm^2 realised at the drSPE opposed to that obtained at the more traditional macro electrode. Once more, comparison of the slopes for the two contrasting calibration plots for the sensing of nitrite provides an insight into the vastly improved sensitivity towards the detection of nitrite offered through the utilisation of the drSPE, with typical slopes obtained for the drSPE and traditional macro electrode being 0.5 and 3.49 x 10^{-7} μA M^{-1} respectively. Such values demonstrate the drSPE's enhanced efficiency per area of electrode in comparison to that of the traditional co-planar macro electrode. The limit of detection (3σ) for nitrite using the

drSPE within this phosphate buffer solution was determined to equate to 7.28 µM. Previously, composite copper electrodes modified with carbon powder and epoxy resin have been utilised for the sensing of nitrite; with a limit of detection claimed to be 600 µM.[36]

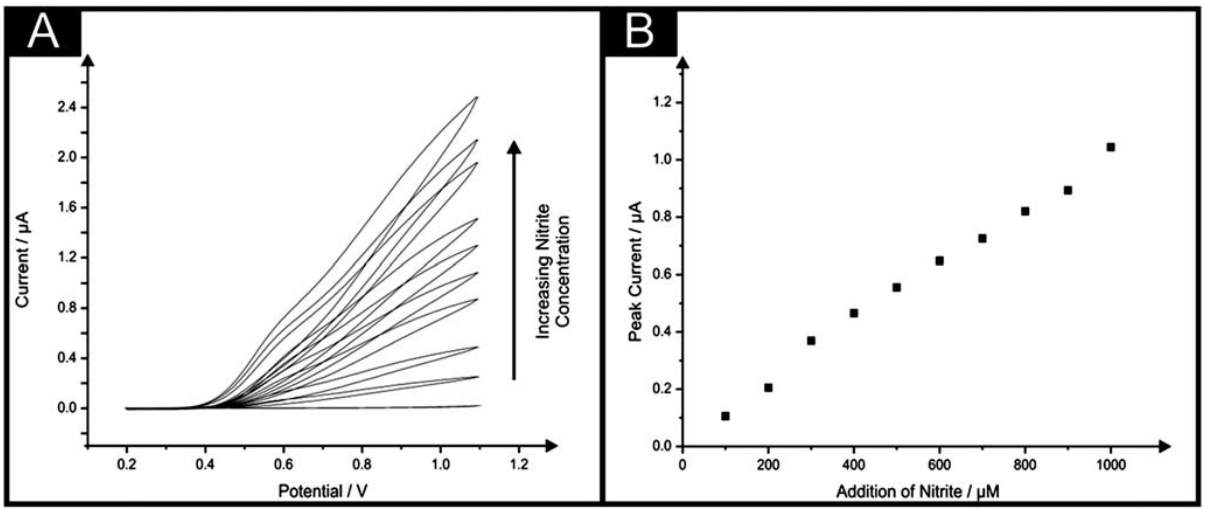

Fig. 4.5: Typical cyclic voltammetric responses **(A)** and the corresponding calibration plot **(B)** resulting from additions of nitrite into a phosphate buffer (pH 7) using the drSPE; additions were made over the range 100 to 1000 µM. Scan rate: 50 mV s^{-1}.

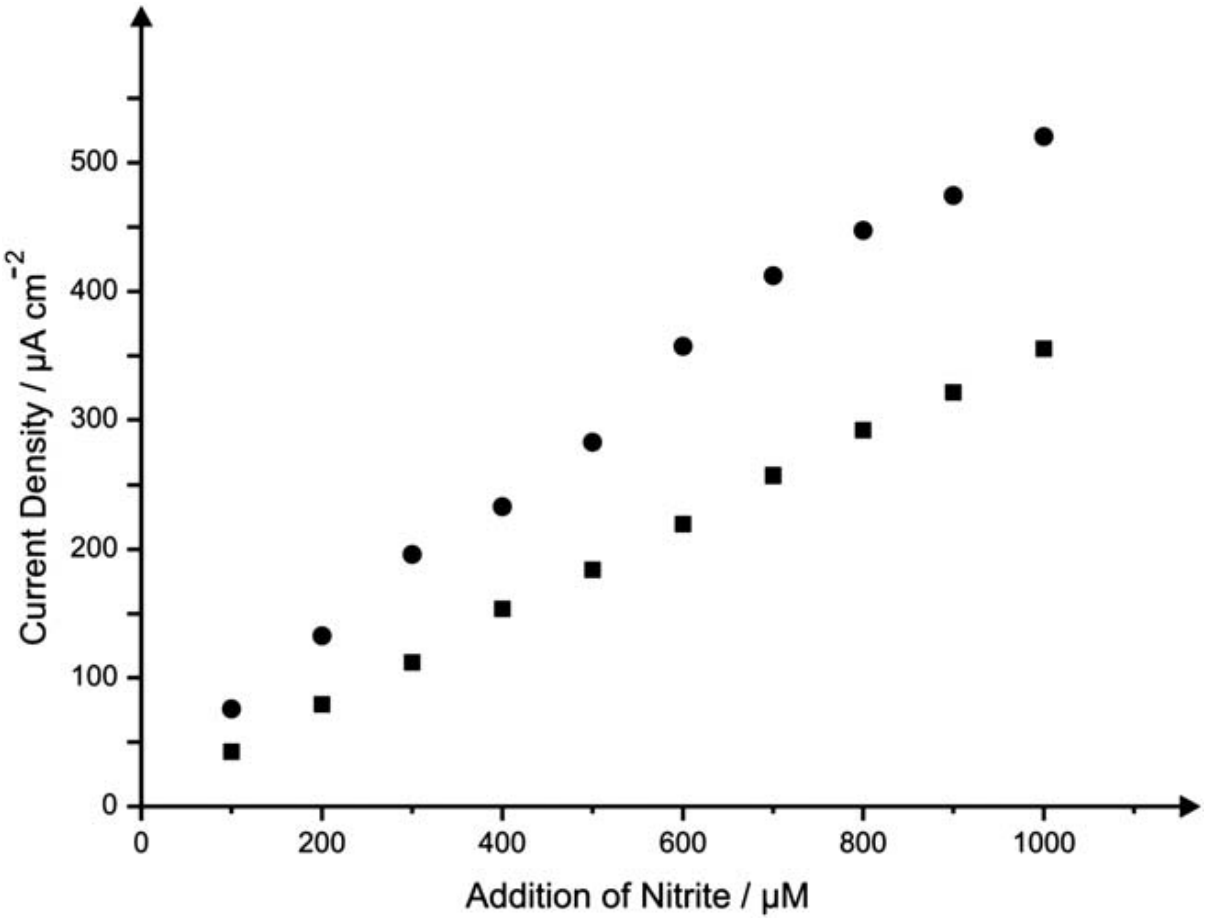

Fig. 4.6: An overlay of typical current density calibration plots resulting from cyclic voltammetric measurement of additions of nitrite into a phosphate buffer over the range of 100 to 1000 µM using the drSPE (circles) versus a standard 3 mm diameter SPE (squares).

Other reports such as that by Chen *et al*.[37] utilising a nanodiamond powder electrode state a nitrite limit of detection of 120 µM. Again it has been noted that, as with the sensing of NADH, lower limits of detection have been reported at other electrode configurations, for example 0.05 µM at a glassy carbon modified with $CuPtCl_6$ film.[38] Next the feasibility of the analytical protocol towards the accurate determination of nitrite within a true environmental sample was determined. Additions of nitrite, over the range 100 to 1000 µM, were made into a canal water sample (collected and prepared as detailed within the Experimental section) with cyclic voltammetric measurements made. As is evident through the corresponding calibration plot for the sensing of nitrite in a canal water sample (I/µA = 2.807 x 10^{-1} µA/µM + 13.864 µA; R^2 = 0.99, N = 10; see Fig. 4.7) which is compared with a typical calibration

recorded in ‘ideal’ conditions, a reduction in the sensitivity of the sensor occurs, likely thought to be due to contaminants present within the sample. These could be biological in nature. It is however not copper since this needs to be reduced to Cu^0 metal which occurs only at negative potential.

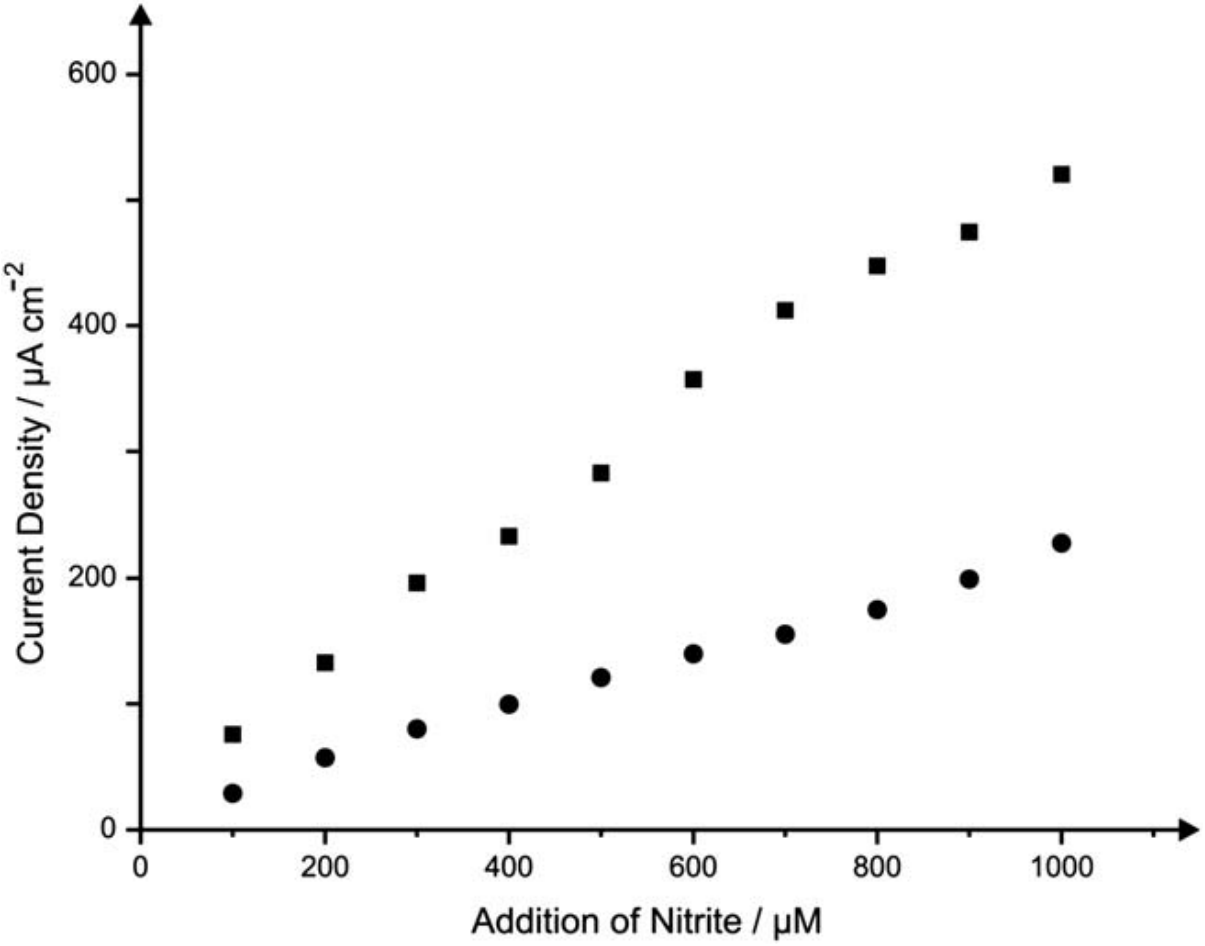

Fig. 4.7: An overlay of typical current density calibration plots resulting from cyclic voltammetric measurement of additions of nitrite into a phosphate buffer (squares) and a canal water sample (circles) over the range of 100 to 1000 µM using the drSPE.

Although it has been ascertained that there is a reduction in the sensitivity of the sensor when applied to the determination of nitrite in canal water samples, the detection of nitrite within the environmental sample was still possible over the entire range studied, with a limit of detection (3σ) for nitrite within the canal water sample corresponding to 43.6 µM.

Platinum disc-shaped screen printed shallow recessed electrodes

To further explore the potential applications of the shallow recessed screen printed electrodes, further drSPE were fabricated utilising a platinum polymer paste as the working electrode (as described in the Experimental section). The platinum drSPE (denoted throughout as PtdrSPE), of the same form as the carbon based drSPE, were utilised for the detection of two analytes of great interest; hydrazine and hydrogen peroxide. We have previously reported on the utilisation of a platinum based macro screen printed electrode (PtSPE) for the sensing of these two key analytes;[39] thus consequential studies at the PtdrSPE would allow definitive comparisons between the two electrodes to determine if the recessed electrode possessed beneficial characteristics. The PtdrSPEs were first electrochemically characterised using the redox probe potassium hexachloroiridate(III). Firstly, scan rate studies were performed using the PtdrSPE in 1 mM potassium hexachloroiridate(III) in 0.1 M KCl (see Fig. 4.8), where observation of voltammetric peak height, plotted as peak current (I_P) against square root of the applied scan rate over the range 5-200 mV s^{-1} was found to be linear $(I_P/\mu A = 3.37 \times 10^{-2}\ \mu A/(\mu M) + 2.89 \times 10^{-1}\ \mu A$ confirming a diffusional process. Again sigmoidal responses are observed at slow scan rates, with peak-shaped responses at faster scan rates as seen previously at the drSPE. The model analyte, hydrazine, previously reported at a platinum based screen printed electrode[39] was selected for the cyclic voltammetric studies using the PtdrSPE. The sensing of hydrazine was attempted over the analytically relevant concentration range of 50 to 500 μM.

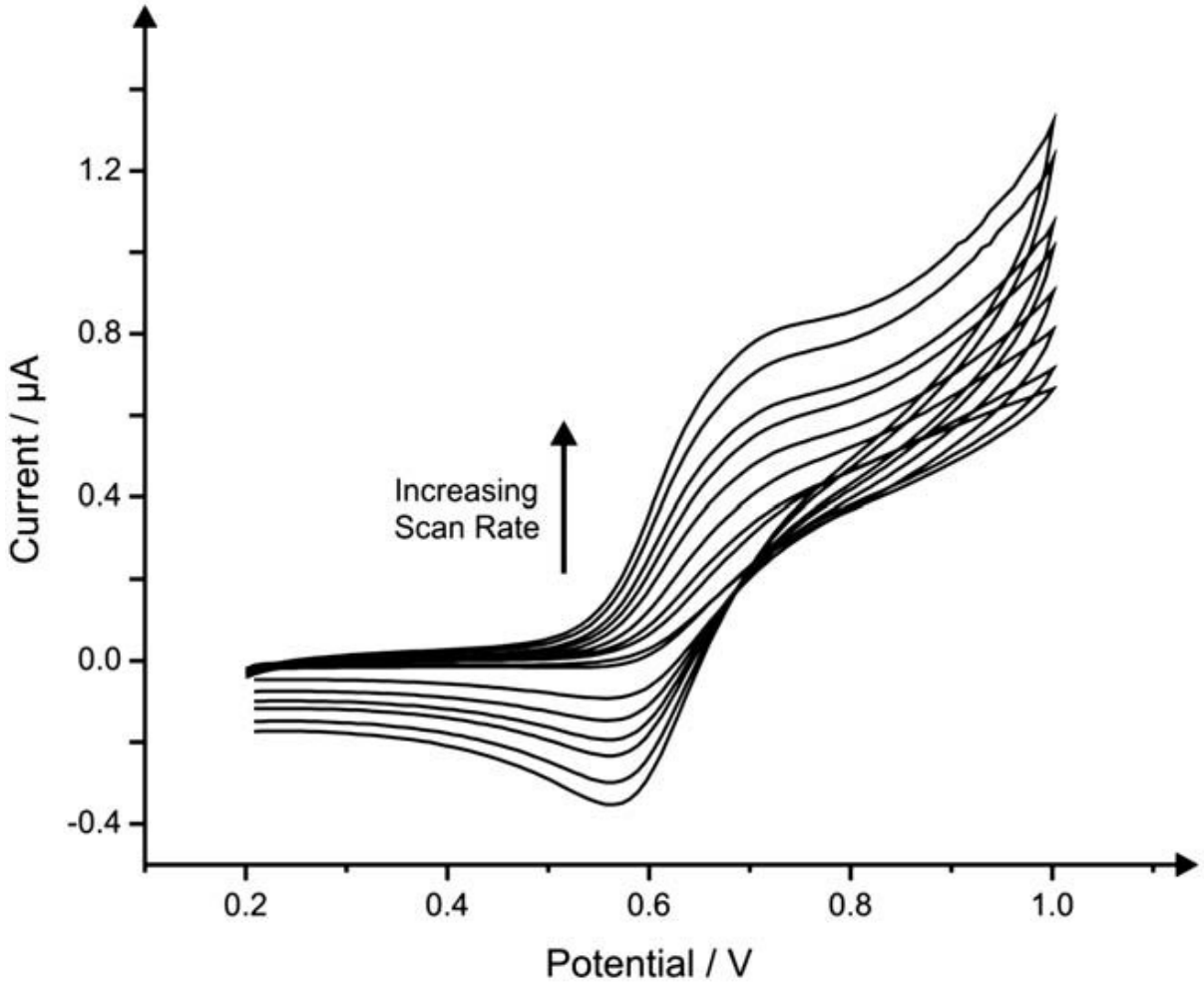

Fig. 4.8: Typical cyclic voltammetric responses observed through scan rate studies using the PtdrSPE in 1 mM potassium hexachloroiridate (III)/0.1M KCl. Scan rates: 5–200 mV s^{-1}.

Fig. 4.9A depicts the cyclic voltammetric response for additions of hydrazine to a pH 5 phosphate buffer solution. As is clear the oxidation of hydrazine is seen to occur at ~+0.4 V (vs. Ag/AgCl), with the resulting wave increasing in peak height ($I_P/\mu A$) at increasing hydrazine concentration over the entire analytical range. The corresponding calibration plot of peak current (I_P) versus concentration (µM) was found to be linear (I/µA = 1.31 x 10^{-2} µA/µM + 5.62 x 10^{-1} µA; R^2 = 0.99, N = 10) exhibiting a limit of detection (3σ) of 26.3 µM. The PtdrSPE was then further utilised for the sensing of hydrazine in a pH 7 phosphate buffer solution using chronoamperometry through holding the potential at +0.5 V (vs. Ag/AgCl) for 120 seconds, selected due to the observed oxidation potential of hydrazine at the PtSPE through earlier cyclic voltammetric analysis. Once again, additions were made to the

phosphate buffer solution over the range 50 to 500 μM of hydrazine at both the previously reported PtSPE and the PtdrSPE. Fig. 4.9B depicts a comparison between the PtdrSPE and PtSPE for the sensing of hydrazine in a phosphate buffer solution. As is evident, greater sensitivity is seen at the PtdrSPE over the PtSPE when comparisons are made between the current densities obtained at increasing hydrazine concentration, demonstrating that some improvement is offered at the PtdrSPE over the previously reported PtSPE.[39] Such observations further highlight, as has been found at the drSPE, that the recessed surface of the electrode offers an improved current density over a co-planar electrode of the same material, thus demonstrating that the findings are applicable to differing electrode materials. The determined limit of detection (3σ) at the Pt drSPE were calculated to be 25.1 μM (I/μA = 6.54 x 10^{-1} μA/μM + 9.79 μA; R^2 = 0.99, N = 10). When the limit of detection realised at the PtdrSPE is compared with previous literature reports it can be seen that although lower limits of hydrazine detection are described at alternative electrode configurations such as at carbon paste electrode modified with copper porphyrin (1 μM),[40]

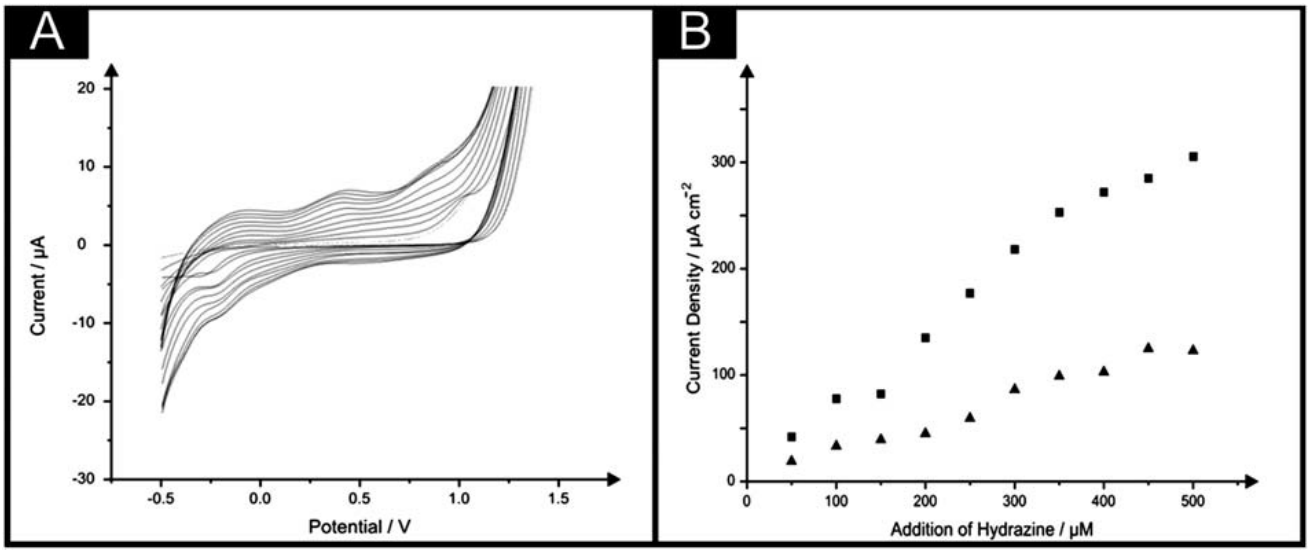

Fig. 4.9: (A) Typical cyclic voltammetric responses resulting from additions of hydrazine into a phosphate buffer (pH 7) (dotted line) at the PtdrSPE; additions made over the range 50 to 500 μM. Scan rate: 50 mV s^{-1}. **(B)** Typical current density calibration plots measured using chronoamperometric measurement (+0.5 V, 120

seconds) for the oxidation of hydrazine, arising from increasing concentrations at the PtdrSPE (squares) and PtSPE (triangles).

iron(III) oxide graphite composite electrodes (1.18 μM)[41] and iron phthalocyanine film upon a gold macro electrode (11 μM),[42] the PtdrSPE offers the unique advantage of being screen printed, with the key attribute of the electrode being the simple configuration with the onboard additions of a reference and counter electrode, in addition to this, no prior treatment of the electrode, nor sample is required with the necessity for potential cycling alleviated as is required in other studies.[43, 44] The PtdrSPE was further utilised for the sensing of hydrogen peroxide, first cyclic voltammetric studies were carried out determining the reduction potential of hydrogen peroxide in a pH 7 phosphate buffer solution to be +0.35 V (vs. Ag/AgCl) in agreement with previous reports.[39] Consequently, chronoamperometric measurements (+0.35 V, 120 s) for the addition of hydrogen peroxide into a pH 7 phosphate buffer solution were obtained over the range 100 to 1000 μM ($I/\mu A = 2.085 \times 10^{-2}\ \mu A/\mu M + 4.066 \times 10^{-4}\ \mu A$; $R^2 = 0.99$, $N = 10$). As with the sensing of hydrazine, the PtdrSPE was found to be much more sensitive for the sensing of hydrogen peroxide in terms of current density, as is depicted in Fig. 4.10.

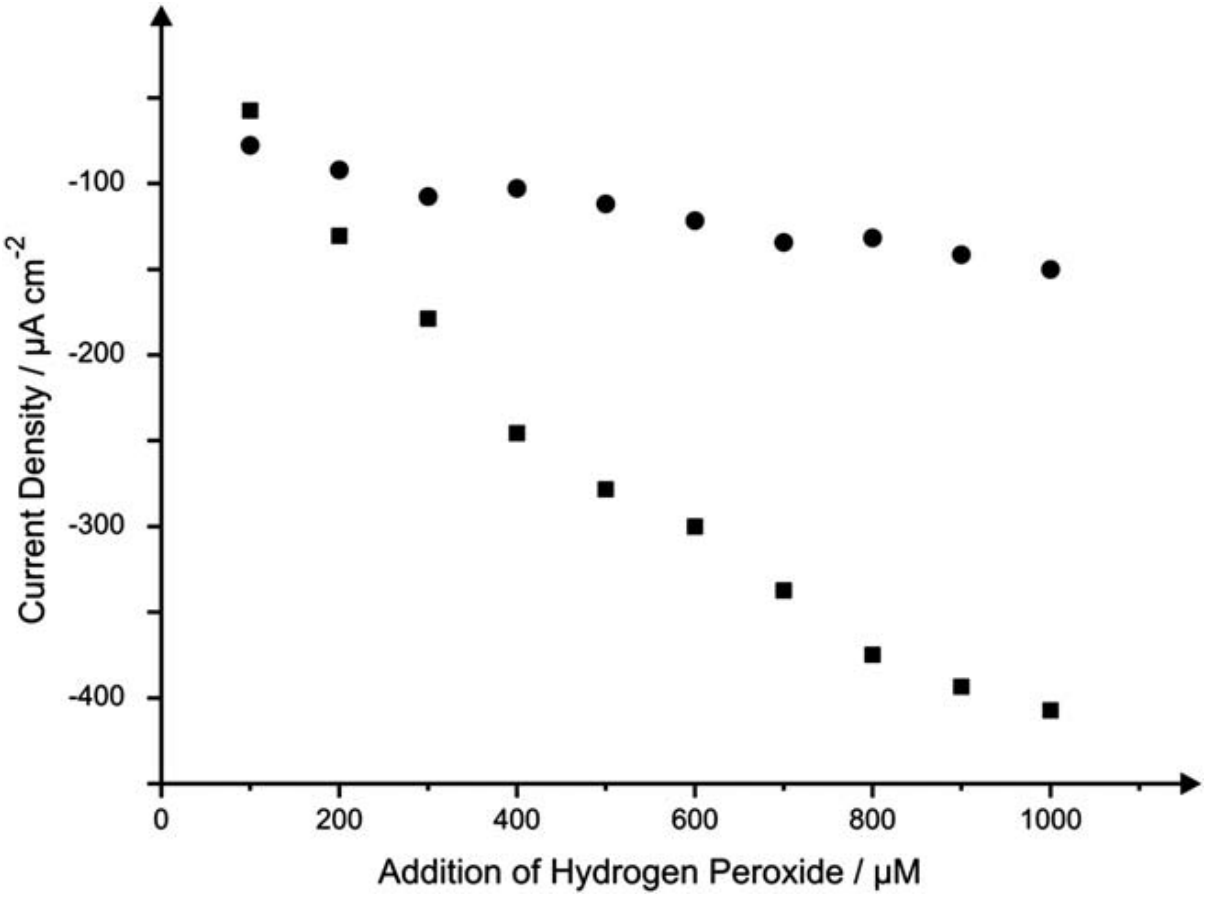

Fig. 4.10: Typical current density calibration plots arising from chronoamperometric measurement (+0.35 V, 120 seconds) of hydrogen peroxide arising from increasing concentrations using the PtdrSPE (squares) and PtSPE (circles).

The determined limit of detection (3σ) at the PtdrSPE was calculated to be 44.3 µM. As was found for the sensing of hydrazine, the limits of detection calculated for hydrogen peroxide at the PtdrSPE are not as low as those reported at differing electrode configurations such as cobalt (II) hexacyanoferrate modified glassy carbon electrode,[45] sol–gel modified glassy carbon[46] and aluminium electrode modified with manganese hexacyanoferrate,[47] but has the potential benefit of being mass produced and single-shot without the requirement of a lengthy fabrication process.

Pentagon-shaped screen printed shallow recessed electrodes

Microsquares have three main modes of diffusion – linear diffusion over the electrode, convergent edge diffusion at the long and the short edges, and point diffusion at the vertices of the electrode; this is depicted in Fig. 4.11.[48] It is this point diffusion at the corners/vertices of the electrode that give rise to enhanced diffusion and hence the move by electrochemists to fabricate square electrodes and utilise the enhancement in mass transport which should ultimately improve the electrochemical response, and in particular electroanalytical performance where the transducer is employed.

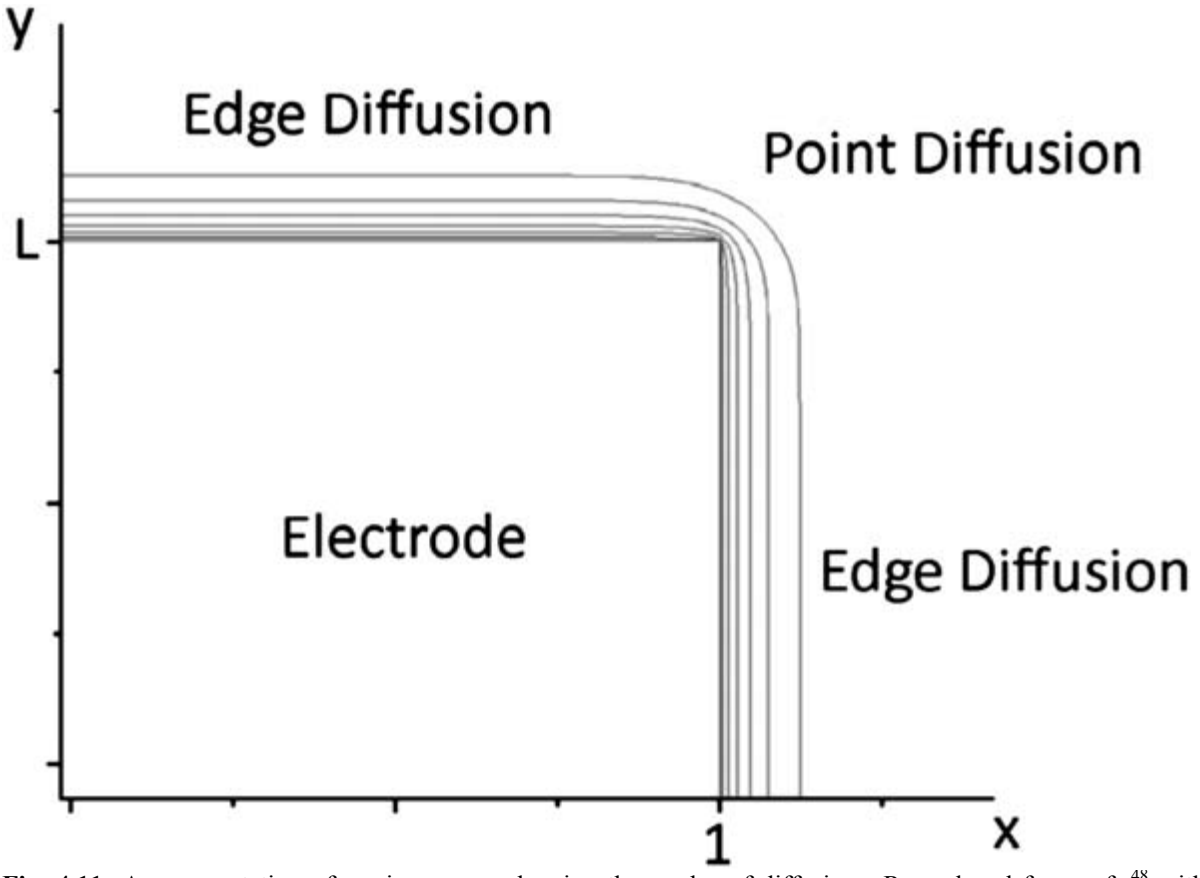

Fig. 4.11: A representation of a microsquare showing the modes of diffusion. Reproduced from ref. [48] with permission of Elsevier.

Indeed it has been shown via numerical simulation[49] that enhanced diffusion at microsquare corners occurs, where the concentration gradients generated are seen to be at their largest.[49] It is here that the current densities are therefore greatest and the diffusion layer is expected to

increase most rapidly with time, faster than at the edge of a microdisc or long edge of a microsquare. Consequently square electrodes have recently been fabricated *via* lithography.[2, 49] An obvious step is then to utilise this point diffusion and make the step from a square, which has four points, to a geometry which has more points and consequently should exhibit even more enhancements in mass transport. Consequently we were inspired to fabricate a pentagon shaped electrode; to the best of our knowledge such an electrode has not yet been reported and will only likely be possible to be fabricated via lithography since the traditional technique of sealing a wire into glass would require a pentagon shaped wire. Here we demonstrate proof-of concept for the fabrication of pentagon-shaped electrodes (prSPE) fabricated entirely via screen printing. The prSPE were fabricated in the same manner as the drSPE (see Experimental section) though the resulting electrode consists of a recessed pentagon-shaped working electrode (45 μm x 45 μm x 45 μm x 35 μm x 25 μm). Presented in Fig. 4.12 are the SEMs obtained for the carbon based prSPE. As is evident, both the drSPE (Fig. 4.1) and prSPE (Fig. 4.12) display the physical properties of a recessed electrode, with the non-conductive layer printed on top of the underlying carbon producing the resultant recess; due to the fabrication approach where the screen define the thickness of the dielectric, the recess is consequently 4 microns resulting in a shallow recessed pentagon shaped screen printed electrode. Note that there is a slight deviation from a true well defined pentagon but approximates well (*viz*. Fig. 4.12). It is important to realise that fabricating a pentagon working electrode in just carbon is not possible with the smallest geometry that can be fabricated being ~100 μm,[28] and as such, to allow smaller electrode geometries to be realised, utilising the dielectric to define the working electrode is the only viable way. The prSPE was characterised using the redox probe hexaammine- ruthenium (III) chloride where the effect of scan rate was explored, the result of which is depicted in Fig. 4.13A. It is readily evident that, as observed with the drSPE, at slow scan rates a steady-state type response is observed where

upon faster scan rates, the voltammetric profile becomes peak shaped. In addition the observed effect of scan rate (Fig. 4.13A) demonstrates that the peak current in hexammine-ruthenium(III) chloride is proportional to the square root of scan rate *($I_P/\mu A$ = -7.315 x 10 $^{-3}$ $\mu A/(\mu M)$ +2.013 x10^{-1} μA)* highlighting a diffusional process.

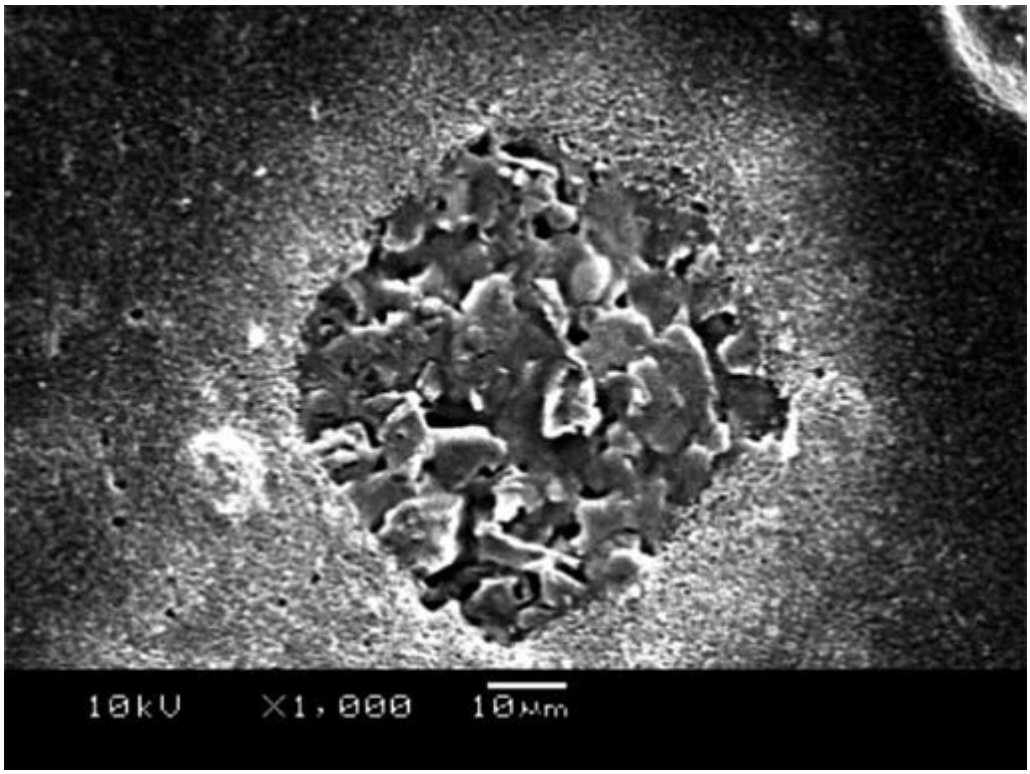

Fig. 4.12: SEM of the prSPE working electrode (x1000 magnification).

Comparison of the responses obtained using the two recessed electrodes (drSPE and prSPE) in terms of current density (μA cm^{-2}) are shown in Fig. 4.13B, clearly demonstrating the apparent superior nature of the prSPE which is due to the large number of points/vertices giving rise to enhanced mass transport. The prSPE was finally assessed for the sensing of manganese (II) and contrasted with analysis at the drSPE. Manganese was chosen as a model analyte since it has been explored at other graphitic based electrodes. In terms of an analytical perspective, manganese is found in tea and is a rich source of dietary manganese.[50] However, there is an analytical need to monitor this due to reports of the neurotoxic effects from chronic exposure to manganese.[51, 52] Though, as described, the toxicity of manganese is rarely

a grave problem, the facile monitoring, and detection of the analyte is still essential. As depicted in Fig. 4.14A, additions of manganese (II) were made into a solution of 0.1 M sodium acetate over the range 73-800 nM at the two recessed electrodes using square wave cathodic stripping voltammetry (E_{dep}= +0.9 V (vs. SCE), 120 s). The sensing strategy is based upon the cathodic stripping voltammetry where the electrode potential is held sufficiently electro-positive for a set accumulation time to form insoluble manganese (IV) dioxide on the electrode surface[53] as described by:

$$Mn^{2+} + 2H_20 \rightarrow MnO_2 + 4H^+ + 2e^- \quad (4.3)$$

The MnO_2 formed upon the electrode surface is then voltammetric stripped by sweeping the potential from positive to negative potential where a stripping peak is observed, giving rise to the electroanalytical signal as depicted in Fig. 4.14A. The resultant calibration plots of manganese concentration versus peak height (I_H) at the drSPE and prSPE (I/μA = 9.988 x10^{-4} μA/μM +1.764 x 10^{-4} μA; R^2 = 0.99, N = 7 and I/μA = 1.01 x 10^{-3} μA/μM + 1.518 x 10^{-16} μA; R^2 = 0.99, N = 7 respectively) are shown in Fig. 4.14B which demonstrate a superior response in terms of peak current is observed at the prSPE as opposed to the drSPE. Such findings are in agreement with the observations made during the electrochemical characterisation of the two recessed electrodes in hexaammine-ruthenium (III) chloride suggesting that the enhancement in point diffusion/mass transport provides benefits in electroanalysis. Linearity is evident at the prSPE from73 to 504 nM with a slight plateau above these manganese (II) concentrations. Respective limits of detection of 63 nM and 36 nM for manganese (II) were determined at the drSPE and prSPE. Such low limits of detection offered by the prSPE highlight the excellent electroanalytical applicability of the recessed electrode and improve even over previous reports at an array of recessed electrodes, which boasted a limit of

detection of 64 nM,[4] which itself was superior over analytical reports such as spectrophotometric techniques[54] and flow-injection with flame atomic absorption spectrometry,[55] and electroanalytical protocols;[56-60] such a response indicates the greater current density observed at the prSPE due to the greater proportion of edges (point diffusion/mass transport), thus highlighting the beneficial utilisation of the prSPE.

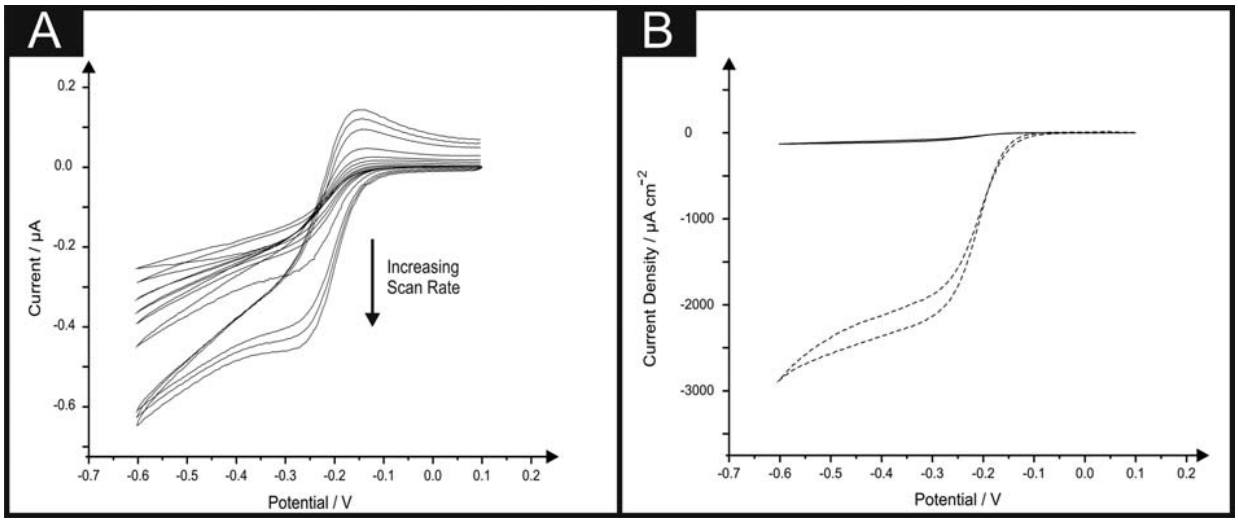

Fig. 4.13: (A) Typical cyclic voltammetric responses observed through scan rate studies using the prSPE in 1mM hexaammine-ruthenium (III) chloride/0.1M KCl. Scan rates: 5–400 mV s^{-1}. **(B)** Comparison between the drSPE (solid line) and prSPE (dashed line) (scan rates of 5 mVs^{-1}) in 1 mM hexaammine-ruthenium (III) chloride/0.1 M KCl.

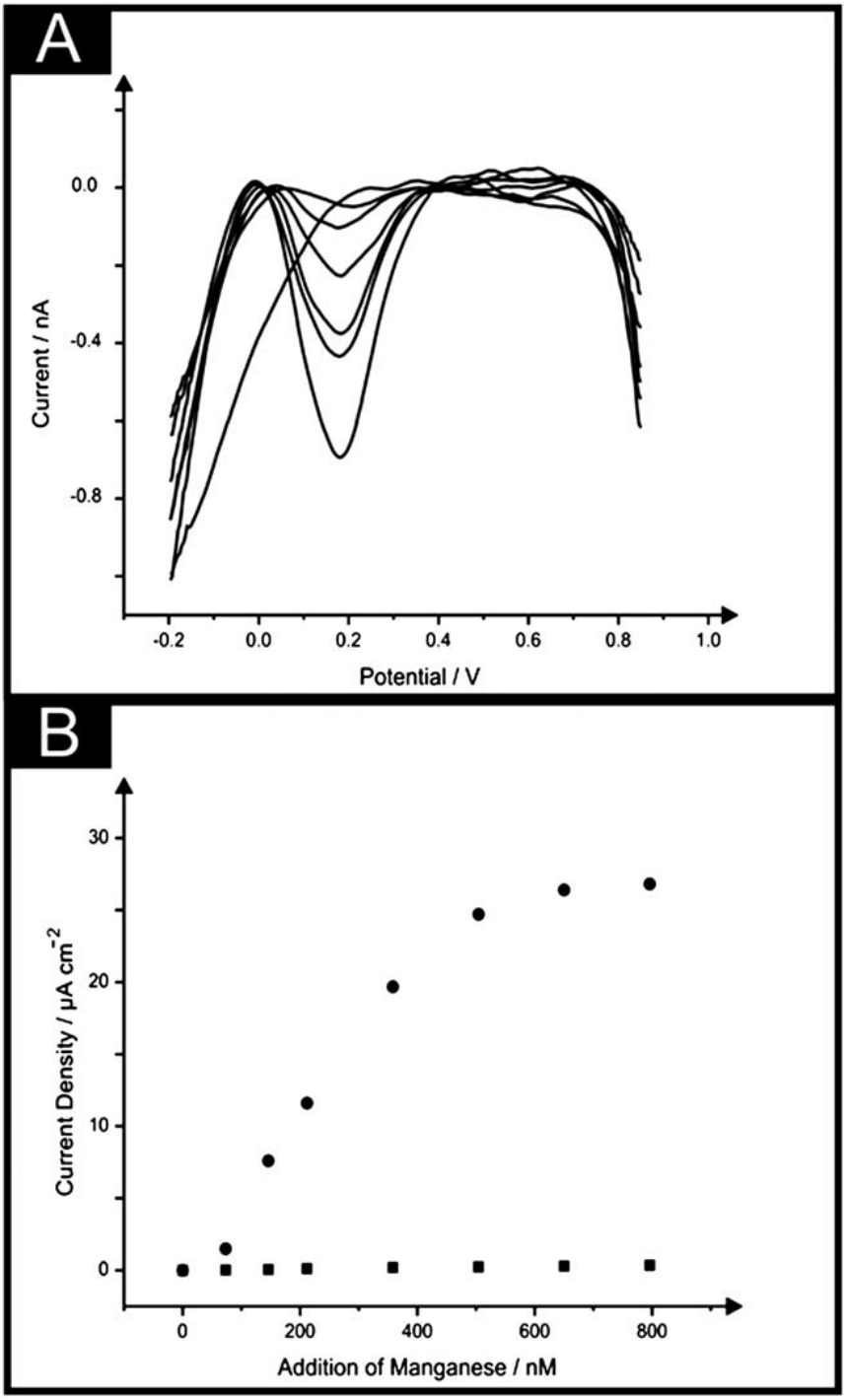

Fig. 4.14: (A) Typical square wave cathodic stripping voltammetry (E_{dep} = +0.9 V (vs. SCE), 120 s) resulting from additions of manganese (II) into a 0.1 M sodium acetate solution. **(B)** An overlay of typical calibration plots resulting from additions of manganese(II) into a 0.1 M sodium acetate solution over the range of 73 to 504 nM at the drSPE (squares) and prSPE (circles) (N = 5).

4.4 Conclusions

The successful fabrication of highly novel screen printed shallow recessed electrodes has been presented. The ease of fabrication and facile modification for beneficial diffusional processes and improved analyte detection is highlighted through the development and implementation of two different types of shallow recessed electrodes; disc-like shallow recessed screen printed electrodes and pentagon shallow recessed screen printed electrodes. Competitive limits of detection for the important analytes nitrite, NADH and manganese are shown to be possible. Interestingly we note that in addition to the clearly described benefits offered by the recessed electrode, the particular shape of the geometry also dominates the observed response and sensitivity offered by the electrode, where a pentagon-shaped shallow recessed electrode being determined to be the most beneficial design likely due to greater point diffusion/mass transport; further work is underway to explore this electrode geometry such as in a pentagon array which would yield even further benefits in mass transport and consequently offer greater electroanalytical performance. Furthermore due to the adaptability and facile modification of screen printed electrode design, the incorporation of electrocatalytic metals of interest within the inks used for fabrication is viable, as determined through the fabrication of a platinum-based recessed screen printed electrode which can be easily extended to other desired metals.

4.5 References

1. H. P. Wu, *Anal. Chem.*, 1993, **65**, 1643.
2. A. Berduque, Y. H. Lanyon, V. Beni, G. Herzog, Y. E. Watson, K. Rodgers, F. Stam, J. Alderman, D. W. M. Arrigan, *Talanta*, 2007, **71**, 1022.
3. P. N. Bartlett, S. L. Taylor, *Electroanal. Chem.*, 1998, **453**, 49.
4. R. O. Kadara, N. Jenkinson, C. E. Banks, *Sens. Actuators, B*, 2009, **142**, 342.
5. R. O. Kadara, N. Jenkinson, C. E. Banks, *Electrochem. Commun.*, 2009, **11**, 1377.
6. J. P. Metters, R. O. Kadara, C. E. Banks, *Analyst*, 2011, **136**, 1067.
7. J. Guo, E. Linder, *Anal. Chem.*, 2009, **81**, 130.
8. J. Guo, E. Linder, *J. Electroanal. Chem.*, 2009, **629**, 180.
9. D. D. Gornall, S. D. Collyner, S. P. Higson, *Electroanalysis*, 2010, **22**, 384.
10. A. C. Barton, S. D. Collyer, F. Davies, D. D. Gornall, K. A. Law, E. C. D. Lawrence, D. W. Mills, S. Myler, J. A. Pritchard, M. Thompson and S. P. J. Higson, *Biosens. Bioelectron.*, 2004, **20**, 328.
11. S. Wilke, M. D. Osborne, H. H. Girault, *Electroanal. Chem.*, 1997, **436**, 53.
12. P. M. Hallam, D. K. Kampouris, R. O. Kadara, C. E. Banks, *Analyst*, 2010, **135**, 1947.
13. S. J. Hood, R. O . Kadara, D. K. Kampouris, C. E. Banks, *Analyst*, 2010, **135**, 76.
14. J. Guo, E. Linder, *Anal. Chem.*, 2009, **77**, 2147.
15. R. Ferrigno, P. F. Brevet, H. H. Girault, *Electrochim. Acta*, 1997, **42**, 1895.
16. F. A. Aguiar, A. J. Gallant, M. C. Rosamond, A. Rhodes, D. Wood, R. Kataky, *Electrochem. Commun.*, 2007, **9**, 879.
17. C. E. Banks, R. G. Compton, A. C. Fisher, I. E. Henley, *Phys. Chem. Chem. Phys.*, 2004, **6**, 3147.
18. Y. Wang, J. G. Limon-Petersen, R. G. Compton, *J. Electroanal. Chem.*, 2011, **652**, 13.
19. D. A. C. Brownson, L. J. Munro, D. K. Kampouris, C. E. Banks, *RSC Adv.*, 2011, **1**, 978.
20. A. Radoi, D. Compagnone, *Bioelectrochemistry*, 2009, **76**, 126.
21. F. Pariente, E. Lorenzo, F. Tobalina, H. D. Abruna, *Anal. Chem.*, 1995, **67**, 3936.
22. Q. Wu, M. Maskus, F. Pariente, F. Tobalina, V. M. Fernandez, E. Lorenzo, H. D. Abruna, *Anal. Chem.*, 1996, **68**, 3688.
23. F. Pariente, F. Tobalina, G. Moreno, L. Hernandez, E. Lorenzo, H. D. Abruna, *Anal. Chem.*, 1997, **69**, 4065.
24. T. Huang, A. Warsinke, T. Kuwana, F. W. Scheller, *Anal. Chem.*, 1998, **70**, 991.
25. T. N. Rao, I. Yagi, T. Miwa, D. A. Tryka, A. Fujishima, *Anal. Chem.*, 1999, **71**, 2506.
26. N. A. Choudhry, D. K. Kampouris, R. O. Kadara, C. E. Banks, *Electrochem. Commun.*, 2010, **12**, 6.
27. M. Zhou, Y. Zhai, S. Dong, *Anal. Chem.*, 2009, **81**, 5603.
28. J. P. Metters, R. O. Kadara, C. E. Banks, *Sens. Actuators, B*, 2012, **169**, 136.
29. W. Lijinskt, S. S. Epstein, *Nature*, 1970, **225**, 21.
30. M. Bru, M. I. Burguete, F. Galindo, S. V. Luis, M. J. Marin, L. Vigara, *Tetrahedron Lett.*, 2006, **47**, 1787.
31. P. Mikuska, Z. Vecera, *Anal. Chim. Acta*, 2003, **495**, 225.
32. I. M. Ferreira, S. Silva, *Talanta*, 2008, **15**, 1598.
33. E. Szoko, T. Tabi, A. S. Halasz, M. Palfi, K. Magyar, *J. Chromatogr.*, 2004, **1051**, 177.
34. V. S. V. C. Y. Lin, K. C. Ho, *Sens. Actuators, B*, 2009, **140**, 51.
35. M. J. Moorcroft, J. Davis, R. G. Compton, *Talanta*, 2001, **54**, 785.
36. B. Sljukic, C. E. Banks, A. Crossley, R. G. Compton, *Electroanalysis*, 2007, **19**, 79.
37. L. H. Chen, J. B. Zang, Y. H. Wang, L. Y. Bian, *Electrochim. Acta*, 2008, **53**, 3442.
38. J. Pei, X. Y. Li, *Talanta*, 2000, **51**, 1107.
39. J. P. Metters, F. Tan, R. O. Kadara, C. E. Banks, *Anal. Methods*, 2012, **4**, 1272.
40. S. V. Guerra, L. T. Kubota, C. L. Xavier, S. Nakagaki, *Anal. Sci.*, 1999, **15**, 1231.
41. B. Sljukic, C. E. Banks, A. Crossley, R. G. Compton, *Electroanalysis*, 2006, **18**, 1757.
42. K. I. Ozoemena, T. Nyokong, *Talanta*, 2005, **67**, 162.
43. L. Aldous, R. G. Compton, *Phys. Chem. Chem. Phys.*, 2011, **13**, 5279.

44. L. Aldous, R. G. Compton, *ChemPhysChem*, 2011, **12**, 1280.
45. M. S. Lin, B. I. Jan, *Electroanalysis*, 1997, **9**, 340.
46. B. Wang, S. Dong, *Talanta*, 2000, **51**, 565.
47. A. Eftekhari, *Talanta*, 2001, **55**, 395.
48. I. J. Cutress, R. G. Compton, *Electroanal. Chem.*, 2010, **645**, 159.
49. J. G. Terry, H. L. Woodvine, A. J. Walton, A. R. Mount, *Analyst*, 2010, **135**, 1058.
50. J. J. Powell, T. J. Burden, R. P. H. Thompson, *Analyst*, 1998, **123**, 1721.
51. A. Iregren, *Neurotoxicology*, 1994, **15**, 671.
52. H. Frumkin, G. Solomon, *Am. J. Ind. Med.*, 1997, **31**, 107.
53. A. J. Saterlay, J. S. Foord, R. G. Compton, *Analyst*, 1999, **124**, 1791.
54. S. Somnam, K. Grudpan, J. Jakmunee, *Spectrosc. Lett.*, 2008, **41**, 221.
55. M. Knap, K. Killian, K Pyrzynska, *Talanta*, 2007, **71**, 406.
56. M. Rievaj, P. Tomick, Z. Janosikova, D. Bustin, R. G. Compton, *Chem. Anal.*, 2008, **53**, 153.
57. B. Rezaei, M. Ghiaci, M. E. Sedaghat, *Sens. Actuators, B*, 2008, **131**, 439.
58. O. M. Filipe, C. M. A. Brett, *Talanta*, 2003, **61**, 643.
59. C. E. Banks, J. Kruusma, R. R. Moore, P. Tomick, J. Peters, J. Davis, S. Komorsky-Lovric, R. G. Compton, *Talanta*, 2005, **65**, 423.
60. L. Lesven, S. M. Skogvold, O. Mikkelsen, G. Billon, *Electroanalysis*, 2009, **21**, 274.

CHAPTER 5

ELECTROANALYTICAL APPLICATION OF SCREEN PRINTED MICROELECTRODE ARRAYS.

5.1 Abstract

The fabrication of screen-printed microelectrode arrays which are comprised of six working electrodes (50 µm radii) which are separated from their nearest neighbour by an average distance of 2272 (± 0.3) µm and arranged in a circular configuration around a common counter and reference electrode are presented. Due to their facile fabrication, different inks can be used to give rise to both graphite-based and gold-based screen-printed microelectrode arrays. Additionally due to their fabrication design, the microelectrodes comprising the array are sufficiently separated to ensure no diffusional overlap which is commonly encountered by microelectrode arrays reported within the literature.

The electrochemical sensing characteristics of the graphite screen-printed microelectrode arrays are evaluated using acetaminophen, dopamine and nitrite giving rise to limits of detection (3σ) of 4.29, 3.24 and 5.24 µM respectively. Further to this, the gold-based screen-printed microelectrode arrays are explored towards the electroanalytical sensing of chromium (VI) yielding a limit of detection (3σ) of 8.28 µM. Proof-of-concept is further demonstrated through the determination of chromium (VI) within an environmental (canal water) sample.

Due to the analytically useful responses observed at the graphite and gold screen-printed microelectrode arrays, these disposable and economical electrodes hold promise for in-the-field sensing applications. Additionally the working electrode composition can be readily changed through the use of the desired screen printing ink (*i.e* Pd, Pt, Cu etc) allowing the tailoring of the electrode surface allowing electrocatalytic microelectrode arrays to be readily derived.

5.2 Introduction

Microelectrodes are utilised by electrochemists due to their reported benefits, which include: improved Faradaic-to-charging current ratios, steady-state (or quasi-steady state) responses for Faradaic processes, reduced ohmic (*IR*) drop, and most importantly when used in sensing, improved signal-to-noise ratios allowing low detection levels to be reached compared to macroelectrodes.[1-5]

The caveat with microelectrodes is that a very small Faradaic current is produced which can be hard or impossible to measure, especially due to their susceptibility to mains interference such that the Faradaic signal is engulfed beneath capacitively coupled mains interference.[6] As pointed out by Fletcher and Horne,[6] to overcome this – that is, to decrease the interference – one has to place all electrochemical apparatus inside earthed screens, and wire all circuits in a common ground plane, greatly complicating the experimental design and significantly limiting sensor implementation into the field.

The well-known solution to overcome these problems yet still use the benefits of microelectrodes is to assemble multiple microelectrodes wired in parallel, with ideally, each microelectrode independent of its neighbours; such an electrode will exhibit all the useful properties of a single microelectrode but generate a signal which is significantly greater.[6-10]

Microelectrode arrays present an opportunity for the integration in 'lab-on-a-chip' devices which can be used in a plethora of applications, such as *in-vitro* and *in-vivo* biological biosensing.[11-16] Typically microelectrode arrays comprise noble metals and are constructed in a variety of approaches (see reference[17] for a thorough overview) which involve sealing the chosen noble metal microwire within an inert substance, for example glass, so as to allow for realisation of micron sized electrode diameters whilst providing sufficient spacing between the microelectrodes comprising the array.[18]

Approaches such as photolithography are thus favoured for the design and production of microelectrode configurations since they offer the ability to fabricate microelectrode arrays with well-defined geometric and inter-electrode spacing[19] such that diffusional interaction from neighbouring microelectrode comprising the array is minimal. Other approaches for the fabricated of arrays have reported the use of screen printing technology.[20-24] Such a method of fabrication is highly advantageous due to their single-shot use alleviating the requirement for preparatory steps such as electrode polishing and also their low-cost nature allowing for economical sensor production without comprising performance or reproducibility.[17]

Screen-printed microelectrode array which comprises six microelectrodes of 50 μm radii and are arranged in a circular configuration around a common counter and reference electrode and are separated from their nearest neighbour by an average distance of 2272 (± 0.3) μm were reported. Due to their design, these screen printed microelectrode arrays are diffusionally independent such that no diffusional interaction occurs between the individual microelectrode comprising the array; such a configuration is seldom reported within the literature and additionally very few microelectrode arrays are produced via screen printing technology.

The microelectrodes comprising the screen-printed microelectrode arrays are fabricated to have working electrodes comprised of either graphite or gold, though an array of any desired noble material could also be realised by using the desired corresponding metal ink (*i.e* Pd, Pt, Cu etc). The microelectrode arrays are first characterised utilising the common electrochemical probe hexaammine-ruthenium (III) chloride and explored, in the case of the graphite microelectrode array towards the electroanalytical sensing of acetaminophen, nitrite and dopamine in the case of the gold microelectrode array, chromium (VI) and in all cases are found to yield analytically useful results. In the latter case, the sensing of chromium (IV)

in an environmental sample is shown to be feasible suggesting these sensors have potential merit in the possible screening of water samples.

5.3 Results and Discussion

Carbon Screen Printed Microelectrode Array (Carbon SPMA)

The carbon screen-printed microelectrode arrays (carbon SPMA) consist of six separate working electrodes (radii 50 μm) surrounding a common counter and reference electrode; images of the carbon SPMA are depicted in figure 5.1. Figure 5.1A shows the entire screen printed disposable sensor, which upon closer inspection with an optical microscope (figure 5.1B) allows measurement of the centre-to-centre distance between the two closest microelectrodes. Since the electrodes are in a circular pattern, the top two microelectrodes are the closest electrodes together which have a separation corresponding to 2249.4 microns; this is relevant in discussions later in terms of the sensors electrochemical response. As shown in figure 5.1C, closer inspection with SEM reveals that the microelectrodes are not typically circular as is found in other microelectrode fabrication routes and is rather, akin to a matchstick head but should still approximate to that of a microelectrode. Note that the microelectrode size is controlled by the screen mesh size and this design is on the limit of fabrication; any smaller attempted electrodes sizes are not feasibly produced and is effectively limited by a combination of the screen mesh and graphite/carbon particle size (with agglomeration a significant factor) used within the commercially utilised screen printing inks. Last, further inspection of the microelectrode (figure 5.1D) reveals the surface to consist of conductive carbon particles and is consistent with previous reports of graphite screen printed electrodes.[25, 26]

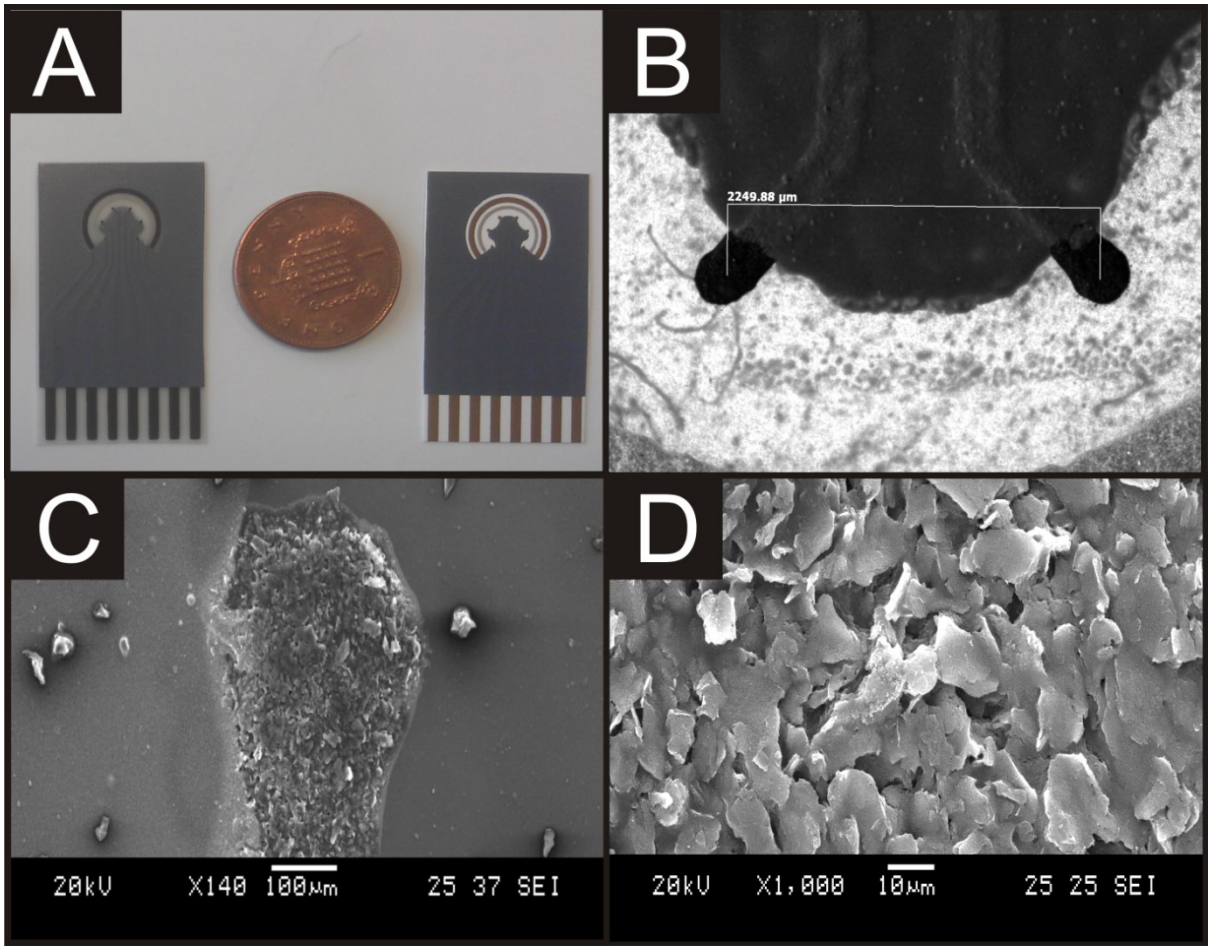

Figure 5.1: Photograph of the carbon (left image) and gold (right image) SPMA **(A)**. An optical microscope image of the carbon SPME **(B)**. Typical SEM images of the carbon SPMA at x140 **(C)** and x1000 magnification **(D).**

The carbon SPMA were next electrochemically characterised using the redox probe hexaammine-ruthenium (III) chloride in 0.1 M KCl. Figure 5.2 depicts the observed cyclic voltammetric signatures utilising the carbon SPMA using scan rates over the range 5 to 200 mVs^{-1}. It is evident through observation of figure 5.2 that at slow scan rates a steady-state type response is observed where upon faster scan rates, the voltammetric profile becomes peak shaped due to the increasing contribution from linear diffusion rather than solely convergent diffusion as expected at true microelectrodes.[27] Figure 5.3 depicts the response of a single electrode from the carbon SPMA contrasted to all the electrodes on the carbon SPMA being utilised as an array, where an apparent improvement in voltammetric peak

height of ~ 2.6 times occurs through utilisation of the SPMA over that of a single microelectrode is readily evident.

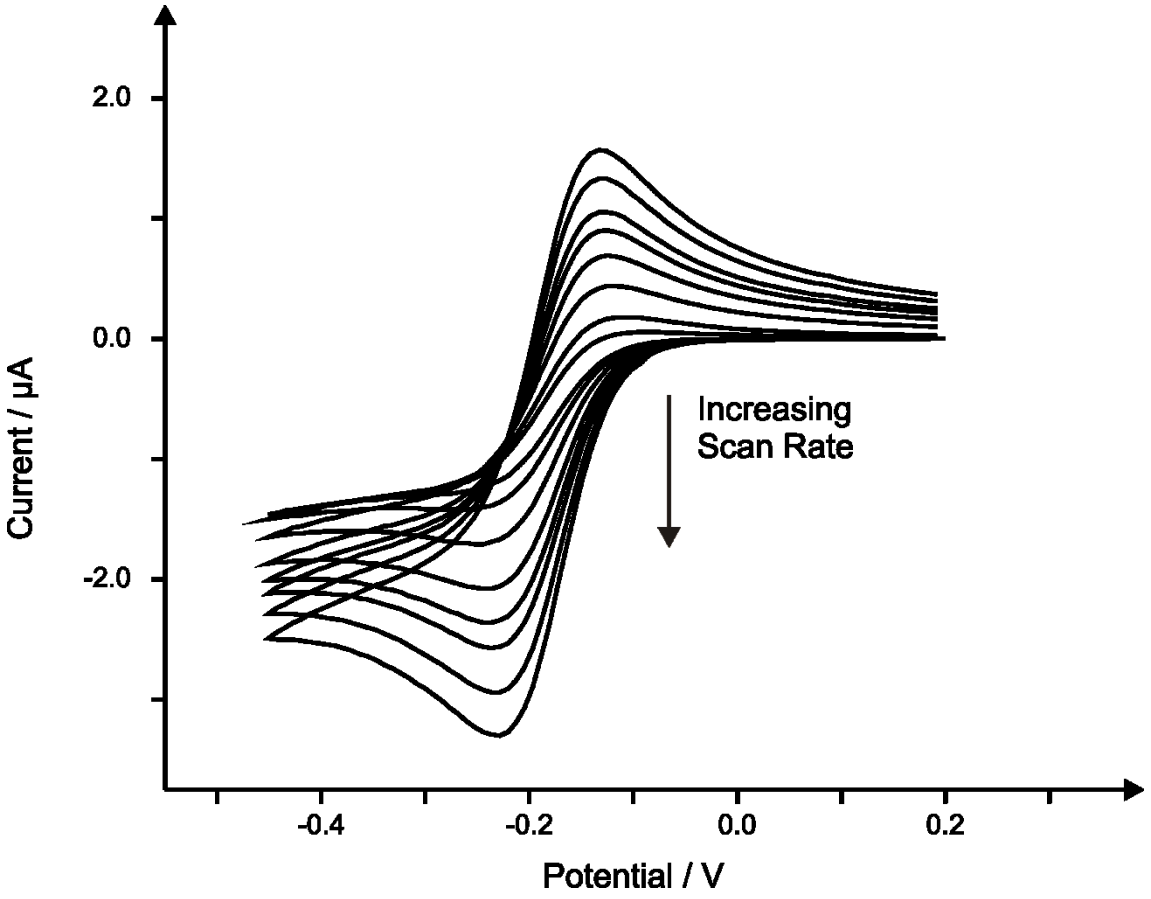

Figure 5.2: Cyclic voltammetric response arising from the carbon SPMA recorded in 1 mM hexaammine-ruthenium (III) chloride / 0.1 M KCl. Scan rates: 5 - 500 mVs^{-1}.

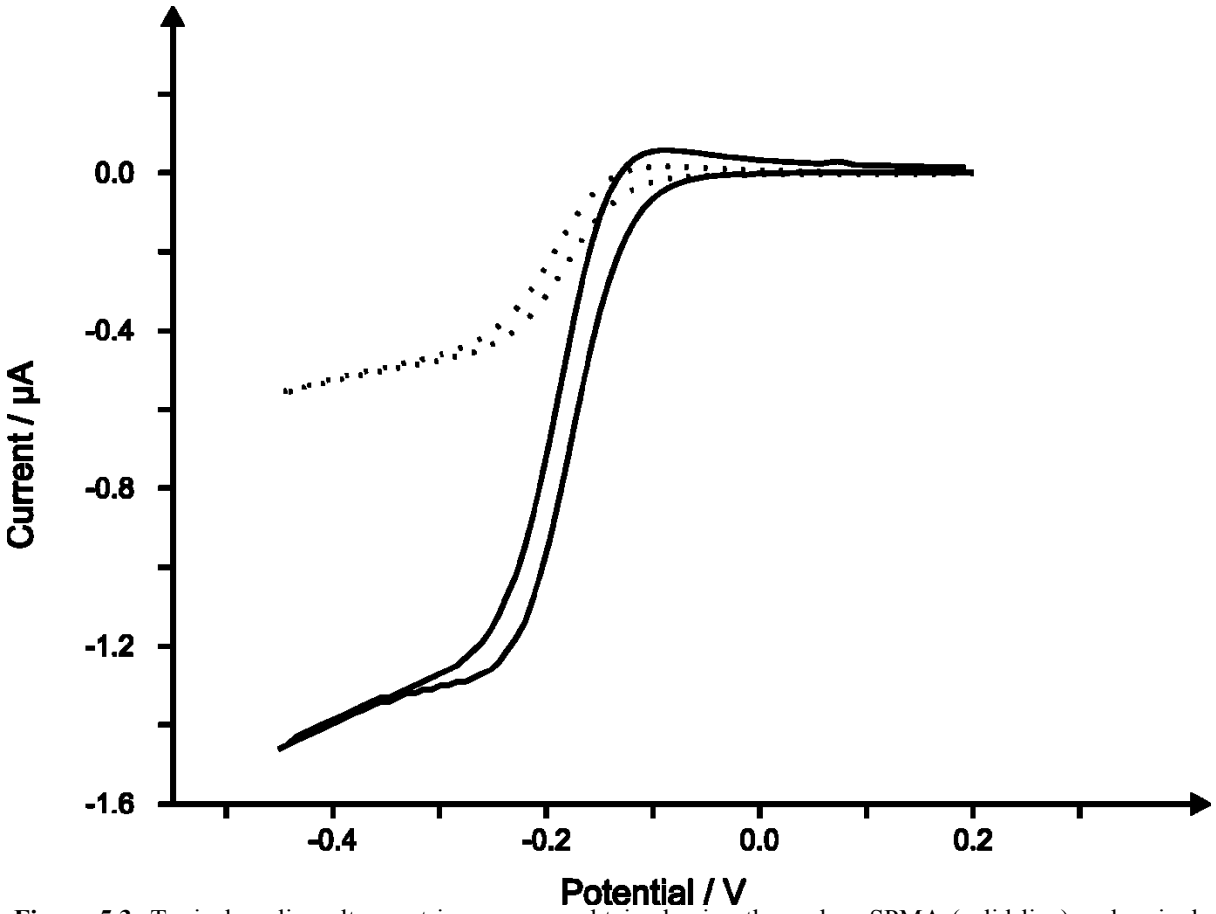

Figure 5.3: Typical cyclic voltammetric responses obtained using the carbon SPMA (solid line) and a single electrode from the carbon SPMA (dotted line) in 1 mM hexaammine-ruthenium (III) chloride / 0.1 M KCl. Scan rate: 5 mVs^{-1}.

Assuming that the dominant form of mass transport is convergent in nature and that the electrochemical response of the carbon SPMA is microelectrode-like, the theoretical predicted current, I_P is given by:

$$I_P = nFrCDN \qquad (5.1)$$

where n is the number of electrons, F the Faraday constant, C is the concentration of the analyte, D the diffusion coefficient of the analyte and r is the electrode radii. Note that N, the number of electrodes comprising the array, is present in equation (5.1) which for when a

single microelectrode on the carbon SPMA is utilised, $N = 1$ while when the whole array is used, $N = 6$. Note that the current is amplified by the total number of electrodes comprising the array. Typically it is expected that equation 5.1 will be valid allowing researchers to determine the radius of the electrodes comprising the array. However this is unfortunately and incorrectly undertaken with little, or no regard to the interaction of diffusion layers of neighbouring electrodes.[28, 29] Instead it is inferred that the diffusion layer is given by:

$$\delta = \sqrt{6Dt} \tag{5.2}$$

where D is the diffusion coefficient and t is the timescale of the experimental analysis, such that:

$$\delta = \sqrt{6D\left(\frac{\Delta E}{\upsilon}\right)} \tag{5.3}$$

If we consider the SPMA shown in figure 5.1, for equation (5.1) to be valid, there should be no diffusion layer interaction between neighbouring microelectrodes such that the diffusion layer, δ, must be less than $f_{greater}$, as given by:

$$f_{greater} = \left(\frac{d_{centre}}{2}\right) - \left(\frac{d_{electrode}}{2}\right) \tag{5.4}$$

where d_{centre} is the centre-to-centre separation between the electrodes and $d_{electrode}$ is the diameter of the electrode. Using equation (5.2), where D is the diffusion coefficient (9.1×10^{-6} cm^2 s^{-1},[30]), υ the voltammetric scan rate employed and ΔE is the potential range over which electrolysis has occurred, the diffusion layer, δ, can be estimated over the range of experimentally utilised scan rates which spans between 67.4 and 465.4 μm for the fastest (200 mVs^{-1}) and slowest (5 mVs^{-1}) applied voltammetric scan rates respectively. Using equation (5.4) $f_{greater}$ was deduced for our carbon SPMA to equate to 1950 μm. Thus given that the diffusion layer will reach a maximum of 268.7 μm at the slowest applied voltammetric scan rate, the carbon SPMA has no diffusional interaction/ overlapping diffusion layers between the electrodes comprising the array; such an array is one of only a few published in the literature where no diffusional interaction is observed and indeed this is the first report of a disposable mass produced carbon SPMA with these characteristics.

Returning to the voltammetry presented in figure 5.3, the question arises as to why, if diffusional overlap doesn't occur in the experimental set-up, an increase from that of a single electrode ($N = 1$) to the array ($N = 6$), is not a factor of 6? The answer simply is that equation (5.1) is for the case of true microelectrodes where the dominant form of mass transport is convergent and the contribution from planar diffusion is minimal; in our case, we have a significant contribution from planar diffusion in addition to convergent diffusion (see figure 5.2) due to the limitations imposed by the fabrication procedure such that electrodes with radii of 50 microns are as small as reliably (limited by the particle size of the graphite/carbon within the ink formulation) can be produced and rather we have *quasi*-microelectrodes comprising the SPMA. Furthermore, the above discussions are for a simple one step electron transfer process; deviation will clearly be observed for multi-step electron transfer processes, as is the case for the analytes explored below, such that a simple 6 times improvement in using the SPMA over a single microelectrode will not be observed.

Following the electrochemical characterisation of the carbon SPMA, the task of assessing the sensor's electroanalytical robustness was explored, first through the sensing of acetaminophen. Acetaminophen, or as it is more commonly known paracetamol, is a widely used antipyretic and analgesic drug.[31] In recent years it has become a more widely preferred alternative to aspirin, particularly for children and those sensitive to aspirin. At the recommended dosage, there are often no side effects, however, doses in excess of those recommended can result in liver and kidney damage.[32] It is suspected that a metabolite of acetaminophen is the actual hepatotoxic agent.[33-35] Clearly, with such wide use, the monitoring of acetaminophen levels within samples is of great interest.

Linear sweep voltammetric measurements were undertaken at increasing concentrations of acetaminophen into a pH 7 phosphate buffer solution; this buffer composition was selected as the optimal solution as it is close to that of biological samples in which acetaminophen sensing is of key interest, but also in line with previous literature reports.[36-39] Figure 5.4A depicts typical linear sweep voltammetric measurements obtained using a carbon SPMA at a scan rate of 5 mVs^{-1} with the quasi-limiting current (I_L) increasing with acetaminophen additions over the range of 10 to 100 μM with figure 5.4B depicting the analysis of the limiting current against acetaminophen concentration which are linear in nature ($I_L/\mu A = 2.02 \times 10^{-3}\ \mu A/\mu M + 8.26 \times 10^{-3}\ \mu A;\ R^2 = 0.98,\ N = 10$). Additionally, figure 5.4A shows the calibration plot corresponding to additions of acetaminophen over the same concentration range using a single electrode from the carbon SPMA. Although a linear response ($I_L/\mu A = 6.41 \times 10^{-4}\ \mu A/\mu M - 1.47 \times 10^{-3}\ \mu A;\ R^2 = 0.99,\ N = 10$) is observed, a reduction in magnitude of the current is noted. The comparison of the gradients for the calibration plots (figure 5.4B) demonstrates a 3.2 x improvement when utilising the carbon SPMA over a single electrode from the SPMA; this deviation from the expected 6 x improvement is due to the array comprising *quasi*-microelectrodes (see earlier).

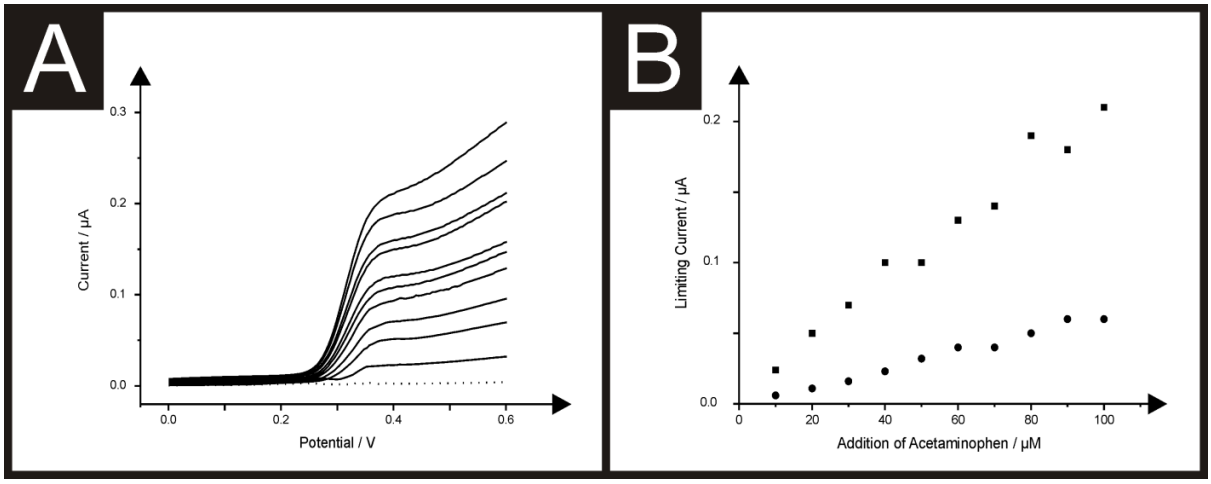

Figure 5.4: Linear sweep voltammograms recorded following the addition of acetaminophen into a pH 7 phosphate buffer solution (dotted line) over the concentration range 10 – 1000 µM using the carbon SPMA **(A)**. Typical corresponding calibration plots using the carbon SPMA (squares) and a single electrode from the carbon SPMA (circles) **(B)**. Scan rate: 5 mVs^{-1}.

The limit of detection (3σ) calculated for acetaminophen in pH 7 phosphate buffer solutions using the carbon SPMA found to correspond to 4.3 µM. Comparison of the determined limit of detection feasible at the carbon SPMA with existing literature finds the SPMA to offer comparable limitations with other electrochemical based sensors, though examples offering lower limits of detection are reported. For example, Wangfuengkanagul *et al*[34] report the sensing of acetaminophen utilising a boron-doped diamond film electrode providing a limit of detection of 10 µM.[34] Further to this an improvement in the limit of detection is reported through the modification of glassy carbon electrodes with carbon-coated nickel magnetic nanoparticles allowing for the sensing of acetaminophen down to 2.3 µM.[40] Similarly, glassy carbon electrodes coated with gold nanoparticles and an organophillic layered double hydroxide have offered a slight improvement with regards to the limit of detection towards acetaminophen of 0.13 µM.[41] The utilisation of carbon nanotubes has also been reported to be highly beneficial towards the sensing of acetaminophen offering ultra-low detection levels in the nM range.[42, 43] A single-walled carbon nanotube / graphene nanosheet

hybrid film modified glassy carbon electrode has been demonstrated to allow for a limit of detection of 38 nM acetaminophen.[42] Improving on this limit of detection Compton *et al*[43] achieve the sensing of acetaminophen to 10 nM using a multi-walled carbon nanotube modified basal plane pyrolytic graphite electrode.[43] Evidently electrode configurations exist within the literature which allow for improvement limits of detection for acetaminophen in comparison to that possible when using the carbon SPMA, it is however important to note that each of the reports discussed utilise electrodes which require preparatory steps prior to utilisation, in some cases resulting in extended time periods involved in their utilisation for analytical sampling and increasing the likelihood of poor reproducibility between electrode modifications. Critically, the carbon SPMA reported herein requires no such pre-treatment or preparation offering great improvements with regards to time and ease of use as is the case in other reported sensors.[41-43]

To further assess the useful analytical nature of the carbon SPMA, linear sweep voltammetric measurements were undertaken for the sensing of the well explored analyte dopamine which is one of the neurotransmitters playing a major role in addiction.[44] As a chemical messenger, dopamine affects brain processes that control movement, emotional response, and ability to experience pleasure and pain. It has also been reported that dopamine has an important role in the pathogenesis or drug treatment of certain brain disease, *e.g.* Parkinson's disease, schizophrenia. Therefore, the rapid and accurate detection of dopamine is important not only for diagnostic but also for pathological research. It possesses very strong electrochemical activity and is one of the main objects of study in the electroanalytical chemistry of neurotransmitters.[45, 46]

Figure 5.5A depicts the electrochemical oxidation of dopamine in a pH 7 phosphate using the carbon SPMA. As observed above, a quasi-steady-state response is observed for the oxidation of dopamine which correlates linearly ($I_L/\mu A = 2.38$ x 10^{-3} $\mu A/\mu M + 2.62$ x 10^{-3} μA;

$R^2 = 0.99, N = 10$) with dopamine concentrations over the range 50 to 500 μM (see figure 5.5B). Comparison of the calibration plot arising from measurements over the analytical range utilising the carbon SPMA with that utilising a single electrode from the array (figure 5.5B) demonstrates the superior response over the entire range studied for the sensing of dopamine. Although a much improved response is facilitated with the carbon SPMA, a single electrode from the array does allow for a linear response ($I_L/\mu A = 3.51$ x 10^{-4} $\mu A/\mu M - 1.01$ x 10^{-4} μA; $R^2 = 0.99, N = 10$) over the range studied where an improvement using the array is evident. Furthermore, a limit of detection (3σ) of 3.24 μM was determined for the sensing of dopamine when using the carbon SPMA. The determination of dopamine is well reported within the literature and therefore comparisons between the carbon SPMA and existing electrode configurations can be made with ease. Examples of such reports include that by Thomas and co-workers[47] who utilise a Poly(Rhodamine B) modified carbon paste electrode enabling the detection of dopamine at a concentration of 4 μM. Additionally, graphene modified electrodes have been shown to offer favourable limits of detection towards the sensing of dopamine. Screen-printed graphene electrodes have been reported by where chemically reduced graphene oxide was utilised to form an ink which could be screen printed. The fabricated sensor was determined to enable the detection of dopamine down to 0.12 μM.[48] Similarly, a graphene has been used in a highly novel form; a three dimensional graphene foam, which when utilised for the sensing of dopamine enables a limit of detection of 25 nM. Again it is clear that alternative electrode materials and configurations allow for improvements for the detection of dopamine in comparison to that possible at the carbon SPMA, however the simplistic nature and removal of the requirement of pre-treatment or electrode preparation necessary at some of the literature reports offers a true advantage, particularly when looking at large scale applications of the sensors at hand.

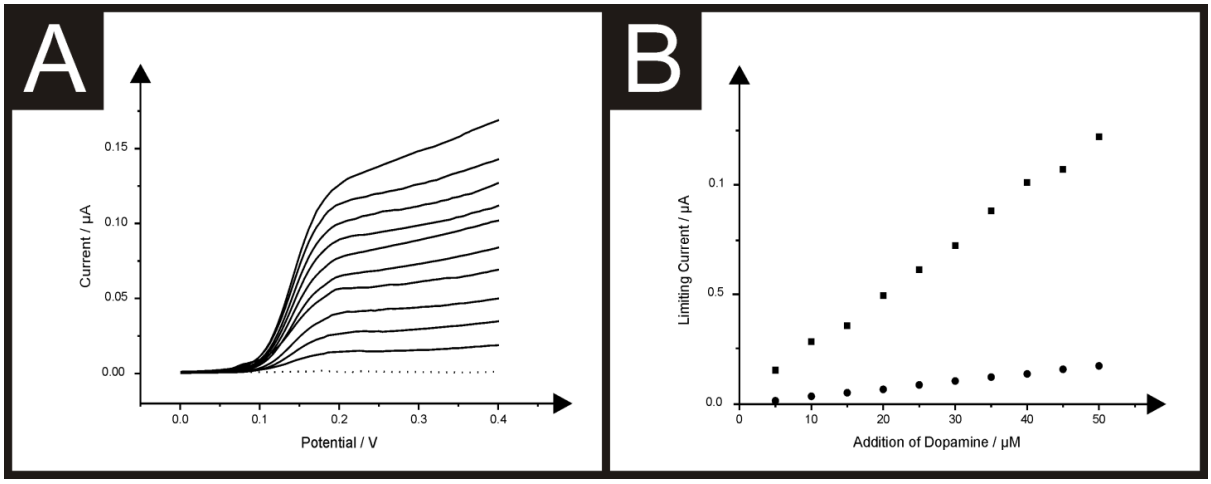

Figure 5.5: Linear sweep voltammograms recorded following the addition of dopamine hydrochloride into a pH 7 phosphate buffer solution (dotted line) over the concentration range 50 – 500 µM using the carbon SPMA **(A)**. Typical corresponding calibration plots using the carbon SPMA (squares) and a single electrode from the carbon SPMA (circles) **(B)**. Scan rate: 5 mVs^{-1}.

The final model analyte selected to ascertain a greater understanding of the analytical potential of the carbon SPMA was sodium nitrite. Nitrite is widely involved in environmental chemistry and public health, so the important roles played by nitrite in these areas were recognized long ago.[49, 50] Although naturally-occurring concentrations of nitrites are usually of no significance to health, wastes from fertilizers and the intentional addition of nitrites for corrosion control are potential sources of nitrite contamination.[51] Nitrite is reported to be a human health-hazard chemical the excess of which may cause poisoning and its derivatives are also major components in low-level radioactive waste solution.[52, 53] The excess uptake of nitrite could cause gastric cancer[54] and it is therefore necessary to develop a reliable and sensitive sensor to detect nitrite in food, drinking water and environmental samples.

Initially cyclic voltammetric studies for a solution of nitrite in a pH 7 phosphate buffer solution at a scan rate of 5 mVs^{-1} demonstrated the oxidation of nitrite was viable through utilisation of the carbon SPMA as shown in figure 5.6A. Voltammetric measurements were made at increasing concentrations (10 to 100 µM) of nitrite using a

carbon SPMA as depicted in figure 5.6A, with the corresponding calibration plot for the carbon SPMA contrasted with the response obtained at a single electrode from the array shown in figure 5.6B. Clearly, both electrodes exhibit a linear response over the entire concentration range studied (SPMA: $I_L/\mu A = 8.22 \times 10^{-3}\ \mu A/\mu M + 5.92 \times 10^{-3}\ \mu A$; $R^2 = 0.98$, $N = 10$ and single electrode from the SPMA: $I_L/\mu A = 1.45 \times 10^{-3}\ \mu A/\mu M + 4.72 \times 10^{-3}\ \mu A$; $R^2 = 0.96$, $N = 10$) where a ~ 5.7 x improvement was evident through use of the carbon SPMA over that at a single electrode. The limit of detection (3σ) using the carbon SPMA for nitrite in a pH 7 phosphate buffer was calculated to be 5.24 μM. This calculated limit of detection for the sensing of nitrite is found to be competative when compared with existing reports within the literature (see *Table 1* for a non-exhaustive list of electrochemical reports). Chen *et al*[55] have described the utilisation of a nano-diamond powder electrode reporting a nitrite limit of detection of 0.12 mM. An improvement upon these limits of detection has been reported through the utilisation of carbon based screen printed shallow recessed electrodes[56] with a limit of detection of 7.28 μM for the sensing of nitrite and furthermore through the use of composite copper – carbon electrodes with a limit of detection of 0.6 μM found to be possible.[57] Improving on these reports a glassy carbon modified with $CuPtCl_6$ film has been described to enable the detection of nitrite at concentrations as low as 0.05 μM.[58] Again the use of a one-shot economical sensor has potential benefits over these literature reports.

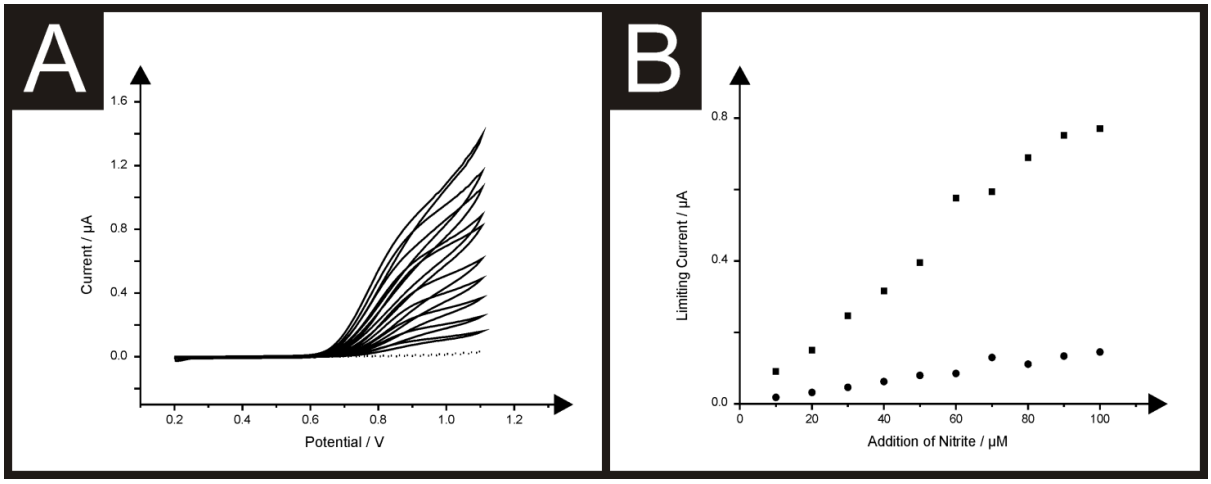

Figure 5.6: Cyclic voltammograms recorded following the addition of nitrite into a pH 7 phosphate buffer solution (dotted line) over the concentration range 50 – 500 µM using the carbon SPMA **(A)**. Typical corresponding calibration plots using the carbon SPMA (squares) and a single electrode from the carbon SPMA (circles) **(B)**. Scan rate: 5 mVs^{-1}.

Gold Screen Printed Microelectrode Array (Gold SPMA)

To further investigate the potential applications of the screen printed microelectrode array and demonstrate the ease of use and versatility of the screen printed design, gold SPMAs were fabricated utilising a gold polymer ink (see Experimental section). These electrodes are exactly the same as the carbon SPMA described above with the only difference being that the carbon work electrode surface is modified with a gold polymeric ink. The gold SPMAs were characterised using the electrochemical redox probe hexaammine-ruthenium (III) chloride in 0.1 M KCl at scan rate over the range 5 – 200 mVs^{-1}. Clearly, as was also determined using the carbon SPMA, use of the gold SPMA at slow scan rates results in a steady-state type response is observed where upon faster scan rates, the voltammetric profile becomes peak shaped. The gold SPMA sensor was utilised for the sensing of chromium (VI)[59, 60] a heavy metal of significant interest which has been demonstrated to be electrochemically viable utilising gold-based electrodes. Chromium (VI) poses a great environmental threat, being around 100 – 1000 times more toxic than chromium (III).[61] This

increased hazardous status is attributed to the high oxidation potential and World Health Organisation (WHO) recommends chromium (VI) to be limited to 0.05 mg L^{-1} (0.17 μM) within groundwater.[62] Due to the previously discussed imposed restrictions relating to chromium (VI) levels within water, areas of industry such as plating industries, cooling towers, timber treatment, leather tanning, wood preservation and steel manufacturing require sensitive and reliable techniques to monitor anthropogenic chromium pollution in ground water.[63, 64]

First, linear sweep voltammetry was performed using the gold SPMA in 0.05 M H_2SO_4 at a scan rate of 5 mVs^{-1}, as depicted by figure 5.7A. Additions of chromium (VI) were made into the 0.05 M H_2SO_4 buffer over the concentration range 10 to 100 μM, measured using linear sweep voltammetry as depicted in figure 5.7A. A linear response through the plot of voltammetric reduction peak height versus concentration (figure 5.7B) was found to be linear ($I_P/\mu A = 6.10 \times 10^{-3}\ \mu A / (\mu M) + 1.70 \times 10^{-2} \mu A$; $R^2 = 0.99$, $N = 10$) over the entire analytical range explored. The limit of detection utilising the gold SPMA for the sensing of chromium (VI) in 0.05 M H_2SO_4 was calculated (3σ) to correspond to 8.28 μM. *Table 2* depicts electrochemical reports present within the literature for the detection of chromium (VI) which shows the gold SPMA to be highly competitive and potentially analytically useful.

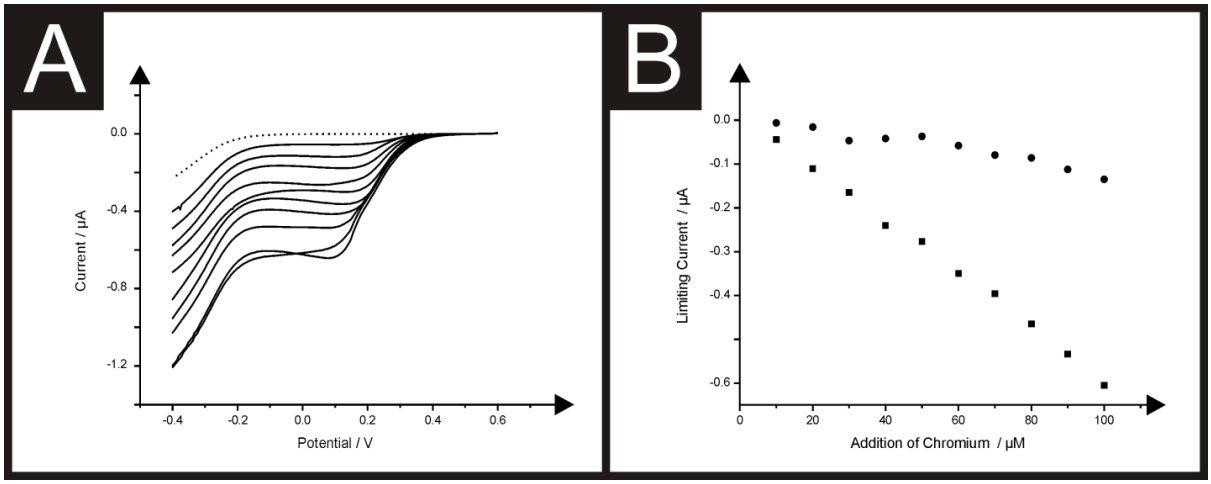

Figure 5.7: Linear sweep voltammograms recorded following the addition of chromium (VI) into a 0.05 M H_2SO_4 solution (dotted line) over the concentration range 10 – 100 µM using the gold SPMA **(A)**. Typical corresponding calibration plots using the gold SPMA (squares) and a single electrode from the carbon SPMA (circles) **(B)**. Scan rate: 5 mVs^{-1}.

In order to assess the true viability of the gold SPMA for the sensitive detection of chromium (VI) in environmental samples, the sensing of chromium (VI) was explored in a canal water sample (sourced and pre-treated as reported in the Experimental Section). Linear sweep voltammetry was utilised as reported above in the '*ideal*' 0.05 M H_2SO_4 buffer solutions, for the measurement of low level additions of chromium (VI) over the concentration range 10 to 100 µM in the canal water sample. The gold SPMA was found to successfully facilitate the sensing of chromium (VI) over the entire analytical range, demonstrating a linear relationship ($I_L/\mu A = 6.30$ x 10^{-3} $\mu A/(\mu M) + 1.95$ x $10^{-2} \mu A$; $R^2 = 0.97$, $N=10$) between the quasi-limiting current and chromium (VI) concentrations even within the canal water sample as shown in figure 5.8 which potentially has other electroactive interferents present. Critically, when the calibration plots obtained under '*ideal*' conditions are contrasted with those using canal water samples (figure 5.8), no deviation is notable in the sensitivity of the gold SPMA, emphasising the robust and reliable nature of the screen printed microelectrode array, even within such difficult media. Further to this, the limit of detection

utilising the gold SPMA for the sensing of chromium (VI) in the acidified canal water sample was calculated (3σ) to be 9.46 µM, showing only a slight deviation from that calculated under '*ideal*' conditions; such results indicate the gold SPMA sensors have potential for chromium (VI) sensing in environmental water samples.

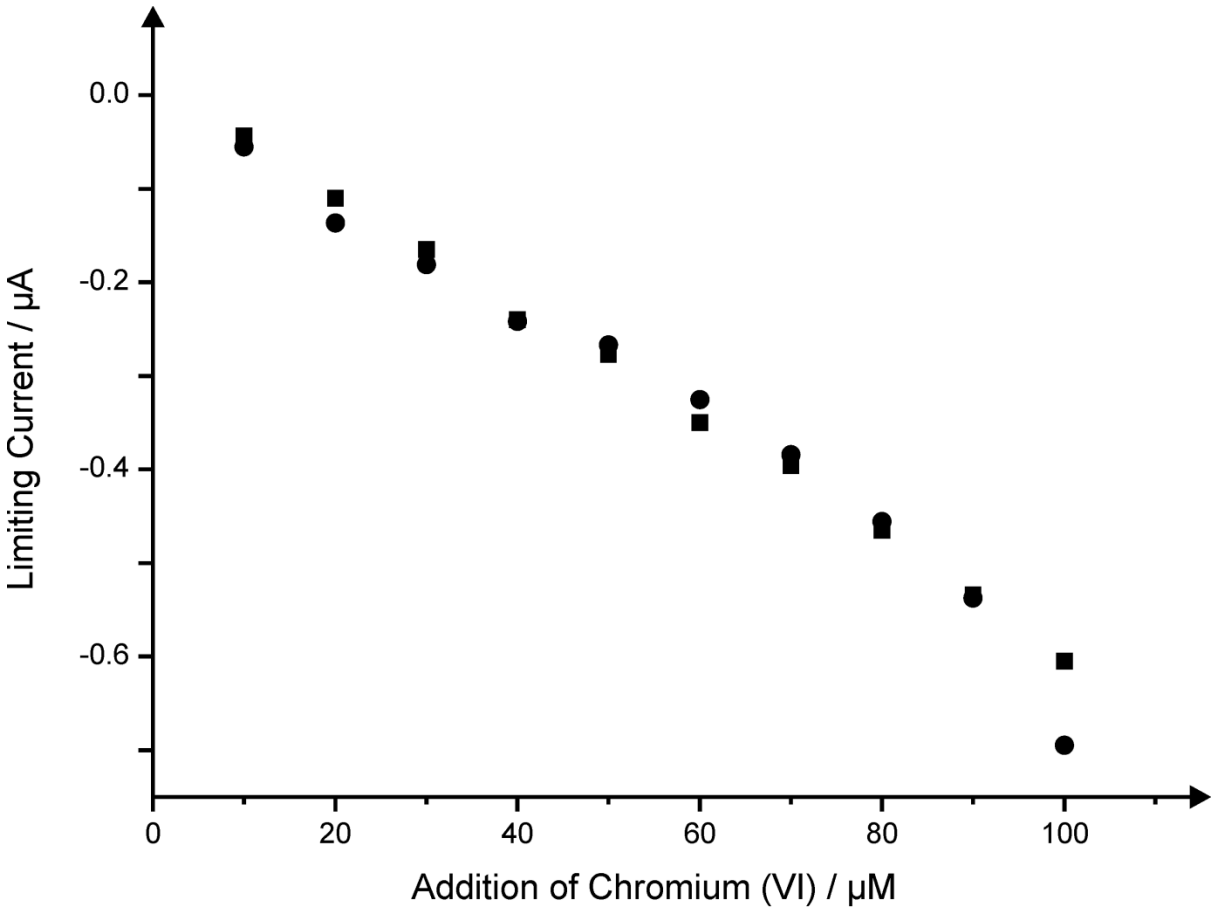

Figure 5.8: An overlay of typical corresponding calibration plots resulting from additions of chromium (VI) made into both an'ideal' 0.05 M H_2SO_4 solution (squares) and a canal water sample (circles). Scan rate: 5 mVs^{-1}.

5.4 Conclusions

We have demonstrated the successful fabrication of a mass-produced disposable screen printed microelectrode arrays utilising both graphite and gold based inks demonstrating the versatility of the screen printing technique for the specific tailoring of sensors. The screen-printed arrays were electrochemically characterised and contrasted with existing literature with the graphite screen-printed microelectrode array benchmarked towards the detection of acetaminophen, dopamine and nitrite.

Similarly the gold based screen-printed microelectrode array was benchmarked towards the sensing of the key analyte chromium (VI) with the analytical protocol further examined for the detection of chromium (VI) within canal water samples. Due to the availability of screen printable inks, other noble metal screen-printed microelectrode arrays can be envisaged and given that these electrode can be mass-produced allowing single-shot disposable sensors to be realised, researchers are able to translate laboratory derived electrochemical protocols into “the field”.

Table 1

A summary of electrochemical reports towards the detection of nitrite

Electrode	Linear Range (µM)	Limit of Detection (µM)	Ref
Composite copper electrode modified with carbon powder and epoxy resin	100 to 1250	600	[57]
Nanodiamond powder electrode	1000 to 20000	120	[55]
poly(3,4-ethylenedioxythiophene) modified carbon screen printed electrode	Δ	1.72	[65]
poly(3,4-ethylenedioxythiophene)/ multiwalled carbon nanotube modified carbon screen printed electrode	Δ	0.96	[65]
Composite lead oxide modified carbon powder and epoxy resin	100 to 700	0.9	[66]
Glassy carbon modified with poly-Nile Blue film	0.5 to 100	0.1	[67]
Glassy carbon electrode modified with alternated layers of iron(III) tetra-(N-methyl-4-pyridyl)-porphyrin (FeT4MPyP) and copper tetrasulfonated phthalocyanine	0.5 to 7.5	0.1	[68]
Graphite screen printed microband	10 to 700	0.05	[26]

Glassy carbon modifed with $CuPtCl_6$ film	0.1 2000	to	0.05	[58]
Glassy carbon modified with an electrodeposited copper nanoparticles/carbon nanotubes/chitosan film	0.1 2500	to	0.024	[69]
Carbon SPMA	10 to 100		5.24	This work

Δ = Not stated

Table 2

A summary of electrochemical reports towards the detection of chromium (VI).

Electrode	Linear Range (μM)	Limit of Detection (μM)	Comments	Ref
Gold macro	20 to 2000	4.5	Detection in the presence of known interferents	[60]
Gold nanoparticle modified screen printed	Δ	0.4	Electrochemical deposition pretreatment was required for the formation of the nanoparticle modified surface	[70]
Silver nanoparticle modified screen printed	Δ	0.85	Electrochemical deposition pretreatment was required for the formation of the nanoparticle modified surface	[70]
Gold nanoparticle modified indium tin oxide	5 to 100	2	Gold nanoparticles induced through electrodeposition	[71]
Gold screen printed macro	10 to 1600	4.4		[59]
Gold nanoparticle modified screen	0.03 to	0.015	Nanoparticles introduced through	[72]

printed	17		electrodeposition	
Graphite screen printed	0.34 to 3.4	0.065		[73]
Sol-gel modified glassy carbon	0.04 to 1.35	0.01	Pretreatment to allow formation of electrodepositd sol-gel film followed by 12h curing in an oven	[74]
Mercury thin film electrode	0.01 to 0.6	0.032	Electrodeposition of a mercury film performed prior to analysis	[75]
Poly(4-vinvlpyridine) coated platinum	0.1 to 10	Δ	Pretreatment required for the formation of the thin film	[76]
Gold SPMA	10 to 100	8.28		This work

Δ = Not stated

5.5 References

1. J. Whitson, D. Kubota, K. Shimono, Y. Jia, M. Taketani, *Adv. Net. Electrophys.*, 2006, 38.
2. M. Fejtl, A. Stett, W. Nisch, K. H. Boven, A. Moller, M. Baudry, M. Taketani, *Advances in Network Electrophysiology Using Multi-Electrode Arrays, New York: Springer Press*, 2006, 24.
3. S. G. Weber, *Anal. Chem.*, 1989, **61**, 295.
4. K. Stulik, C. Amatore, K. Holub, V. Marecek, W. Kutner, *Pure Appl. Chem.*, 2000, **72**, 1483.
5. D. E. Tallman, *J. Solid State Electrochem.*, 2011, **15**, 1703.
6. S. Fletcher, M. D. Horne, *Electrochem. Commun.*, 1999, **1**, 502.
7. N. A. M. Said, K. Twomey, V. I. Ogurtsov, D. W. M. Arrigan, G. Herzog, *J. Phys. : Conf. Ser.*, 2011, **307**.
8. R. G. Compton, G. G. Wilgoose, N. V. Reese, I. Streeter, R. Baron, *Chem. Phys. Lett.*, 2008, **459**, 1.
9. D. W. M. Arrigan, *Analyst*, 2004, **129**, 1157.
10. T. J. Davis, R. G. Compton, *J. Electroanal. Chem.*, 2005, **585**, 63.
11. K. M. Wassum, V. M. Tolosa, J. Wang, E. Walker, H. G. Monbouquette, . N. T. Maidment, *Sensors*, 2008, **8**, 5023.
12. C. B. P. Thiebaud, M. Koudelka-Hep, M. Bove, S. Martinoia, M. Grattarola, H. Jahnsen, R. Rebaudo, J. Zimmer, Y. Dupont, *Biosens. Bioelectron.*, 1999, **14**, 61.
13. G. Jobst, I. Moser, P. Svasek, M. Varahram, Z. Tranjanoski, P. Wach, P. Kotanko, F. Skrabal, G. Urban, *Sens. Actuators, B* 1997, **43**, 121.
14. A. Guiseppi-Elie, S. Brahim, G. Slaughter, K. R. Ward, *Sensors*, 2005, **5**, 345.
15. G. S. Wilson, R. Gifford, *Biosens. Bioelectron.*, 2005, **20**, 2388.
16. J. Piehler, *Curr. Opin. Struct. Biol.*, 2005, **15**, 4.
17. J. P. Metters, R. O. Kadara, C. E. Banks, *Analyst*, 2011, **136**, 1067.
18. R. G. Compton, C. E. Banks, *Understanding Voltammetry, 2nd Ed. Imperial College, London*, 2010.
19. A. E. Cohen, R. R. Kunz, , *Sens. Actuators, B*, 2000, **62**, 23.
20. J. Wang, J. Lu, B. Tian, C. Yarnitzky, *J. Electroanal. Chem.*, 1993, **361**, 77.
21. K. C. Honeychurch, J. P. Hart, , *TrAC, Trends Anal. Chem.*, 2003, **22**, 456.
22. S. Piermarini, L. Micheli, N. H. S. Ammida, G. Palleschi, D. Moscone, *Biosens. Bioelectron.*, 2007, **22**, 1434.
23. B. P. Corgier, C. A. Marquette, L . J. Blum, *Anal. Chim. Acta*, 2005, **538**, 1.
24. V. M. B. V. Chikkaveeraiah, V. Patel, J. S. Gutkind, J. F. Rusling, *Biosens. Bioelectron.*, 2011, **26**, 4477.
25. R. O. Kadara, N. Jenkinson, C. E. Banks, *Sens. Actuators, B*, 2009, **138**, 556.
26. J. P. Metters, R. O. Kadara, C. E. Banks, *Sens. Actuators, B*, 2012, **169**, 136.
27. C. G. Zoski, *Electroanalysis*, 2002, **14**, 1041.
28. T. J. Davis, S. Ward-Jones, C. E. Banks, J. del Campo, R. Mas, F. X. Munoz, R. G. Compton, *J. Electroanal. Chem.*, 2005, **585**, 51.
29. A. O. Simm, C. E. Banks, S. Ward-Jones, T. J. Davis, N. S. Lawrence, T. G. J. Jones, L. Jiang, R. G. Compton, *Analyst*, 2005, **130**, 1303.
30. F. Marken, J. C. Eklund, R. G. Compton, *J. Electroanal. Chem.*, 1995, **395**, 335.
31. D. A. C. Brownson, J. P. Metters, D. K. Kampouris, C. E. Banks, *Electroanalysis*, 2011, **23**, 894.
32. N. Hanawa, M. Shinohara, B. Saberi, W. A. Gaarde, D. Han, N. Kaplowitz, *J. Biol. Chem.*, 2008, **283**, 13565.
33. D. L. Laskin, C. R. Gardner, V. F. Price, D. J. Jollow, *Hepatology*, 1995, **21**, 1045.
34. O. C. N. Wangfuengkanagul, *J. Pharm. Biomed. Anal.*, 2002, **28**, 841.
35. M. Black, *Annual Rev. Med.*, 1984, **35**, 577.
36. A. Babaei, M. Afrasiabi, M. Babsadeh, *Electroanalysis*, 2010, **22**, 1743.
37. Q. Wan, X. Wang, F. Yu, X. Wang, N. Yang, *J. Appl. Electrochem.*, 2009, **39**, 1145.

38. F. Ghorbani-Bidkorbeh, S. Shahrokhian, A. Mohammadi, R. Dinarvand, *Electrochim. Acta*, 2010, **55**, 2752.
39. S. A. Kumar, C. F. Tang, S. M. Chen, *Talanta*, 2008, **76**, 997.
40. S. F. Wang, F. Xie, R. F. Hu, *Sens. Actuators, B*, 2007, **123**, 495.
41. H. Yin, K. Shang, X. Meng, S. Ai, *Microchim. Acta*, 2011, **175**, 39.
42. X. Chen, J. Zhu, Q. Xi, W. Yang, *Sens. Actuators, B*, 2012, **161**, 648.
43. G. G. W. R. T. Kachoosangi, R. G. Compton, *Anal. Chim. Acta*, 2008, **618**, 54.
44. J. N. Stuart, A. B. Hummon, J. V. Sweedler, *Anal. Chem.*, 2004, **76**, 120.
45. Y. Sun, B. Ye, W. Zhang, X. Zhou, *Analytica Chimica Acta*, 1998, **363**, 75.
46. T. F. Kang, G. L. Shen, R. Q. Yu, *Analytica Chimica Acta*, 1997, **354**, 343.
47. T. Thomas, R. J. Mascarenhas, B. E. Kumara Swamy, *J. Mol. Liq.*, 2012, **174**, 70.
48. J. Ping, J. Wu, Y. Wang. Y. Ying, *Biosens. Bioelectron.*, 2012, **34**, 70.
49. T. R. Camp, *Water and its Impurities. Reinhold Publishing, New York*, 1963.
50. D. E. Metzler, *Biochemistry: The Chemical Reaction of Living Cells. Academic New York*, 1977.
51. N. Spataru, T. N. Rao, D. A. Tryk, A. Fujishima, *J. Electrochem. Soc.*, 2001, **148**, E112.
52. D. W. Standards, *US Department of Health, Education and Wlefare, Public Health Service, Washington DC*, 1962, 1988.
53. J. M. Concon, *Food Toxicology: Principles and Concepts, Part A, Marcel Dekker, New York*, 1988.
54. W. Lijinskys, S. S. Epstein, *Nature*, 1970, **225**, 21.
55. L. H. Chen, J. B. Zang, Y. H. Wang, L. Y. Bian, *Electrochim. Acta*, 2008, **53**, 3442.
56. J. P. Metters, F. Tan, R. O. Kadara, C. E. Banks, *Anal. Methods*, 2012, **4**, 3140.
57. B. Sljukic, C. E. Banks, A. Crossley, R. G. Compton, *Electroanalysis*, 2007, **19**, 79.
58. J. Pei, X. Y. Li, *Talanta*, 2000, **51**, 1107.
59. J. P. Metters, R. O. Kadara, C. E. Banks, *Analyst*, 2012, **137**, 896.
60. C. M. Welch, O. Nekrassova, R. G. Compton, *Talanta*, 2005, **65**, 74.
61. M. C. Y.-B. R. M. Cespon-Romero, M. P. Bermejo-Barrera, *Anal. Chim. Acta*, 1996, **327**, 37.
62. WHO, *Guidance for Drinking Water Quality, 2nd Ed., Vol. 1. Recommendations. Geneva*, 1993.
63. D. Golub, Y. Oren, *J. Appl. Electrochem.*, 1989, **19**, 311.
64. R. J. Kieber, J. D. Wiley, S. D. Zvalaren, *Environ. Sci. Technol.*, 2002, **36**, 5321.
65. C. Y. Lin, V. S. Vasantha, K. C. Ho *Sens. Actuators, B*, 2009, **140**, 51.
66. B. Sljukic, C. E. Banks, A. Crossley, R. G. Compton, *Anal. Chim. Acta*, 2007, **587**, 240.
67. X. Chen, F. Wang, Z. Chen, *Anal. Chim. Acta*, 2008, **623**, 213.
68. W. J. R. Santos, P. R. Lima, A. A. Tanaka, S. M. C. N. Tanaka, L. T. Kubota, *Food. Chem.*, 2009, **113**, 1206.
69. S. Yang, X. Liu, X. Zeng, B. Xia, J. Gu, S. Luo, N. Mai, W. Wei, *Sens. Actuators, B*, 2010, **145**, 762.
70. O. Dominguez-Renedo, L. Ruiz-Espelt, N. Garcia-Atorgano, J. Acros-Martinez, *Talanta*, 2008, **76**, 854.
71. M. C. Tsai, P. Y. Chen, *Talanta*, 2008, **76**, 533.
72. G. Liu, Y. Y. Liu, H. Wu, Y. Lin, *Environ. Sci. Technol.*, 2007, **41**, 8129.
73. P. M. Hallam, D. K. Kampouris, R. O. Kadara, C. E. Banks, *Analyst*, 2010, **135**, 1947.
74. N. A. Carrington, L. Yong, Z. L. Xue, *Anal. Chim. Acta*, 2006, **572**, 17.
75. C. M. A. Brett, O. M. S. Filipe, C. S. Neves, *Anal. Lett.*, 2003, **36**, 955.
76. J. A. Cox, P. J. Kulesza, *Anal. Chim. Acta*, 1993, **154**, 71.

CHAPTER 6. OVERALL CONCLUSIONS

Overall, new screen printed electrochemical sensors have been fabricated and explored towards a range of target analytes which were: i) the first example of a true platnium screen printed macroelectrode was presented which was found to be electroanalytically useful; ii) a novel, disposable, single-shot palladium screen printed macro electrodes has been fabricated and evaluated towards the sensing of formaldehyde, hydrazine, protons and hydrogen gas; iii) shallow recessed electrodes made entirely via screen printing has also been fabricated and benchmarked, with a new pentagon electrode shown to be useful; iv) the successful fabrication of a mass-produced disposable screen printed microelectrode array exhibiting diffusional independence comprising graphite and gold have been realised

In a wider context, these designs can be tailored with new catalytic surfaces for target analyte sensing, which will be reliant upon the availability of screen printable inks. Given that these electrodes can be mass-produced allowing single-shot disposable sensors to be realised, researchers are able to translate laboratory derived electrochemical protocols into “the field” using the benefits of the desired electrode surface configuration and enhancements in mass transport.